UCRL-17783

c.2

University of California

Ernest O. Lawrence Radiation Laboratory

MASS AND SPECTROSCOPIC MEASUREMENTS
OF COMPLETE ISOSPIN QUARTETS
IN THE LIGHT NUCLEI

Gilbert W. Butler
(Ph.D. Thesis)

August 30, 1967

DISCLAIMER

UCRL-17783

UNIVERSITY OF CALIFORNIA
Lawrence Radiation Laboratory
Berkeley, California

AEC Contract No. W-7405-eng-48

MASS AND SPECTROSCOPIC MEASUREMENTS OF COMPLETE ISOSPIN QUARTETS IN THE LIGHT NUCLEI

Gilbert W. Butler

(Ph.D. Thesis)

August 30, 1967

MASS AND SPECTROSCOPIC MEASUREMENTS OF COMPLETE ISOSPIN QUARTETS IN THE LIGHT NUCLEI

Contents

MASS AND SPECTROSCOPIC MEASUREMENTS OF COMPLETE ISOSPIN QUARTETS IN THE LIGHT NUCLEI

Gilbert W. Butler

Lawrence Radiation Laboratory
University of California
Berkeley, California

August 30, 1967

ABSTRACT

The mass 13, 21, and 37 isospin T = 3/2 quartets have been completed through a series of nuclear reaction investigations. A standard particle identifier was used to measure the mass of the T_z = -3/2 nuclide ^{13}O via the $^{16}O(^3He,^6He)^{13}O$ reaction at 65 MeV. An improved particle-identification system, which employed two transmission (dE/dx) and one stopping (E) detector, was used to determine the masses of the T_z = -3/2 nuclei ^{21}Mg and ^{37}Ca via the $^{24}Mg(^3He,^6He)^{21}Mg$ and $^{40}Ca(^3He,^6He)^{37}Ca$ reactions at 56 MeV. The first three T = 3/2 levels in ^{21}Ne were established by a simultaneous study of the $^{22}Ne(d,t)^{21}Ne$ and $^{22}Ne(d,^3He)^{21}F$ reactions at 39.6 MeV, while the $^{23}Na(p,t)^{21}Na$ reaction at 42 MeV was utilized to observe the lowest T = 3/2 level in ^{21}Na. Excitation energies of the lowest T = 3/2 levels in ^{37}K and ^{37}Ar were determined via the $^{39}K(p,t)^{37}K$ and $^{39}K(p,^3He)^{37}Ar$ reactions induced by 45-MeV protons. Data from the complete isospin quartets were used to test the isobaric multiplet mass equation and the various predictions of masses of neutron-deficient nuclei. Preliminary studies of the angular distributions of the $^{16}O(^3He,^6He)^{13}O$, $^{16}O(^3He,^6Li)^{13}N$, $^{16}O(^3He,^7Li)^{12}N$, and $^{16}O(^3He,^7Be)^{12}C$ reactions at 70 MeV are also presented.

I. INTRODUCTION

Of particular interest in the general study of nuclear spectroscopy is the delineation throughout the nuclear chart of the line of particle stability—that is, the determination of the lightest and heaviest isotopes of each element which are stable with respect to nucleon emission. In general, theoretical approaches to this problem (see Refs. 1-3) have concerned themselves with the lighter nuclei and have been either somewhat qualitative in their predictions or were unable to predict nuclear masses unless the mass of the conjugate nucleus was known. The recent theory of Kelson and Garvey[4] overcomes these objections and makes explicit mass predictions for all particle-stable nuclei with a high degree of accuracy, as far as it can be tested. It is one of the purposes of this thesis to develop an experimental technique capable of measuring the masses of nuclei that are three neutrons removed from β-stability ($T_z = -3/2$ nuclei such as ^{13}O) by the three-neutron transfer reaction (^3He,^6He) as a method of evaluating the various theoretical approaches toward the prediction of the line of particle stability.

Of additional interest is the fact that nuclei three neutrons from β-stability in the light elements (e.g., ^9C, ^{37}Ca) complete isospin quartets, thereby permitting one to test the isobaric multiplet mass equation[5,6] (IMME):

$$M(A,T,T_z) = \underline{a}(A,T) + \underline{b}(A,T)T_z + \underline{c}(A,T)T_z^2.$$

Since this equation relating the masses of members of an isospin multiplet possesses three coefficients, its validity can be independently tested only if four or more members of an isospin multiplet with $T \geq 3/2$ are known. Although this equation was originally proposed by Wigner and Feenberg[5] in 1941, its experimental study has only very recently become possible and results have been reported only for the mass 9 isospin quartet.[7] We wish to continue this study and investigate the IMME over a reasonable change in the Coulomb energy through the completion of the mass 13, 21, and 37 isospin quartets.

In order to complete these quartets it was necessary to employ various one- and two-nucleon transfer reactions, such as the (d,t) and (p,t) reactions, on appropriate targets to locate the $T = 3/2$ states in the $T_z = +1/2$ and $-1/2$ members of the quartets. These data, in conjunction with the data from the (^{3}He,^{6}He) experiments, completed the isospin quartets since the masses of the $T_z = +3/2$ nuclei were already known.

II. THE ISOBARIC MULTIPLET MASS EQUATION

Evidence is continually being found in low-energy nuclear processes for the presence of a further constant of the motion that is similar to the well-known angular momentum and parity constants of the motion. These observations may be simply interpreted if the charge independence of nuclear forces is assumed, and the isobaric spin formalism provides a useful expression of this hypothesis—it states in effect that total isobaric spin is conserved in fundamental nuclear processes. To be more specific, the charge-independence hypothesis states that the specifically nuclear forces between pairs of nucleons in corresponding states of relative motion are independent of charge. For example, the nuclear forces in the proton-proton, neutron-neutron, and proton-neutron systems in the ^1S state of relative motion are all assumed equal. The first direct evidence for the credibility of the charge-independence hypothesis came from low-energy proton-proton scattering experiments.[8] When compared with existing information on the neutron-proton interaction, which was derived from the scattering cross section for slow neutrons by protons and from the binding energy of the deuteron, these results suggested a very similar central potential for the proton-proton and neutron-proton systems in the ^1S state of relative motion.

In the isobaric spin formalism it is possible to treat low Z nuclei as assemblies of identical particles by introducing a general particle (the nucleon) with two isobaric spin projections: $+1/2$ for a neutron and $-1/2$ for a proton. These are then defined to be eigenvalues of T_z, the z-component of the isobaric spin quantum number T. T is a constant of the motion for the charge-independent nuclear Hamiltonian (which omits Coubomb forces), and the constancy of T_z expresses the conservation of charge. The z-component of the isobaric spin of a complex nucleus consisting of Z protons and N neutrons is clearly $T_z = (1/2)(N-Z)$. Since the charge-independence hypothesis implies that T is a good quantum number, there must exist isobaric spin multiplets consisting of $2T + 1$ isobaric nuclei with T_z values ranging from $-T$ to $+T$. Each nucleus of this multiplet possesses an energy

level (not necessarily the ground state) of the same binding energy (after taking into account Coulomb forces and the neutron-hydrogen atom mass difference) and the same parity and total angular momentum. As may be seen from the expression for T_z, the isobaric spin T is integral for even A and half-integral for odd A.

The 2T + 1 members of an isobaric multiplet have eigenstates $|TT_z\rangle$ that are then identical except for T_z. If the total charge-dependent perturbation (nuclear plus Coulomb) to the nuclear forces is V, then, under the assumption that the nuclear wave functions are unaffected by the perturbation to first order, the masses of the members of an isobaric multiplet are given by the formula:[5,6,9]

$$M(A,T,T_z) = \text{constant} + \langle TT_z|V|TT_z\rangle .$$

If V is the sum of two-body interactions only, then its expansion into a set of irreducible tensors in isobaric spin space does not go beyond the second rank:

$$M(A,T,T_z) = \text{constant} + \sum_k a_k \langle TT_z|T_0^{(k)}|TT_z\rangle \qquad k \leq 2.$$

By the Wigner-Eckart theorem this becomes (using a 3-j symbol):

$$\begin{aligned} M(A,T,T_z) &= \text{constant} + \sum_k a_k (-1)^{T-T_z} \begin{pmatrix} T & k & T \\ -T_z & 0 & T_z \end{pmatrix} \langle T\|T^{(k)}\|T\rangle \qquad k \leq 2 \\ &= \text{constant}_1 + \text{constant}_2 \times T_z + \text{constant}_3 \times [T_z^2 - (1/3)T(T+1)] \\ &= \underline{a}(A,T) + \underline{b}(A,T)T_z + \underline{c}(A,T)T_z^2 , \end{aligned}$$

which is the usual form of the isobaric multiplet mass equation (IMME). Second- or higher-order perturbations in V or three-body forces would cause a breakdown of the parabolic character of the IMME.

Since this equation relating the masses of members of an isobaric spin (isospin) multiplet possesses three coefficients, its validity can be independently checked only if four or more members of a

multiplet with $T \geq 3/2$ are known. In this case the masses of three members of the multiplet determine the coefficients and hence the position of the fourth (or higher) member of the multiplet without further assumptions. In the past a lack of experimental data on complete isospin multiplets with $T \geq 3/2$ prevented any testing of the IMME. It should be pointed out that agreement with the IMME does not necessarily imply that nuclear forces are completely charge independent, though the magnitude of any observable disagreement would certainly be of theoretical importance. If agreement with the IMME is found within the experimental errors, then one can test the charge-independence hypothesis only by calculating the $b(A,T)$ and $c(A,T)$ coefficients of the IMME using realistic Coulomb interactions.

The mass 9 isospin quartet was the first quartet in which all four members were experimentally determined and good agreement with the IMME was found.[7] Prior to this work, some calculations involving the IMME in the light nuclei had been made,[10] but due to insufficient data had to rely on various assumptions, such as the assumption that the $b(A,T)$ and $c(A,T)$ coefficients of the IMME do not change with isospin. Wilkinson[11] has parameterized the $b(A,T)$ and $c(A,T)$ coefficients for nuclei in the 1p shell into various expected charge-independent and charge-dependent terms and obtained fairly good agreement with the data from isobaric doublets and triplets. Such an approach will presumably be necessary to test more precisely the charge independence of nuclear forces as more data on isobaric quartets and quintets become available.

III. EXPERIMENTAL PROCEDURES

A. Cyclotron, Beam Optics, and Scattering Chamber

Conventional cyclotrons were usually limited to accelerating ions of a fixed charge-to-mass ratio q/m to a fixed energy, whereas the sector-focused (SF) cyclotron (e.g., the Berkeley 88-inch cyclotron) can accelerate ions having a variety of q/m values to a wide range of final energies. With the more elaborate magnetic field configuration of the SF cyclotron, the requirements of phase stability and axial focusing can each be precisely satisfied. Therefore acceleration is more efficient and the quality of the beam from the SF cyclotron relative to the earlier cyclotrons is greatly improved in terms of energy, geometric dispersion, and intensity. The decoupling of the problems of phase stability and axial focusing means that accelerating ions to moderately relativistic velocities is possible. In our case, the 88-inch cyclotron can accelerate protons to a maximum energy of 55 MeV, deuterons to 60 MeV, ^{3}He-particles to 150 MeV, and ^{4}He-particles to 130 MeV.

The layout of the 88-inch cyclotron and experimental area is shown in Fig. 1. The beam was extracted from the cyclotron at a radius of 39.3 inches by means of a tungsten septum and an electrostatic deflector. After the beam passed through a radial collimator, a quadrupole doublet and a vertical collimator, it entered a beam analysis magnet where it was deflected toward the experimental cave. Another quadrupole lens was required to produce a radial focus at the analyzing slit, which was an adjustable slit that permitted a momentum analysis of the beam. The expected energy resolution of the beam after analysis was $\sim$0.14%. The beam was then focused to a spot typically 0.06 inch wide by 0.10 inch high in the center of a 20-inch scattering chamber by means of two additional magnetic quadrupole doublets. Four adjustable tantalum collimator blades were located 28 inches in front of the scattering chamber but these collimators were usually set at 0.4 inch wide by 0.4 inch high so that they served only as clean-up collimators. A 1/4-inch-square tantalum clean-up collimator was located 8 inches in front of the scattering chamber center. The angle at which the beam

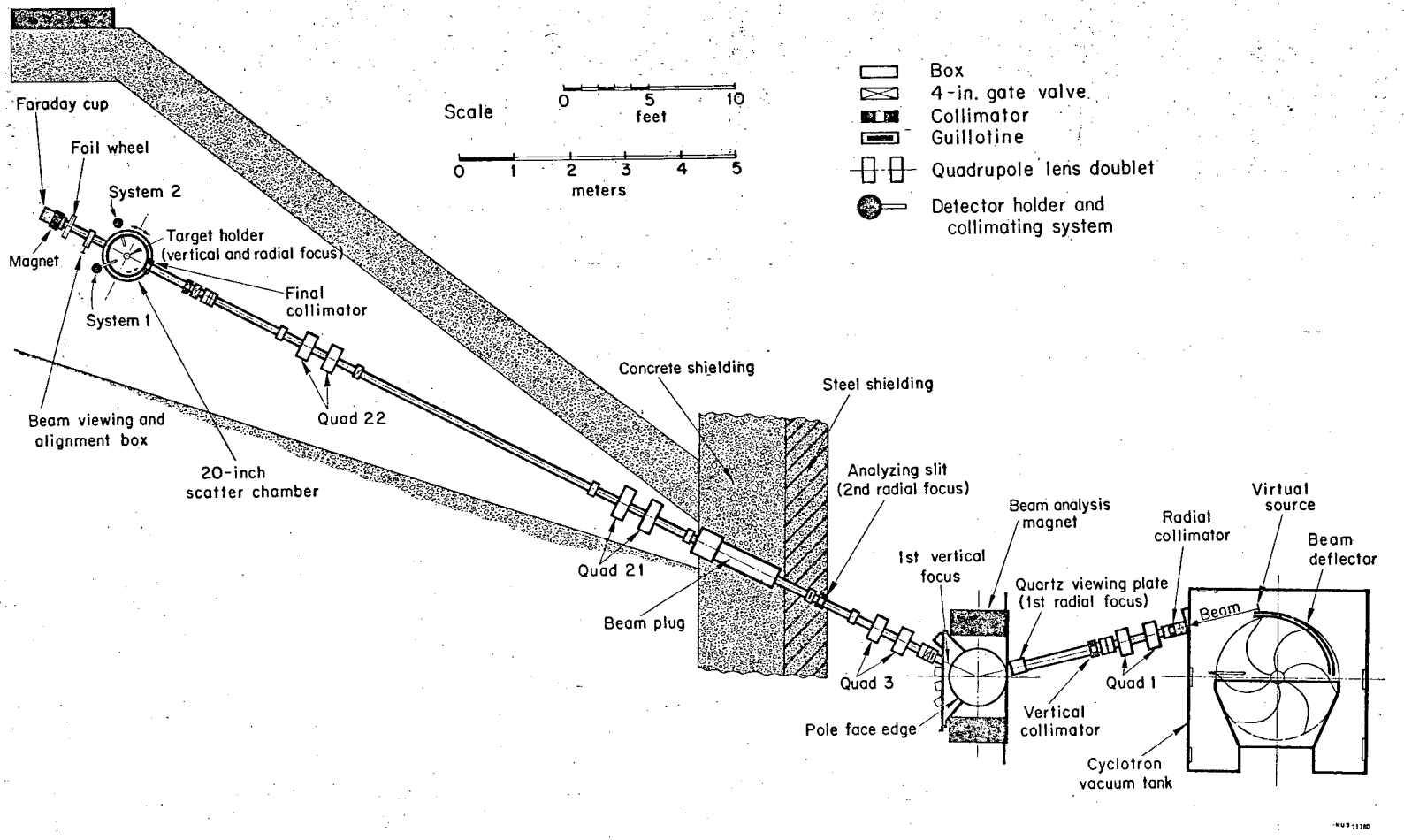

Fig. 1. Schematic diagram of the 88-inch cyclotron and the relevant beam optics and equipment.

passed through the center of the scattering chamber was determined by observing (via remote television) its impact on luminous foils placed at the center of the chamber and 28 inches downstream.

Beam intensities used in these experiments varied from 0.05 to 1.5 μA, depending on the scattering angle and the nuclear reaction being studied. The accumulated beam was measured with a Faraday cup (protected against charge loss and gain by a permanent magnet) and an integrating electrometer. Five remotely controlled ten-position foil wheels—located between the scattering chamber and the Faraday cup, and containing various thicknesses of aluminum absorber—were used to determine the mean energy of the beam. A plot of beam intensity at the Faraday cup versus thickness of aluminum absorber was used to determine the amount of absorber corresponding to one-half the maximum beam intensity. These ranges in aluminum were converted into energies by means of range-energy tables that were coded at this laboratory[12] and agreed very well with available experimental data and prior computations.[13]

The scattering chamber had two independently moveable turrets with counter axes that passed through the center of the chamber at angles 10 deg above and below the median plane so that scattering angles from 10 to 170 deg were observable. The details of the scattering chamber have been described in Ref. 14, so we will only present here those places in which significant changes have been made. Counter telescope assemblies (completely different from those used in Ref. 14) were located just outside the scattering chamber and could be isolated from it by a vacuum valve. The detectors were mounted on aluminum detector holders which were then fastened to the lid of the external counter telescope assembly.

Rectangular tantalum collimators with approximate dimensions of 0.085 inch wide by 0.200 inch high were used and were located approximately 18.9 inches from the center of the scattering chamber, thereby subtending an angular width (radial) of 0.26 deg and a solid angle of 5×10^{-5} sr. The counter assembly could be rotated symmetrically about the axis which passed through it and the center of the scattering

chamber; this enabled the vertical collimator height to be positioned always perpendicular to the scattering plane. When a gas target was used, an additional set of collimators (radial only) was attached to the counter assembly at a distance of 4.3 inches from the center of the scattering chamber.

A counter which monitored the target stability and the beam energy was located in one of the viewing ports of the center stationary section of the scattering chamber. This counter was in the median plane at a fixed scattering angle of 27.5 deg and was collimated so that it subtended approximately the same solid angle as the counter telescope systems. The monitor counter was normally used to detect the elastically scattered beam particles. Exceptions occurred when a high-energy proton or deuteron beam was used and the available detectors were not thick enough to stop the elastically scattered beam particles; in this case, a reaction such as (p,α) was monitored.

B. Targets

1. Gas Targets

A target gas cell 3.0 inches in diameter by 1.25 inches in height and with a 315 deg continuous window made of 0.1 mil Havar[15] foil (2.11 mg/cm^2) was employed for the bombardment of gas targets. Gas pressures were determined by means of a mercury manometer and the temperatures by a thermometer placed near the scattering chamber. A mercury displacement pump was available for the recovery or rare gases. Dry natural oxygen at pressures of 23.8 to 32.4 cm Hg was used for the ^{16}O target during the study of the $^{16}O(^3He,^6He)^{13}O$ reaction. Neon gas enriched[16] to 91.3% ^{22}Ne (8.2% ^{20}Ne and 0.5% ^{21}Ne) for the study of the $^{22}Ne(d,t)^{21}Ne$ and $^{22}Ne(d,^3He)^{21}F$ reactions was contained in this cell at a pressure of 21 cm Hg. Nitrogen gas enriched[17] to > 99% ^{15}N, which was used as a calibration target during the $^{16}O(^3He,^6He)^{13}O$ experiment, was bombarded in this gas cell at a gas pressure of 24 cm Hg.

2. Solid Targets

Several ^{12}C targets were used to provide calibration reactions during some of the experiments. These targets were obtained by preparing a dilute solution of colloidal graphite in alcohol and acetone and then spreading a thin layer of the solution onto a mirror. Once the solution had evaporated, the residual film was floated off in water, collected, and then dried. Self-supporting targets about 0.5 mg/cm^2 thick were obtained by this method. The oxygen impurity was removed by heating the targets to 1400°C in a vacuum and allowing them to cool to below 200°C before exposure to air.

The ^{23}Na target was prepared by evaporating NaH (which decomposed when heated) onto a glass plate in vacuum. The glass plate had previously been coated with a thin, evaporated layer of hexadecylamine so that the sodium target was readily floated off in dry hexane. This self-supporting target (~1 mg/cm^2) was transferred to the scattering chamber under an inert (argon) atmosphere but was found to contain appreciable oxygen contamination.

A ^{24}Mg target, enriched[18] to 99.8% ^{24}Mg, was prepared by evaporation onto a glass plate in vacuum. The target (1.1 mg/cm^2) was then peeled off in a mixture of water and alcohol, and mounted in a target frame.

A ^{39}K target was prepared by evaporating natural potassium (93.1% ^{39}K) metal onto a glass plate in vacuum and then floating it off in hexane. This self-supporting target (0.8 mg/cm^2) was allowed to oxidize slowly before it was transferred to the scattering chamber—the oxygen impurity provided convenient internal calibration points.

An evaporated, self-supporting natural calcium (97.0% ^{40}Ca) foil 0.75 mg/cm^2 thick served as the ^{40}Ca target. This target was also transferred to the scattering chamber under an inert (argon) atmosphere, and it was found to contain only a small amount of ^{16}O impurity.

C. Particle Identification

For bombarding energies above a few MeV simple single-counter detection systems generally can not be employed because of the many nuclear reactions which obscure the reaction of interest. The method of particle identification used in these experiments made use of a transmission counter which measured an energy loss ΔE proportional to the rate of energy loss dE/dx, and a stopping counter which measured the remaining energy E. The total energy of the particle can then be easily calculated ($\Delta E + E = E_{total}$) and, by performing a more elaborate calculation (discussed below) based on a range-energy relationship, the particle type can be determined from the relative values of ΔE and E.

Two types of calculation have been employed by different workers to determine the particle type from knowledge of the ΔE and E signals. The first method was based on a simplified form of Bethe's equation for the rate of energy loss.[19] The second method (used in all these experiments) was originally used at Berkeley[20] and is based on the empirical range-energy relationship $R = \underline{a}E^{1.73}$, where R is the range of the particle, E is its energy, and $\underline{a}$ is a proportionality constant characteristic of the particle. It has been shown[20] that this range-energy relationship is accurate to within about 2% for protons, deuterons, tritons, ^{3}He-particles, and α-particles in the energy range from ~10 MeV to ~150 MeV. The use of this range-energy relationship in a particle identifier is illustrated in Fig. 2. The calculation given in Fig. 2 shows that a quantity $T/\underline{a}$ (here T is the ΔE counter thickness) can be calculated by generating the function $(E + \Delta E)^{1.73} - E^{1.73}$; this quantity is characteristic of the type of particle and therefore serves to identify it. The electronic method of performing the above calculation is also shown in Fig. 2.

D. Procedures For High-Yield Nuclear Reactions

High-yield nuclear reactions were investigated by utilizing two of these particle identifiers fed by two independent ΔE-E silicon detector telescopes. A schematic diagram of the electronic setup for

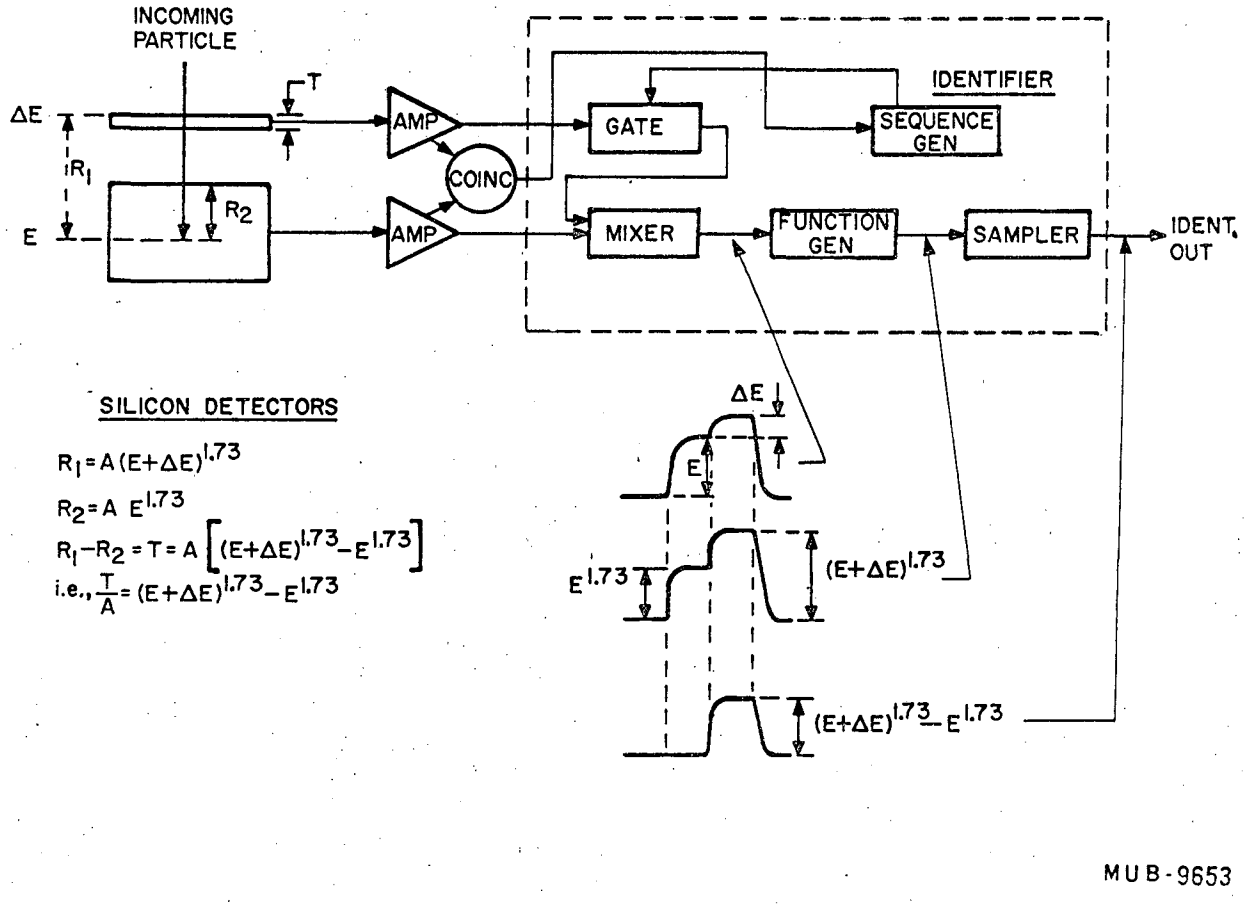

Fig. 2. Block diagram of the standard (double-counter) particle identifier.

one of these two systems is shown in Fig. 3. The ΔE detectors were 5.6-mil phosphorus-diffused silicon transmission counters,[21,22] whereas the 120-mil E detectors, the 20-mil rejection detectors, and the various monitor detectors were all lithium-drifted silicon counters.[22] Signals from the rejection detectors were used in anti-coincidence with those from the ΔE-E counter telescope to eliminate long-range particles traversing the first two counters. Each detector was connected by a short length of low-capacity cable to the input of a fast rise-time (10-15 nsec, depending on the capacitance of the detector) charge-sensitive preamplifier,[22] and via a 10-MΩ resistor to the detector bias voltage supply. Detector bias voltages used in these experiments varied from 50 to 1000 V., depending on the detector, and the leakage currents varied from 0.5 to 10 μA. The preamplifiers were connected by about 150 ft. of 125-Ω cable to the counting area where the signals were fed into linear amplifiers[22] with delay-line shaping networks. To obtain complete charge collection from the silicon detectors and also to obtain good energy resolution, the amplifier shaping networks were operated with time constants in the 1 μsec range. After coincidence requirements in the respective ΔE and E amplifiers were met, the amplified signals were sent to the particle identifiers.

This "standard" particle identifier has been quite adequate for studying nuclear reactions which have a reasonable cross section. This is illustrated in Fig. 4, which shows a typical particle-identifier spectrum from the bombardment of a sodium target with 42-MeV protons. Clearly very good separation was obtained between the various hydrogen and helium isotopes in this spectrum. For the study of the $^{23}Na(p,t)^{21}Na$ and $^{23}Na(p,^{3}He)^{21}Ne$ reactions, particle-identifier pulses were fed into two four-channel routers where single-channel analyzers were set around the triton, ^{3}He, and ^{4}He peaks (the fourth channel was a narrow one centered about the deuteron-triton valley to make certain no tritons were lost). The energy spectrum of a given particle was then routed into one of the four 1024-channel memory units of a Nuclear Data 4096-channel pulse-height analyzer; data from the second counter telescope were recorded in an on-line PDP-5 computer (which served as

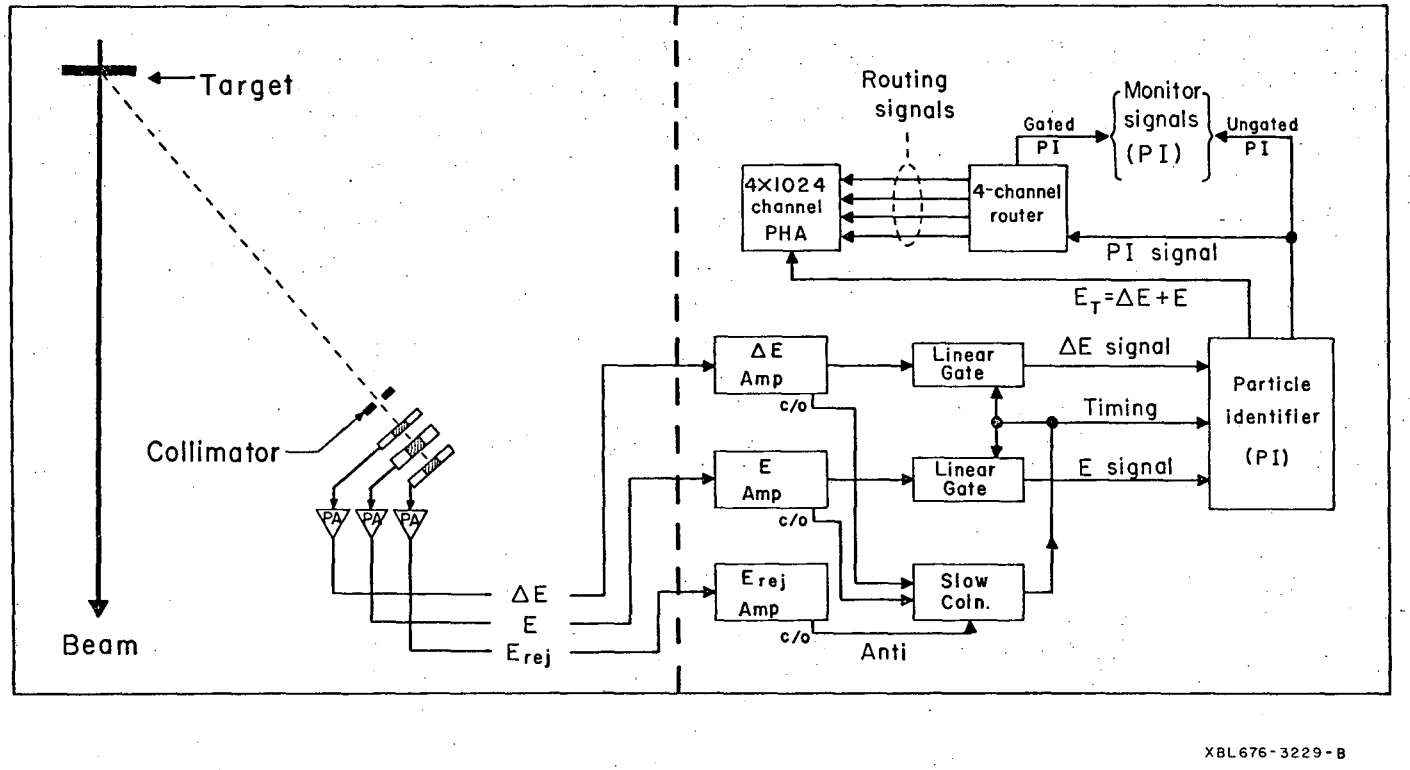

Fig. 3. Schematic diagram of the electronic setup for the standard particle-identifier system.

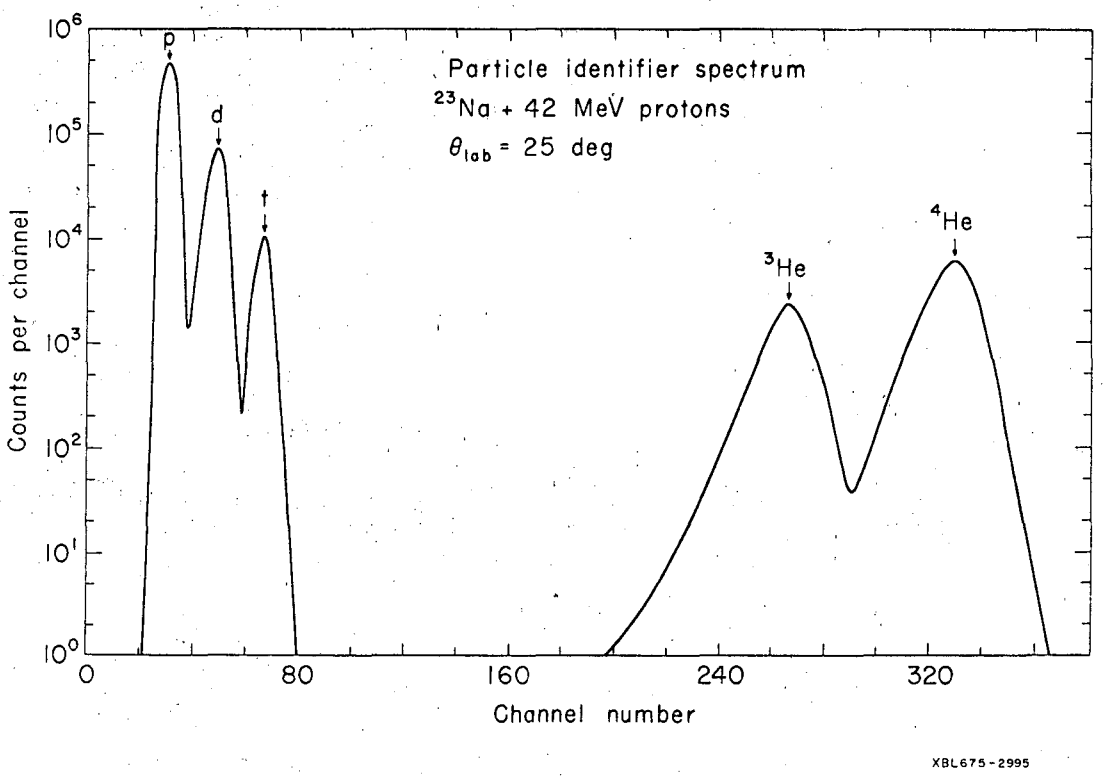

Fig. 4. Standard particle-identifier spectrum from the bombardment of a sodium target with 42-MeV protons. The ΔE counter thickness was 5.6 mils.

a second 4096-channel analyzer) via an eight-channel pulse multiplexer and a 4096-channel analogue-to-digital converter (ADC).

E. Procedures For Low-Yield Nuclear Reactions

The performance of the standard particle identifier in the study of low-yield nuclear reactions was not very good. Although this identifier was used in the determinations of the masses of ^{9}C and ^{13}O via the $^{12}C(^{3}He,^{6}He)^{9}C$ and $^{16}O(^{3}He,^{6}He)^{13}O$ reactions,[7,23] the presence of a relatively high background in the ^{6}He region of the identifier spectra complicated the measurements. This background arose primarily from rare events in which a few of the large number of α-particles stopping in the counter telescope deposited an abnormally large amount of energy in the ΔE detector (due to blocking, Landau tail, "nuclear reactions," etc.), causing their identification signal to be significantly higher than normal. When survey experiments on the $(^{3}He,^{6}He)$ reaction on heavier targets showed a decreasing cross section, it became necessary to develop an identification system which eliminated this background. The system which accomplished this was developed at Berkeley[24] and a schematic diagram of a typical counter telescope and the electronics for this improved particle-identification system is shown in Fig. 5.

The counter telescope was augmented to incorporate two ΔE detectors (denoted $\Delta E2$ and $\Delta E1$ on Fig. 5) and an E detector. Pulses in these detectors were amplified and fed to a fast-slow coincidence system with a fast-coincidence resolving time of 50 nsec. If the coincidence requirements were met, these three pulses were sent to the particle identifier along with timing pulses. The rejection detector performed the same function as described in the preceding section. The triple-counter identifier produced three identification pulses for each particle and a schematic derivation of these three pulses using the three energy signals ($\Delta E2$, $\Delta E1$, and E) and the relationship $R = \underline{a}E^{1.73}$ is presented in Fig. 6. It can be seen that the three identification signals are proportional to the $\Delta E2$, $\Delta E1$, and ($\Delta E2$ + $\Delta E1$) detector thicknesses, respectively. The Ident. 1 and Ident. 2 pulses

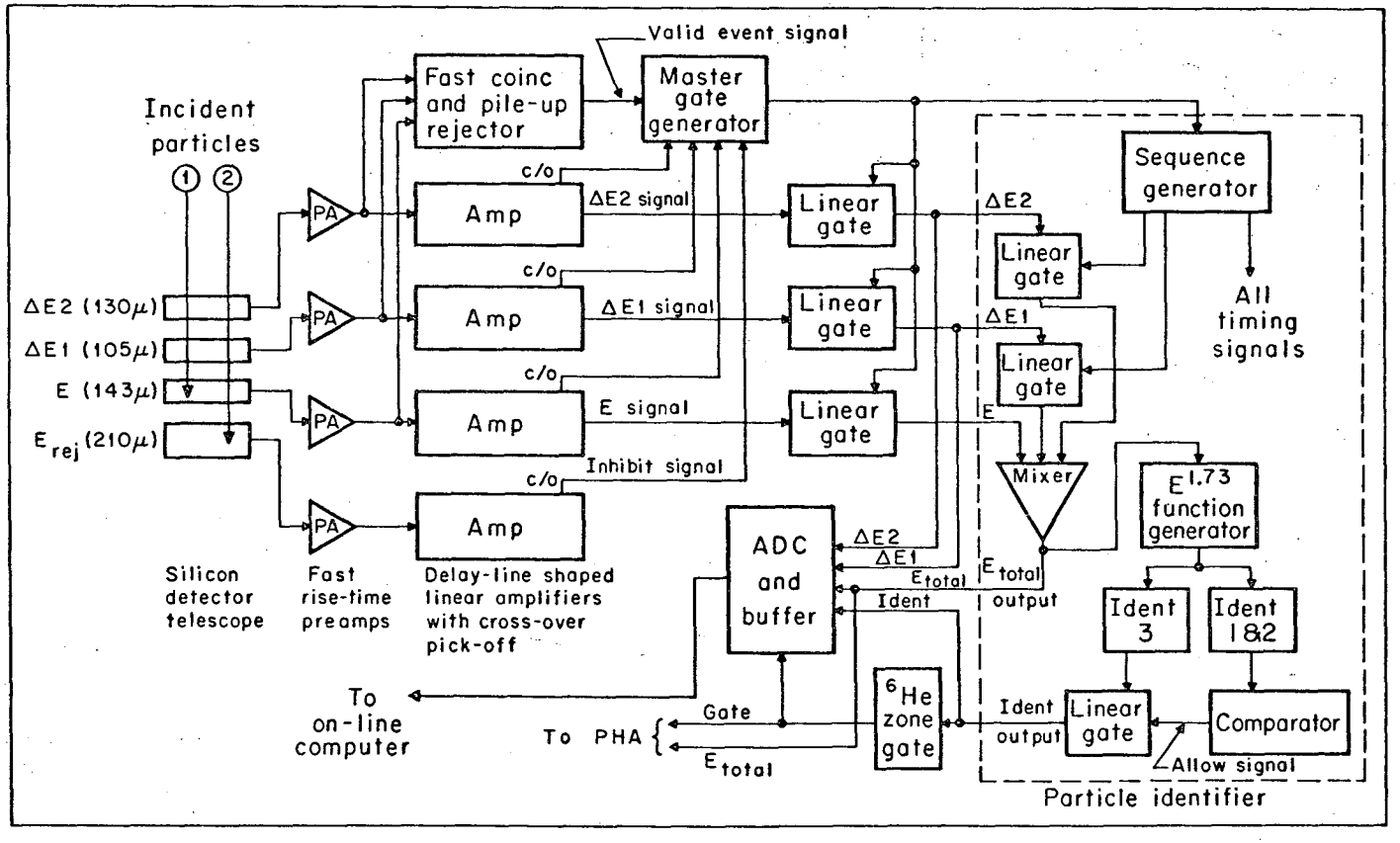

MUB-9482-A

Fig. 5. Schematic diagram of the electronics for the triple-counter particle-identification system.

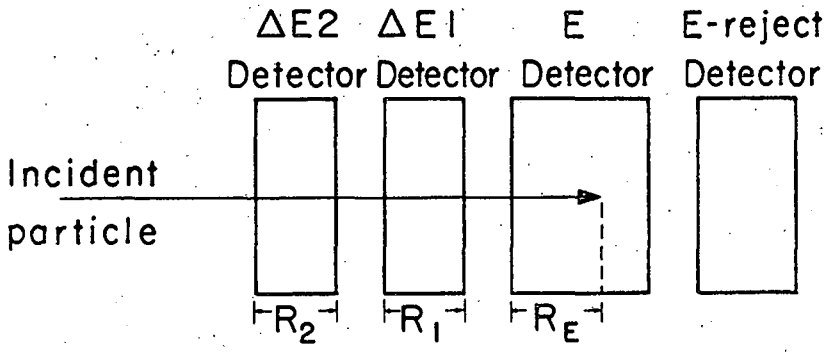

Empirical relationships:

$$\text{Total range } (R_T) = R_2 + R_1 + R_E$$

$$\text{Total energy } (E_T) = \Delta E2 + \Delta E1 + E$$

$$R_T = a\, E_T^{1.73}$$

$$R_E = a\, E^{1.73}$$

Ident. 1:

$$R_1 + R_E = a\,(\Delta E1 + E)^{1.73}$$

$$R_2 = R_T - (R_1 + R_E)$$

$$R_2 = a\,E_T^{1.73} - a\,(\Delta E1 + E)^{1.73}$$

$$\text{Ident. 1} \propto R_2/a = E_T^{1.73} - (\Delta E1 + E)^{1.73}$$

Ident. 2:

$$R_1 = a\,(\Delta E1 + E)^{1.73} - R_E$$

$$R_1 = a\,(\Delta E1 + E)^{1.73} - a\,E^{1.73}$$

$$\text{Ident. 2} \propto R_1/a = (\Delta E1 + E)^{1.73} - E^{1.73}$$

Ident. 3:

$$R_2 + R_1 = R_T - R_E$$

$$R_2 + R_1 = a\,E_T^{1.73} - a\,E^{1.73}$$

$$\text{Ident. 3} \propto (R_2 + R_1)/a = E_T^{1.73} - E^{1.73}$$

MUB-12880

Fig. 6. A schematic derivation of the three identification pulses generated by the triple-counter particle identifier.

(see Figs. 5 and 6) were then compared; if their ratio agreed within preset adjustable limits, a linear gate was opened allowing the third identification pulse (Ident. 3 on Figs. 5 and 6) to emerge as the output of the particle identifier. Since there was only a very small chance that both ΔE signals for a particular event would deviate markedly from normal in the same direction by about the same amount, very few incorrect identifications resulted after the comparison-rejection process. Tests had shown that those particles which lost an abnormal amount of energy in a ΔE detector and were identified improperly (predominantly filling the valleys of the identifier spectrum) could be eliminated while 95-99% of the total counts were retained.

The following data contrast the performance of the standard and the triple-counter identifier systems. First, Fig. 7 shows standard particle-identifier spectra from the two-neutron pick-up reaction $^{12}C(\alpha,{}^{6}He)^{10}C$ at 70 MeV with $d\sigma/d\Omega_{g.s.}$ ~30-40 μb/sr and from the three-neutron pick-up reaction $^{12}C(^{3}He,{}^{6}He)^{9}C$ at 65 MeV with $d\sigma/d\Omega_{g.s.}$ ~1-4 μb/sr. Although a ^{6}He identification peak was resolved in the former experiment, the lower cross section of the latter reaction was insufficient to cause a peak above the general background in this region of the identifier spectrum. Figure 8 is a ^{6}He energy spectrum from the $^{12}C(^{3}He,{}^{6}He)^{9}C$ reaction[7] using the standard particle identifier and showing the presence of a large background. The improvement acquired with a triple-counter particle-identifier system is apparent in Fig. 9, which presents an identifier spectrum from ^{12}C + 65-MeV ^{3}He—note particularly the greatly improved peak-to-valley ratios. Finally, Fig. 10 is a ^{6}He energy spectrum from the $^{12}C(^{3}He,{}^{6}He)^{9}C$ reaction obtained using the triple-counter particle-identification system and showing essentially no background.

Previous experiments had shown that chance coincidences between two particles "simultaneously" traversing the counter telescope were a significant problem in the study of low-yield nuclear reactions (see Refs. 25 and 26) in that some of these coincidences produced identification signals near those of the particles of interest. Even though a 50 nsec fast coincidence was required between the cross-over pickoff

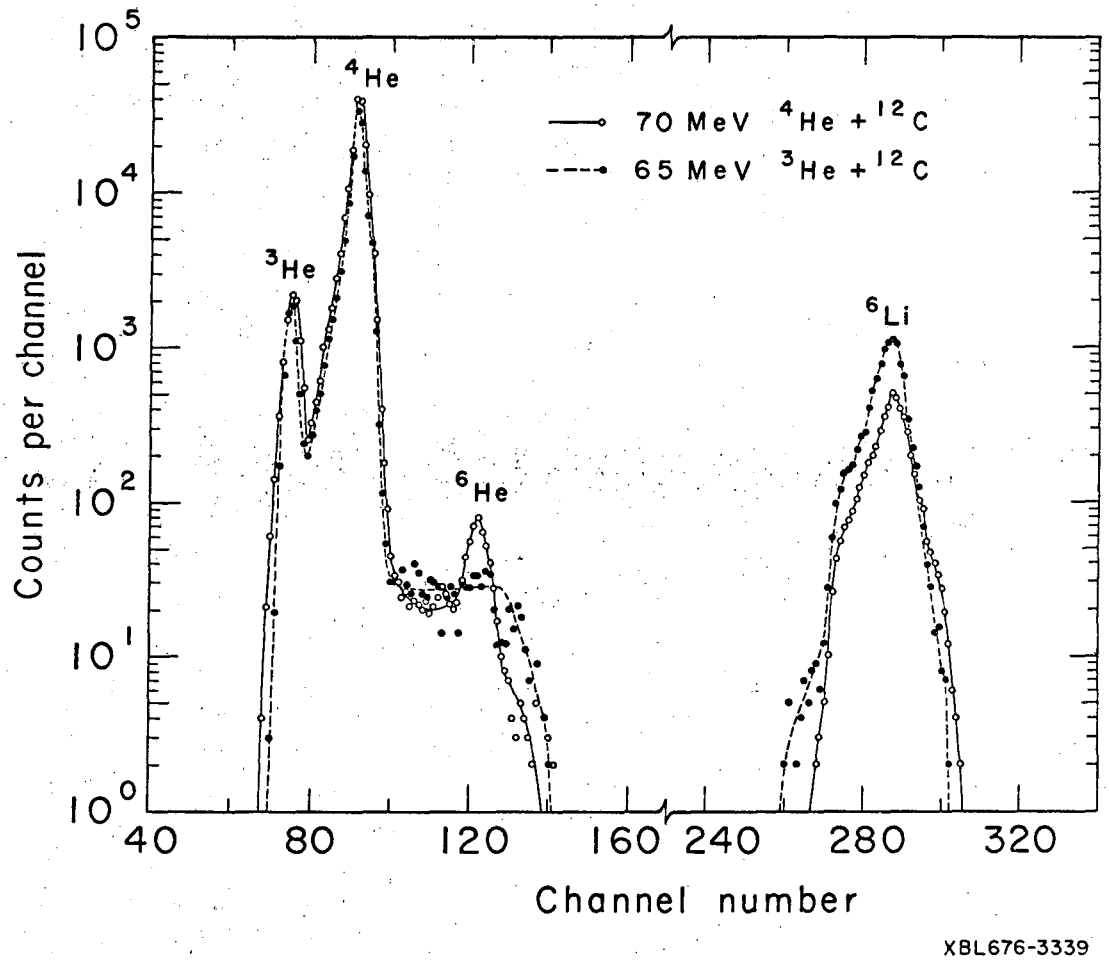

Fig. 7. ^{12}C Standard particle-identifier spectra from the bombardment of a target with 70-MeV ^{4}He ions (open circles) and with 65-MeV ^{3}He ions (filled circles). The ΔE and E detector thicknesses were 8.5 mils and 120 mils, respectively.

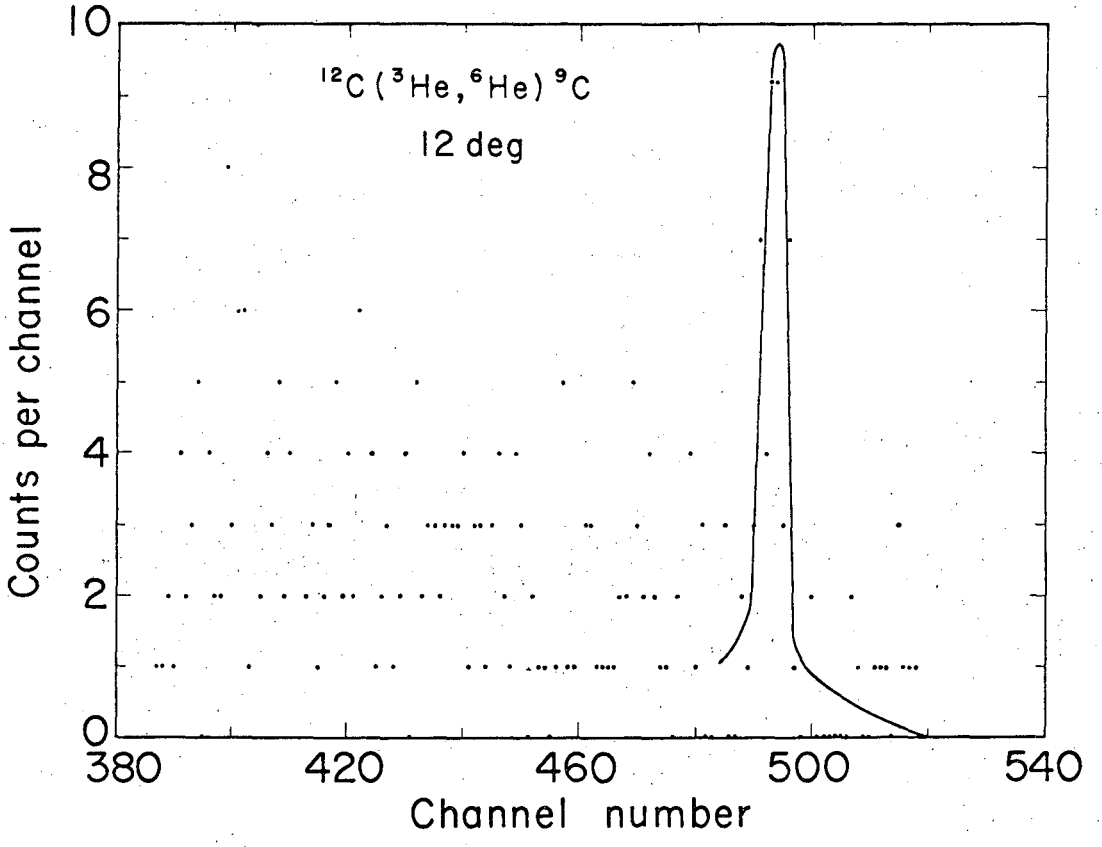

Fig. 8. A ^{6}He energy spectrum from the $^{12}C(^{3}He,^{6}He)^{9}C$ reaction at 65 MeV. This reaction was investigated using the standard particle identifier.

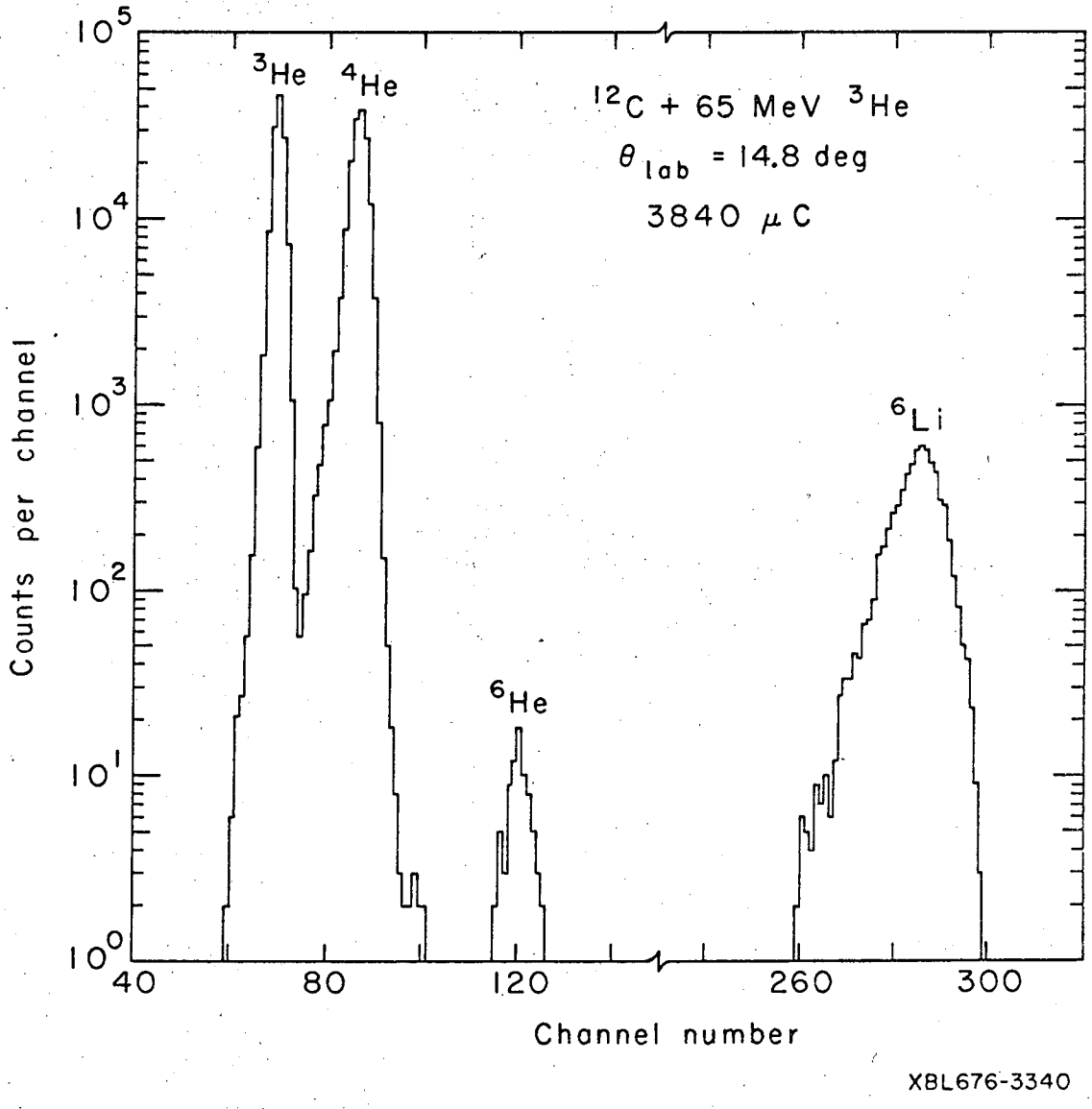

Fig. 9. Triple-counter particle-identifier spectrum from ^{12}C + 65-MeV ^{3}He-particles. The $\Delta E2$, $\Delta E1$, and E detector thicknesses were 5.2 mils, 4.2 mils, and 5.6 mils, respectively.

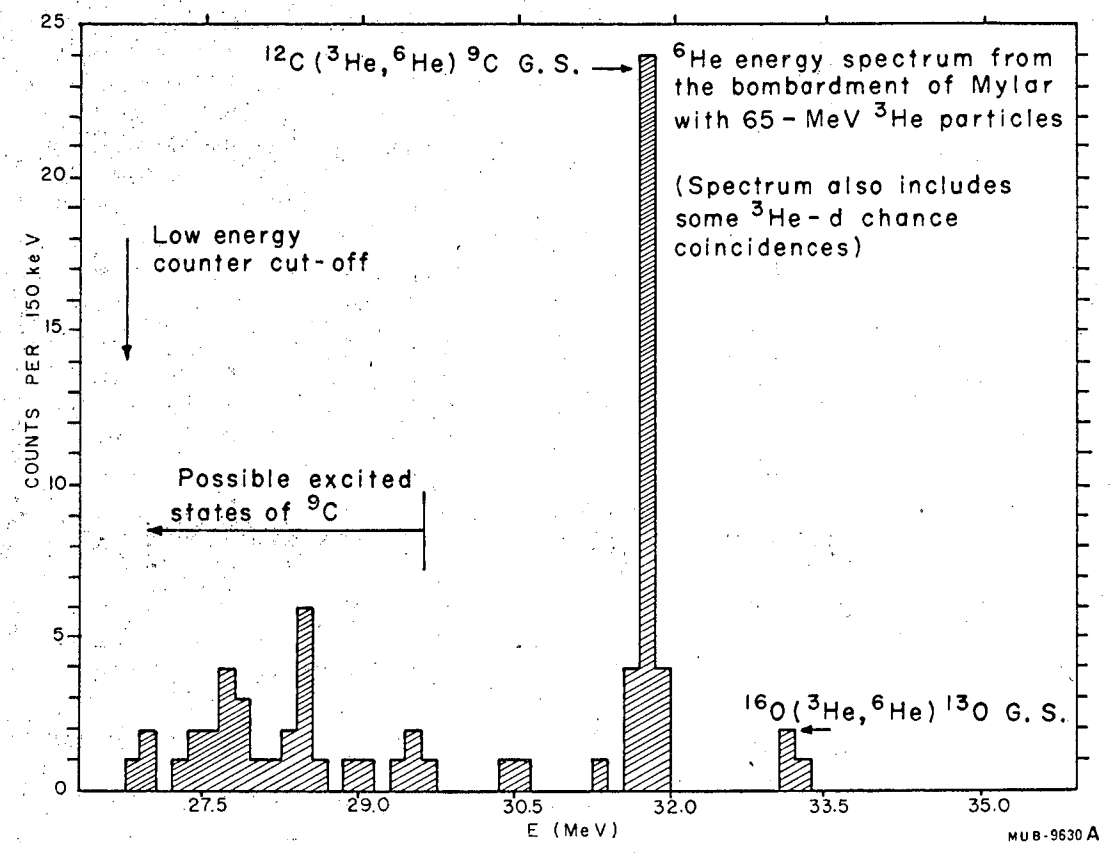

Fig. 10. Energy spectrum of the $^{12}C(^{3}He,^{6}He)^{9}C$ reaction at 65 MeV; the counts due to the $^{16}O(^{3}He,^{6}He)^{13}O$ reaction resulted from the oxygen in the Mylar target. These results were obtained using the triple-counter particle-identification system.

signals from the three detectors, it was found that two light particles of appropriate energies traversing the detector telescope within a time $\Delta t \leq 400$ nsec could satisfy the fast coincidence requirements because the cross-over points of all three (pile-up) energy signals were shifted in the same direction by approximately the same amount. Note Fig. 11(c), which shows a pulser-simulated triple-counter particle-identifier spectrum for all the particle-stable nuclides from ^{3}He to ^{7}Li, while Fig. 11(b) shows the pulser-simulated particle-identifier positions of various ^{3}He + light particle (proton, deuteron, triton, ^{3}He, or ^{4}He) chance coincidences, and Fig. 11(a) shows the same for various ^{4}He + light particle chance coincidences. The different particles shown in Fig. 11 were restricted to the same narrow limits of energy that were allowed experimentally in the (^{3}He,^{6}He) investigations using the particular three-counter telescope shown in Fig. 5. As under our normal experimental conditions, a minimum energy loss of 5 MeV in the E detector was required. The silicon range-energy relations that were necessary for these calculations were similar to those discussed earlier.[12] It is apparent from Fig. 11 that a ^{3}He-d chance coincidence can very nearly simulate a ^{6}He-particle and an α-d chance coincidence can simulate a ^{8}He-particle.

Table I is a list of the calculated energy losses of various particles in the three-counter telescope indicated, assuming no detector dead layers. Energy losses for a ^{6}He-particle and a typical ^{3}He-d chance coincidence with the same total energy are listed in the upper portion of the table; although the ^{3}He-d chance coincidence event would be identified just above the ^{6}He region of the particle-identifier spectrum (see Fig. 11), an analysis of the ΔE2 and ΔE1 energy losses would distinguish this chance coincidence event from a ^{6}He-particle. (See next section for a discussion of this procedure.) Unfortunately, not all ^{3}He-d chance coincidences can be positively distinguished from ^{6}He events, and these non-removable events appear as a residual background in the ^{6}He energy spectra. Also listed in the lower portion of

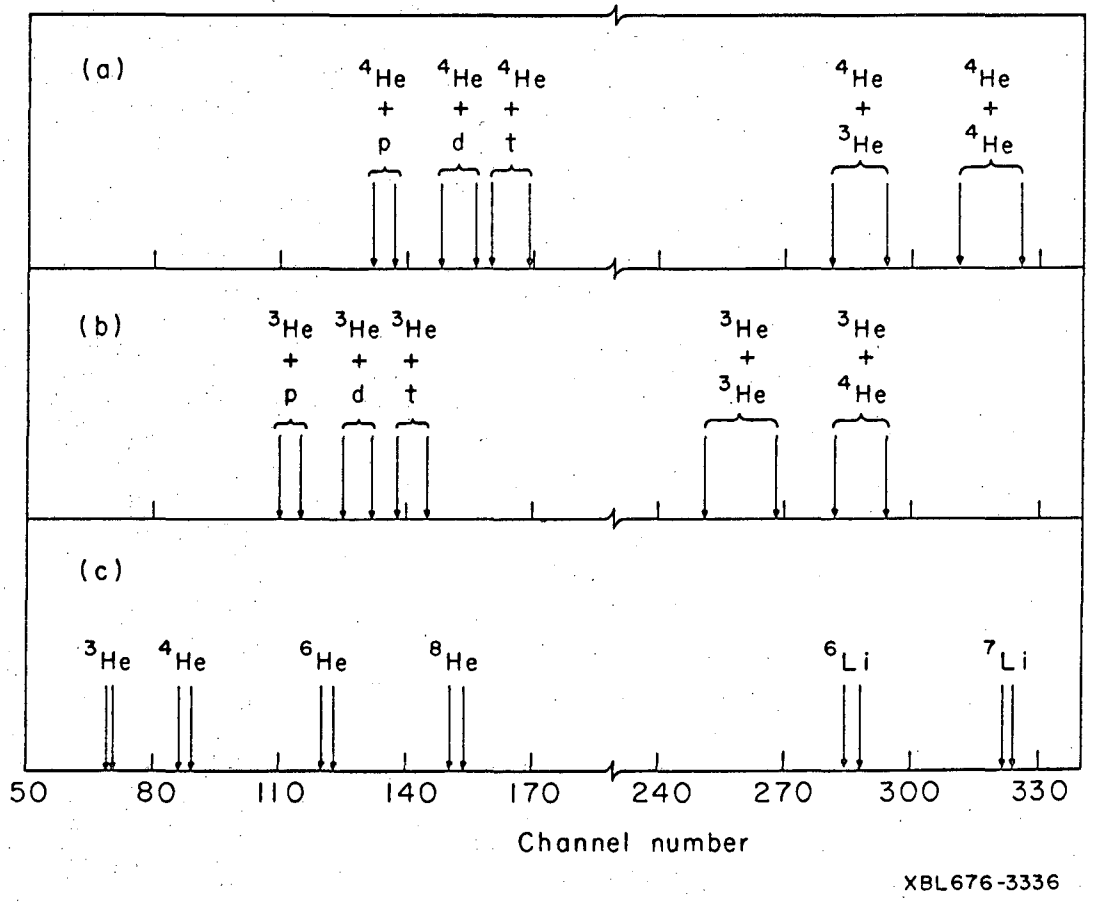

Fig. 11. Pulser-simulated particle-identifier spectra for the triple-counter system using the detector thicknesses shown in Fig. 5; (c) shows the normal positions of the particle-stable nuclei from ^{3}He to ^{7}Li, while (a) and (b) show the positions of ^{4}He + X and ^{3}He + X (X denotes p, d, t, ^{3}He, or ^{4}He) chance coincidences, respectively.

Table I. Energy losses of various particles in a triple-counter telescope.

Particle	E_{total} (MeV)	Energy Losses In Counters (MeV)		
		5.2 mil ΔE2 ctr	4.2 mil ΔE1 ctr	6.5 mil E ctr
^{6}He	29.00	8.27	9.17	11.56
^{3}He	21.25	6.25	7.15	7.85
d	7.75	2.53	2.94	2.28
^{3}He + d (sum)	29.00	8.78	10.09	10.13
^{8}He	35.50	8.67	8.93	17.90
^{4}He	27.50	6.18	6.24	15.08
d	8.00	2.39	2.69	2.92
^{4}He + d (sum)	35.50	8.57	8.93	18.00
^{4}He + d (sum)	35.50	8.66	9.45	17.39

Table I are the energy losses for a ^{8}He-particle and two sets of α-d chance coincidences—all three events having the same total energy. The first α-d chance coincidence has ΔE2 and ΔE1 energy losses such that it could not be distinguished from the ^{8}He-particle (see Fig. 11 and Refs. 25 and 26), whereas the second α-d chance coincidence, for which only the summed energy losses are given, could be distinguished from the ^{8}He-particle by an analysis of the ΔE2 and ΔE1 energy losses.

Two techniques were used to reduce these chance coincidences. First, the pile-up rejector shown schematically in Fig. 5 was designed at this laboratory[24] to decrease the background due to chance coincidences. When coincident pulses occurred on the three input lines to the pile-up rejector, an inspection period of ~800 nsec was started. If any pile-up occurred during this time, the lack of a "valid event" signal from the pile-up rejector prevented the processing of the event by the remainder of the system. Using this pile-up rejector, events which consisted of two particles traversing the counter telescope spaced in time by $\geq$ 47 nsec were rejected—thus restricting all chance coincidence events to those occurring in a single cyclotron beam burst. (For 70-MeV α-particles, the cyclotron oscillator frequency is ~10 Mcs and the cyclotron produces bursts of particles of about 6 nsec duration every 100 nsec.) Second, the ΔE2, ΔE1, E_{total} (E_{total} = ΔE2 + ΔE1 + E), and particle-identifier pulses for each event in any desired region of the identifier spectrum were recorded in an on-line PDP-5 computer via an eight-channel pulse multiplexer and a 4096-channel ADC and were later individually analyzed (see following section) using the known detector thicknesses and range-energy relations in silicon. This procedure both rejected some coincidence events and enabled us to attach a higher degree of reliability to the "good" events. Accurate analysis of these rare events of interest required two further procedures. First, a pulser-stabilized monitor detector independently measured the beam energy variation with time by recording the ^{3}He elastic scattering peak; Fig. 12(a) is a time plot of the ^{3}He beam energy as followed by the monitor detector. Second, the computer stored a pulser-

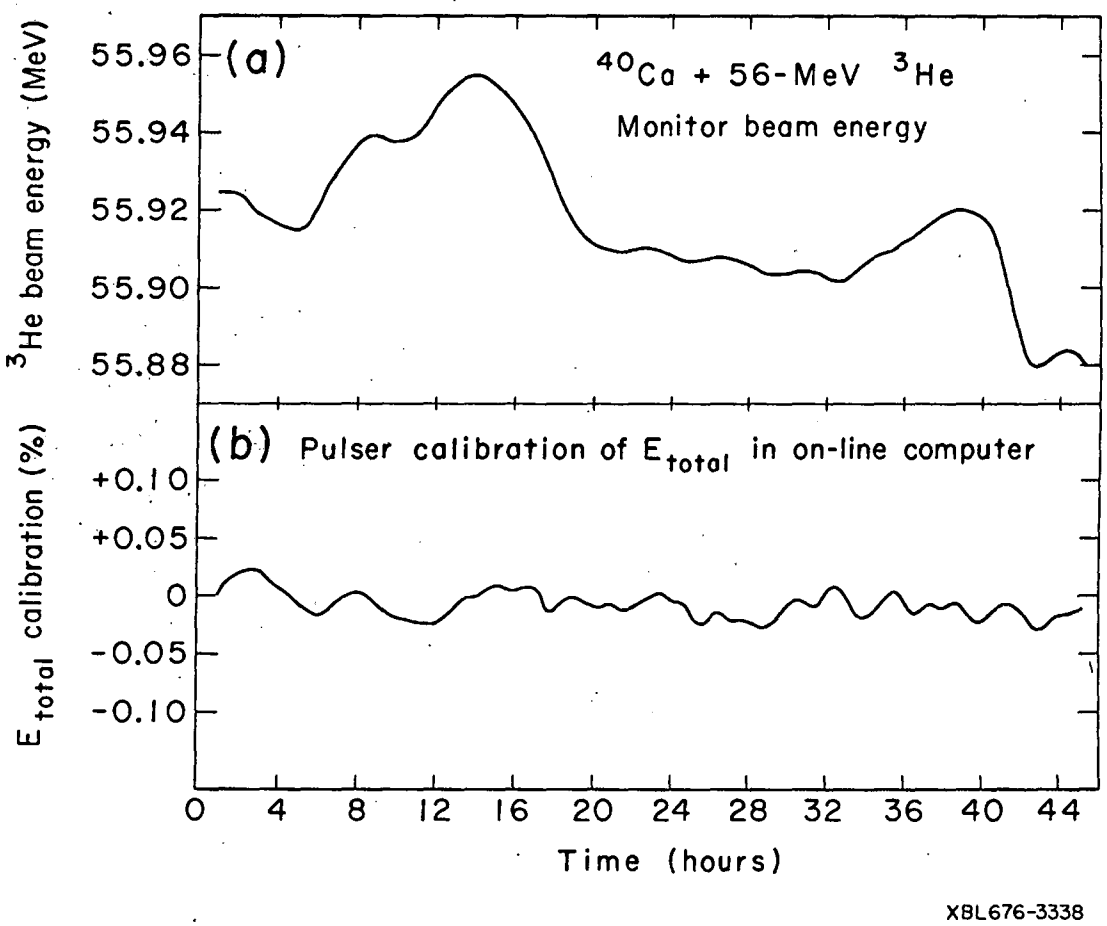

Fig. 12. Time plots of (a) the ^{3}He beam energy as determined by elastic scattering in the monitor detector and (b) the electronic drifts in the E_{total} pulse of one triple-counter ^{6}He detection system during a study of the ^{40}Ca(^{3}He,^{6}He)^{37}Ca reaction.

simulated ^{6}He event every 12 minutes to check the entire system and provide an accurate measure of electronic drifts during the long data-collection times necessary in the (^{3}He, ^{6}He) experiments; Fig. 12(b) shows the electronic stability of the E_{total} pulse from one triple-counter particle-identification system during a 45-hour cyclotron run.

Detector thicknesses in the triple-counter telescopes were selected to provide optimum operation only for the ^{6}He-particles and a few ^{6}Li groups from the (^{3}He, ^{6}Li) reaction, which served as a calibration reaction. Diffused-junction silicon transmission detectors were used (including the rejection detectors) to obtain minimum detector window thicknesses. Each detector was calibrated by comparing a precision pulser[24] with the energy losses of α-particles from a ^{212}Po - ^{212}Bi natural α-source.

F. Data Analysis Procedures For (^{3}He, ^{6}He) Reactions

As an example of our analysis procedures for these low-yield reactions, we will utilize the data from the $^{40}Ca(^{3}He, ^{6}He)^{37}Ca$ experiment since it had a considerably lower cross section than either the $^{16}O(^{3}He, ^{6}He)^{13}O$ or the $^{24}Mg(^{3}He, ^{6}He)^{21}Mg$ reactions. Figure 13 presents a triple-counter particle-identifier spectrum from ^{40}Ca + 56-MeV ^{3}He-particles; the positions of ^{3}He-p, ^{3}He-d, and ^{3}He-^{3}He chance coincidences are indicated on the spectrum. The ^{3}He and ^{4}He peak heights in this spectrum (and in other similar triple-counter particle-identifier spectra) are not representative since over 98% of these particles were rejected either by the rejection detector or by single-channel analyzers which were set to pass only the ^{6}He and ^{6}Li ions of interest (thus recording only ^{3}He-particles between 20.0 and 24.7 MeV and α-particles between 22.3 and 27.8 MeV). Each event in the ^{6}He region of the identifier spectrum (and including the ^{3}He-p and ^{3}He-d chance coincidence regions) was routed to the on-line computer where its $\Delta E2$, $\Delta E1$, E_{total} and particle-identifier signals were stored on magnetic tape.

In order to discriminate between good and bad events, a plot of the $\Delta E2$ and $\Delta E1$ energy losses versus E_{total} for each event in the

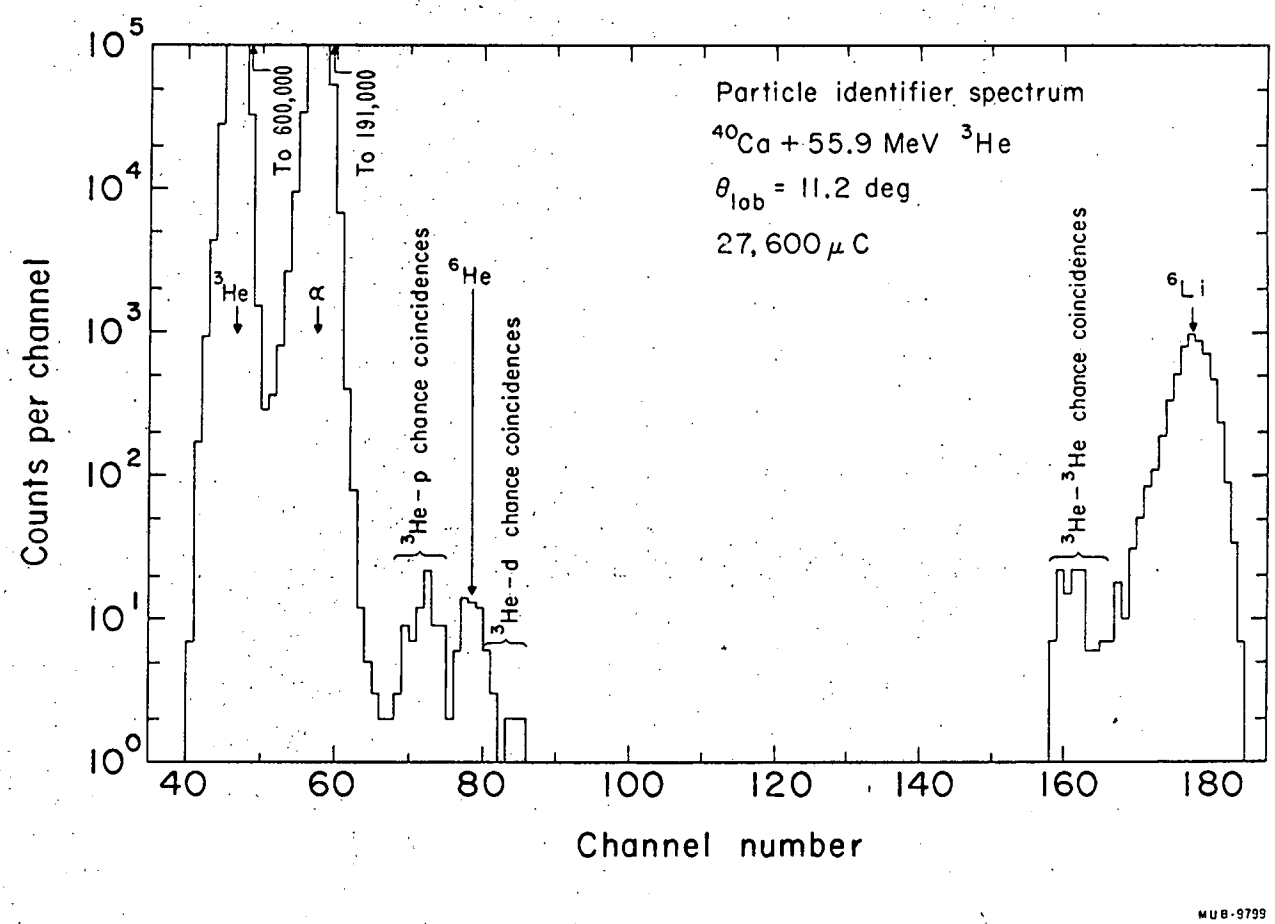

Fig. 13. Triple-counter particle-identifier spectrum from 55.9-MeV ^{3}He ions incident on a ^{40}Ca target.

^{6}He region of the identifier spectrum was made; such a plot for all "^{6}He" events observed in the System Two counter telescope during the ^{40}Ca(^{3}He,^{6}He)^{37}Ca experiment is shown in Fig. 14. Events in which the ΔE2 and/or the ΔE1 energy loss deviated more than ±5% from the smooth curves, which were calculated from the average detector thicknesses, were rejected (these are the circled events and they amount to about 20% of all the events) and were attributed primarily to chance coincidences. Some residual background due to non-rejectable coincidences plus other rare events remains. The peak near E_{total} channel 2160 corresponds to the ^{40}Ca(^{3}He,^{6}He)^{37}Ca ground-state transition and the peak near channel 2040 corresponds to a transition to an excited state of ^{37}Ca; some of the data in Fig. 14 were obtained at a scattering angle of 14.1 deg and some at a scattering angle of 11.4 deg so that these two peaks are really sharper than they appear to be. All of the valid ^{6}He events were then individually corrected for beam energy and electronic drifts (see Fig. 12) as well as for target and detector dead layer energy losses—the energy of each event was determined from the ^{6}He energy scale discussed below. Data from the ^{40}Ca(^{3}He,^{6}Li)^{37}K calibration reaction (Q = -9.205 MeV)[27] was collected at intervals throughout the run to observe whether any energy shifts occurred arising from radiation damage to the counters.

The problem of establishing an absolute beam energy was treated as follows: calibration curves for ^{6}He and ^{6}Li ions were obtained by observing highly negative Q-value (α,^{6}He) and (α,^{6}Li) reactions on suitable targets at scattering angles and beam energies chosen so that the ground-state groups stopped in the E detector. For the ^{21}Mg and ^{37}Ca experiments the calibration target was ^{12}C, and the ^{12}C(α,^{6}He)^{10}C (Q = -30.831 MeV) and ^{12}C(α,^{6}Li)^{10}B (Q = -23.716 MeV) reactions were studied at an α-particle beam energy of 71 MeV to provide ^{6}He and ^{6}Li particles of the desired energies. Since each individual detector was previously energy calibrated by comparing a precision pulser with the energy losses of α-particles from a ^{212}Po - ^{212}Bi natural α-source (the α-particle groups used for the detector calibrations had energies of 6.051, 6.090, and 8.785 MeV[28]), an absolute α-particle beam energy

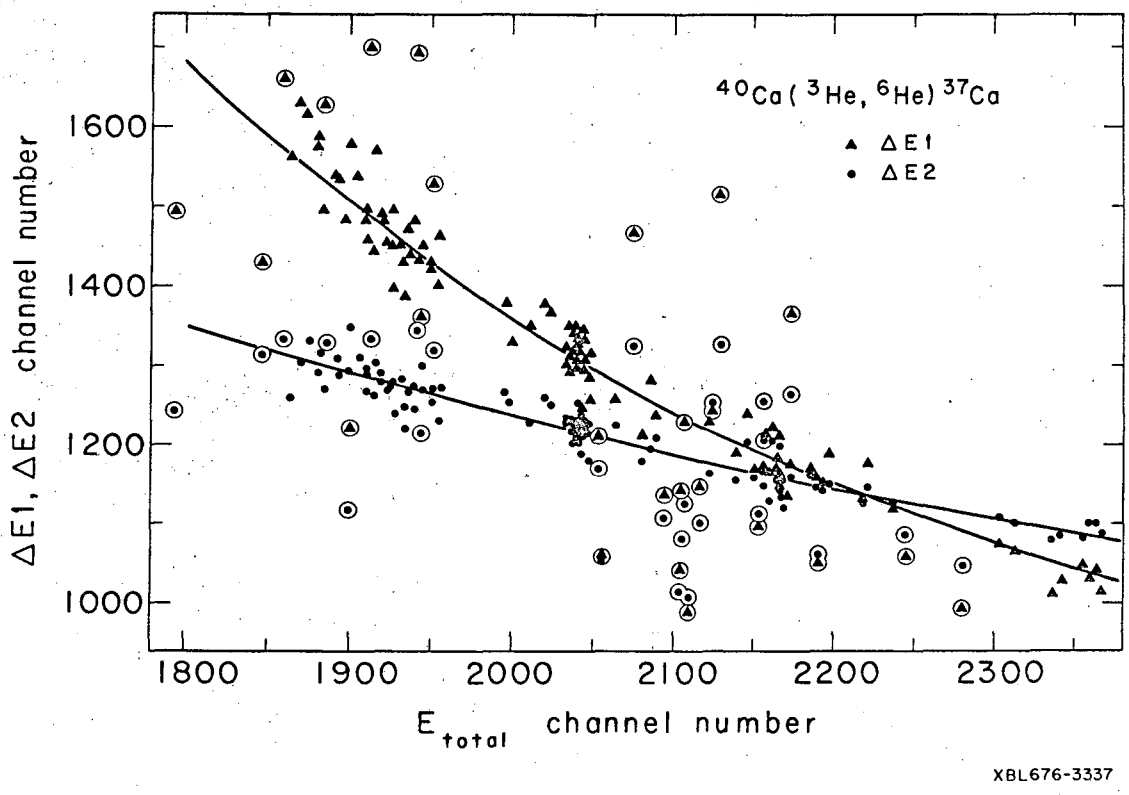

Fig. 14. Plots of ΔE2 and ΔE1 versus E_{total} for the events in the ^{6}He region of the particle-identifier spectrum during the $^{40}Ca(^{3}He,^{6}He)^{37}Ca$ experiment.

of 71.0 MeV was established from these calibrations and the known Q-value and kinematic relations, after energy losses in the detector dead layers and in the target itself were taken into account. (Since stopping ^{6}He-particles possessed energies of ~30 MeV and ^{6}Li-particles ~45 MeV and since these energies were distributed among the three counters in the counter telescope, the (α,^{6}He) and (α,^{6}Li) calibrations were such that minor extrapolations of the previously established α-source energy scale were required for the ^{6}He-particles and reasonable ones for the ^{6}Li-particles.) This α-particle beam energy agreed within 0.5% with that obtained from range-energy measurements in aluminum. The incident beam was then changed to ^{3}He-particles at the appropriate energy (approximately 56 MeV). This beam energy was again measured via aluminum range-energy measurements, but, more importantly, its energy was also determined from the ^{6}Li-particles from a known Q-value calibration reaction (here ^{40}Ca(^{3}He,^{6}Li)^{37}K, see Fig. 15) to be 55.9_2 MeV—this was again obtained from the earlier α-source calibration and it agreed with the range-energy measurements to 0.6%. This is equivalent to forcing the ^{6}Li ions from the (^{3}He,^{6}Li) reaction to be on the same energy scale as those from the earlier (α,^{6}Li) reaction, so that the ^{6}He ions from the (^{3}He,^{6}He) reaction should be on the (α,^{6}He) line established earlier. Using this procedure, an error of 1 MeV in the ^{4}He beam energy would make a difference of only about 40 keV in the ^{37}Ca mass.

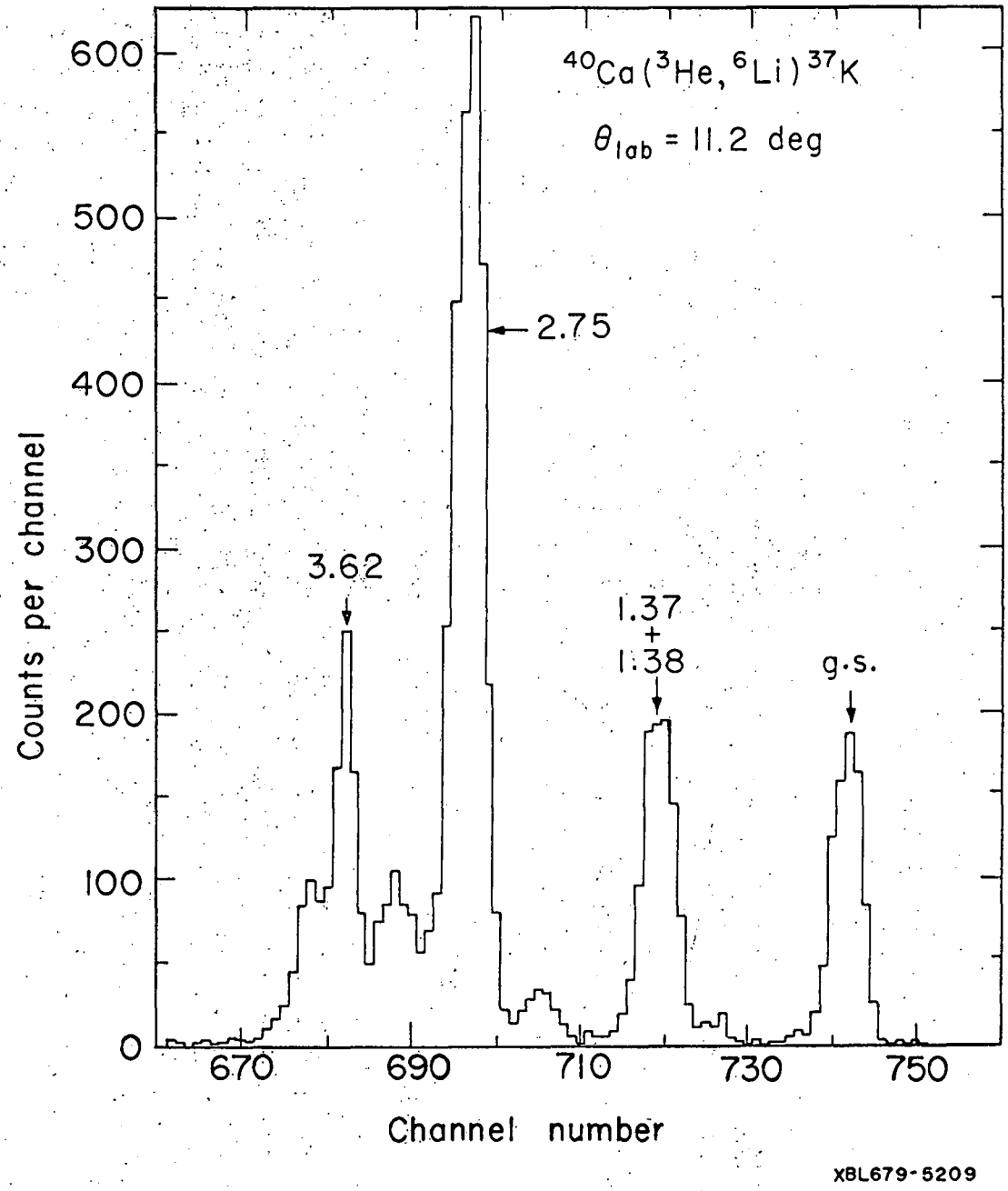

Fig. 15. Energy spectrum of the $^{40}Ca(^{3}He,^{6}Li)^{37}K$ reaction at 55.9 MeV.

IV. RESULTS AND DISCUSSION

A. Mass Measurements via (^{3}He, ^{6}He) Reactions

1. Mass of ^{13}O

The mass of ^{13}O, which is the $T_z = -3/2$ member of the mass 13 isospin quartet, was determined via the ^{16}O(^{3}He, ^{6}He)^{13}O reaction at 65.3 MeV,[23] utilizing the double-counter particle identifier. A ^{6}He-^{6}Li energy scale had been established earlier by studying the ^{15}N(α, ^{6}He)^{13}N (Q = -20.418 MeV) and ^{15}N(α, ^{6}Li)^{13}C (Q = -14.688 MeV) reactions at 64.5 MeV. The ^{16}O(^{3}He, ^{6}Li)^{13}N (Q = -9.239 MeV) reaction was studied simultaneously with the ^{16}O(^{3}He, ^{6}He)^{13}O reaction, and typical energy spectra from these two reactions are presented in Fig. 16. Although there is a fairly high background, one can clearly see the sharp ^{13}O ground-state transition in the ^{6}He energy spectrum. An average differential cross section for measurements at four angles between 10 and 20 deg (lab) was only 1 μb/sr. The average Q-value for the ^{16}O(^{3}He, ^{6}He)^{13}O ground-state transition was determined to be -30.51 ±0.07 MeV, which corresponds to an ^{13}O mass excess of 23.11±0.07 MeV (^{12}C = 0). Thus ^{13}O is stable with respect to proton emission by 1.52±0.07 MeV. The mass of ^{13}O completed the mass 13 isospin quartet since the lowest T = 3/2 levels in ^{13}N ($T_z = -1/2$) and ^{13}C ($T_z = +1/2$) had already been established[23] and the mass of ^{13}B ($T_z = +3/2$) was known.[27] Energy level diagrams for the members of the mass 13 isospin quartet are shown in Fig. 17, in which, for clarity, ground-state energies of mirror nuclei have been equated and many of the energy levels of ^{13}N and ^{13}C below the first T = 3/2 level have been deleted. The four members of the completed ground-state T = 3/2 quartet are shown and are connected by dashed lines. A tabulation and discussion of the results of this and the two following completed isospin quartets will be found in Sec. V.

2. Mass of ^{21}Mg

The mass of ^{21}Mg, which is the $T_z = -3/2$ member of the mass 21 isospin quartet, was determined by the ^{24}Mg(^{3}He, ^{6}He)^{21}Mg reaction

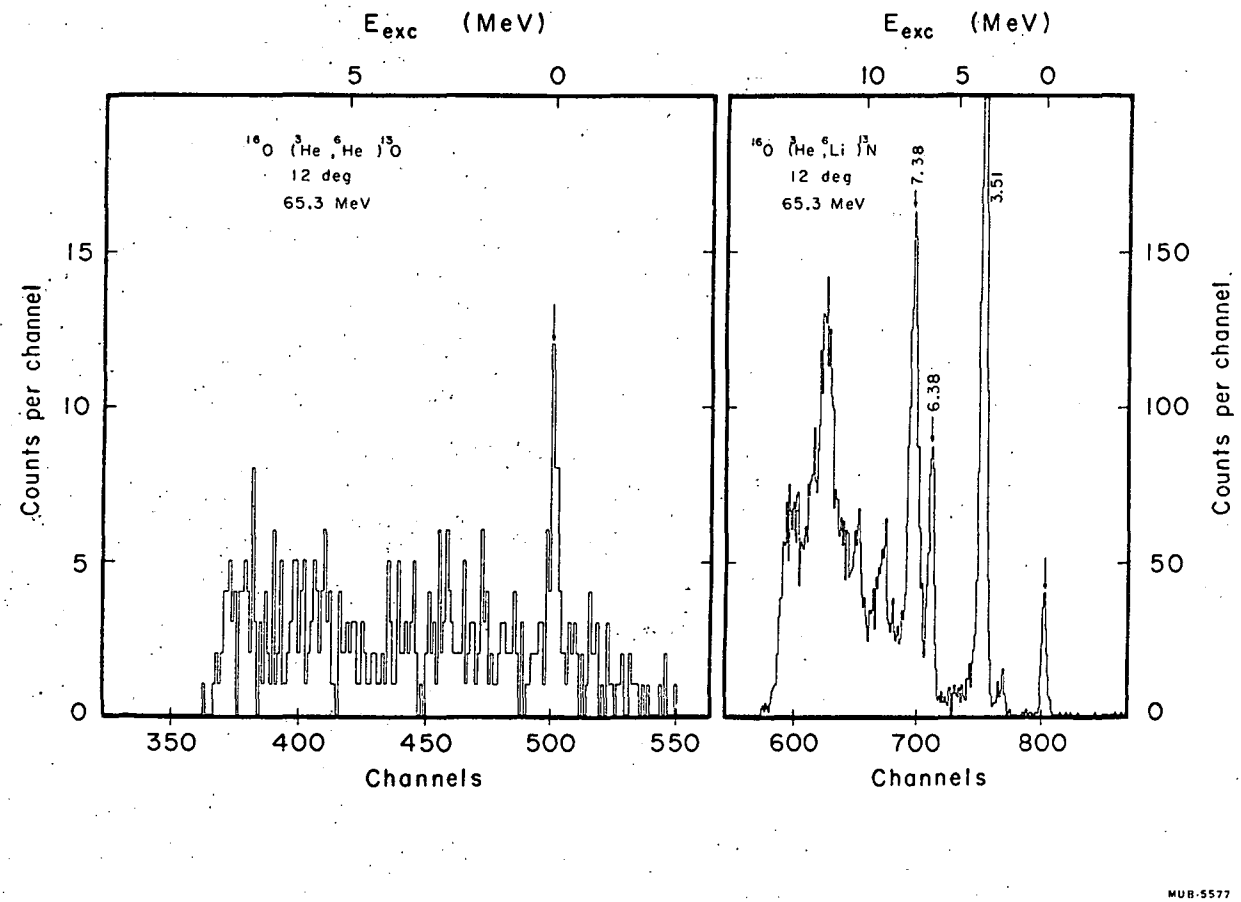

Fig. 16. Energy spectra for the $^{16}O(^{3}He,^{6}He)^{13}O$ and $^{16}O(^{3}He,^{6}Li)^{13}N$ reactions at 12 deg and 65.3 MeV.

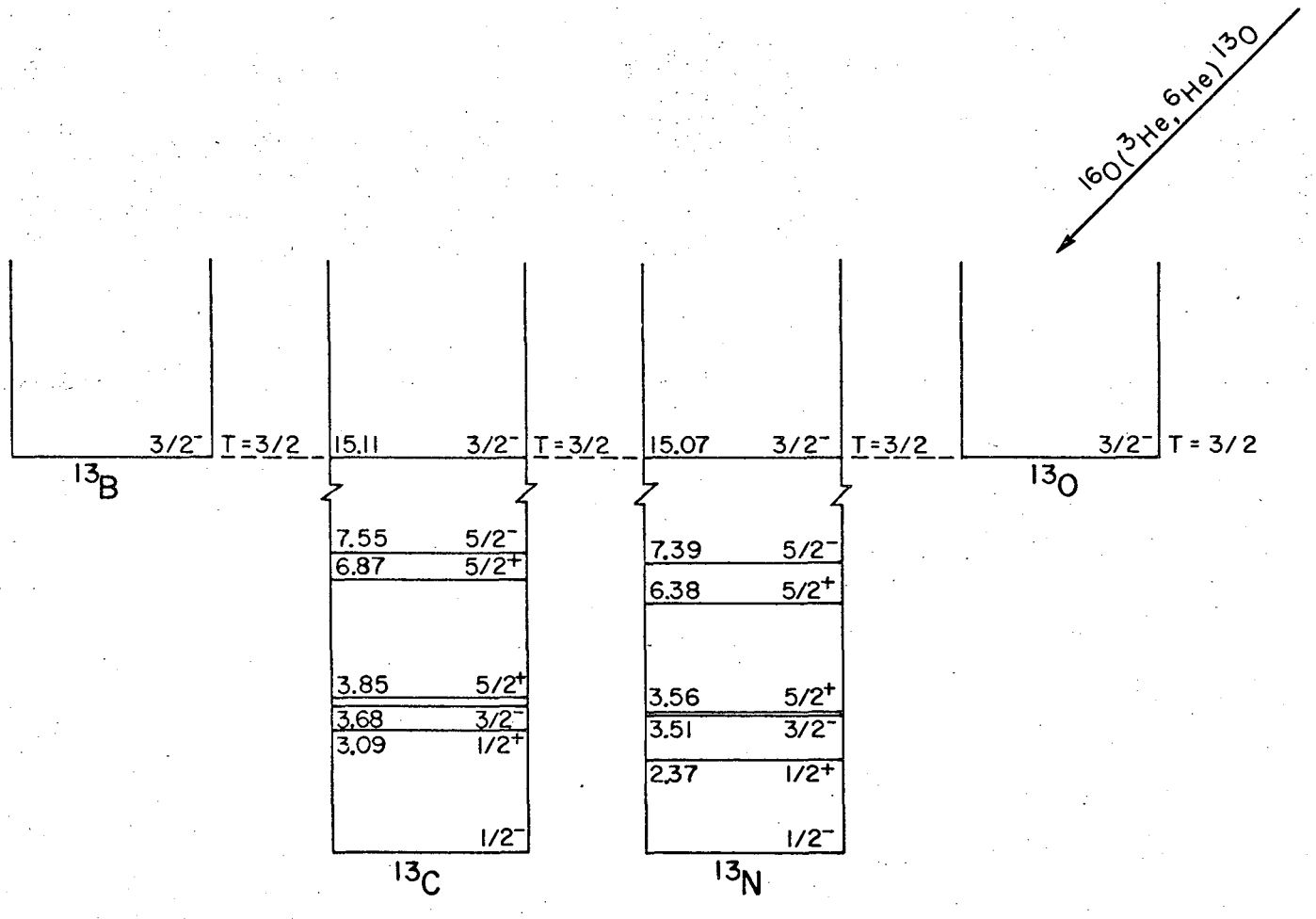

XBL678-5168

Fig. 17. Energy level diagrams for the members of the mass 13 isospin quartet showing the positions of the lowest T = 3/2 levels in each nucleus.

at 55.9 MeV utilizing the triple-counter particle identifier , and Fig. 18 shows an identifier spectrum obtained during this experiment. Figure 19 is an energy spectrum from the $^{24}Mg(^{3}He,^{6}Li)^{21}Na$ reaction (Q = -10.905 MeV), which was recorded simultaneously and used as a calibration reaction. Two independent ^{6}He energy spectra from the $^{24}Mg(^{3}He,^{6}He)^{21}Mg$ reaction are shown in Fig. 20—these spectra represent a 12-hour run at a beam intensity of 400 nA. Each event in both spectra was corrected for beam energy variations, electronic drifts (see Fig. 12 and Sec. III F for a discussion of these procedures), and for energy losses in the target and detector dead layers. Each block in Fig. 20 represents a single event and the block width was chosen to be 100 keV. There appear to be five peaks common to the two spectra which correspond to the ground state and four excited states of ^{21}Mg. The average differential cross section for the ^{21}Mg ground-state transition at 14.1 deg (lab) was 0.84 μb/sr and the average Q-value was determined to be -27.22±0.12 MeV, which corresponds to a ^{21}Mg mass excess of 10.62±0.12 MeV (^{12}C = 0); therefore ^{21}Mg is stable to proton emission by 3.65±0.12 MeV. Average excitations of the observed ^{21}Mg excited levels were 0.22 ±0.03, 1.27±0.06, 1.62±0.04, and 1.89±0.04 MeV; these are consistent with the known[29] level structure of the T_z = +3/2 nucleus ^{21}F. It is interesting to note that ^{21}Mg and ^{37}Ca (presented below) are the first two T_z = -3/2 nuclei in which excited levels have been experimentally observed.

3. Mass of ^{37}Ca

The mass of ^{37}Ca (T_z = -3/2) was determined via the $^{40}Ca(^{3}He,^{6}He)^{37}Ca$ reaction at 55.9 MeV. (Refer back to Fig. 13 for a triple-counter particle-identifier spectrum from this experiment.) Corrected ^{6}He energy spectra from two independent observations of this reaction are shown in Fig. 21—a 45-hour run at a beam intensity of 400 nA was required to obtain these data (higher ^{3}He beam intensities were available but were not used because of the chance coincidence problem in the ^{6}He spectra). Each block in the ^{6}He spectra represents a single event and the block width is 100 keV. Although two angles were observed

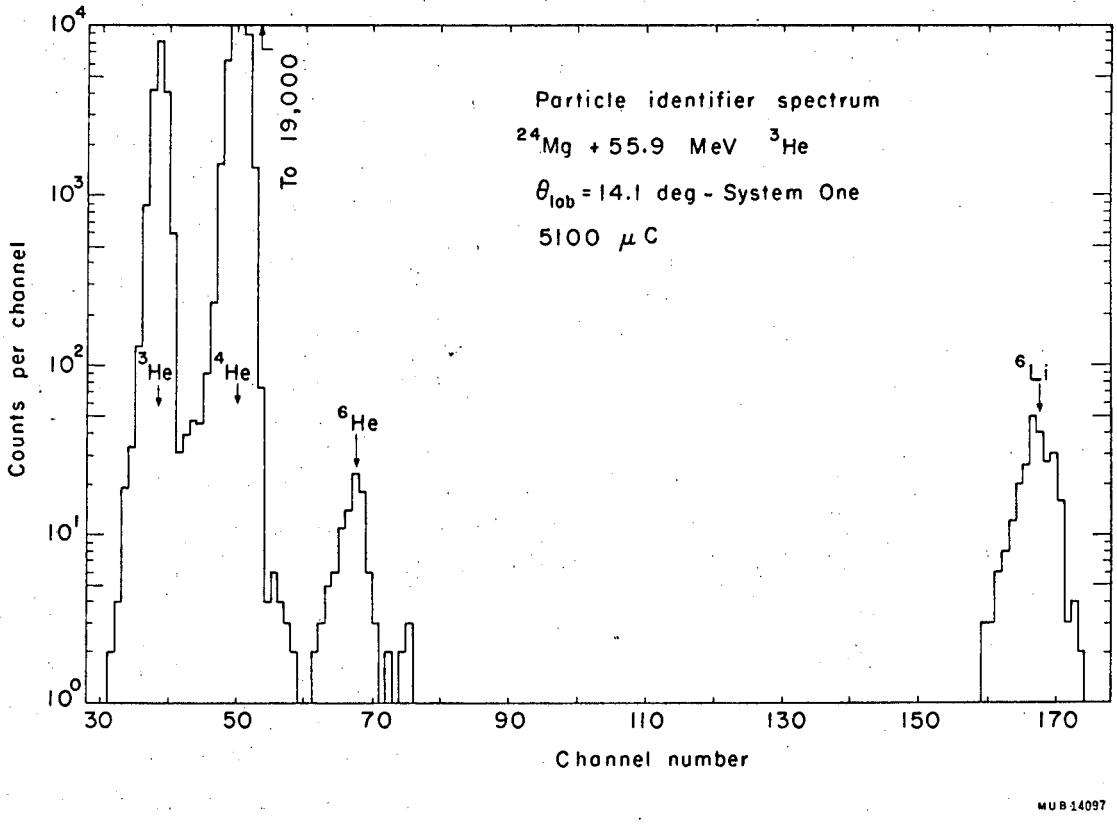

Fig. 18. Triple-counter particle-identifier spectrum resulting from the bombardment of ^{24}Mg with 55.9-MeV ^{3}He ions.

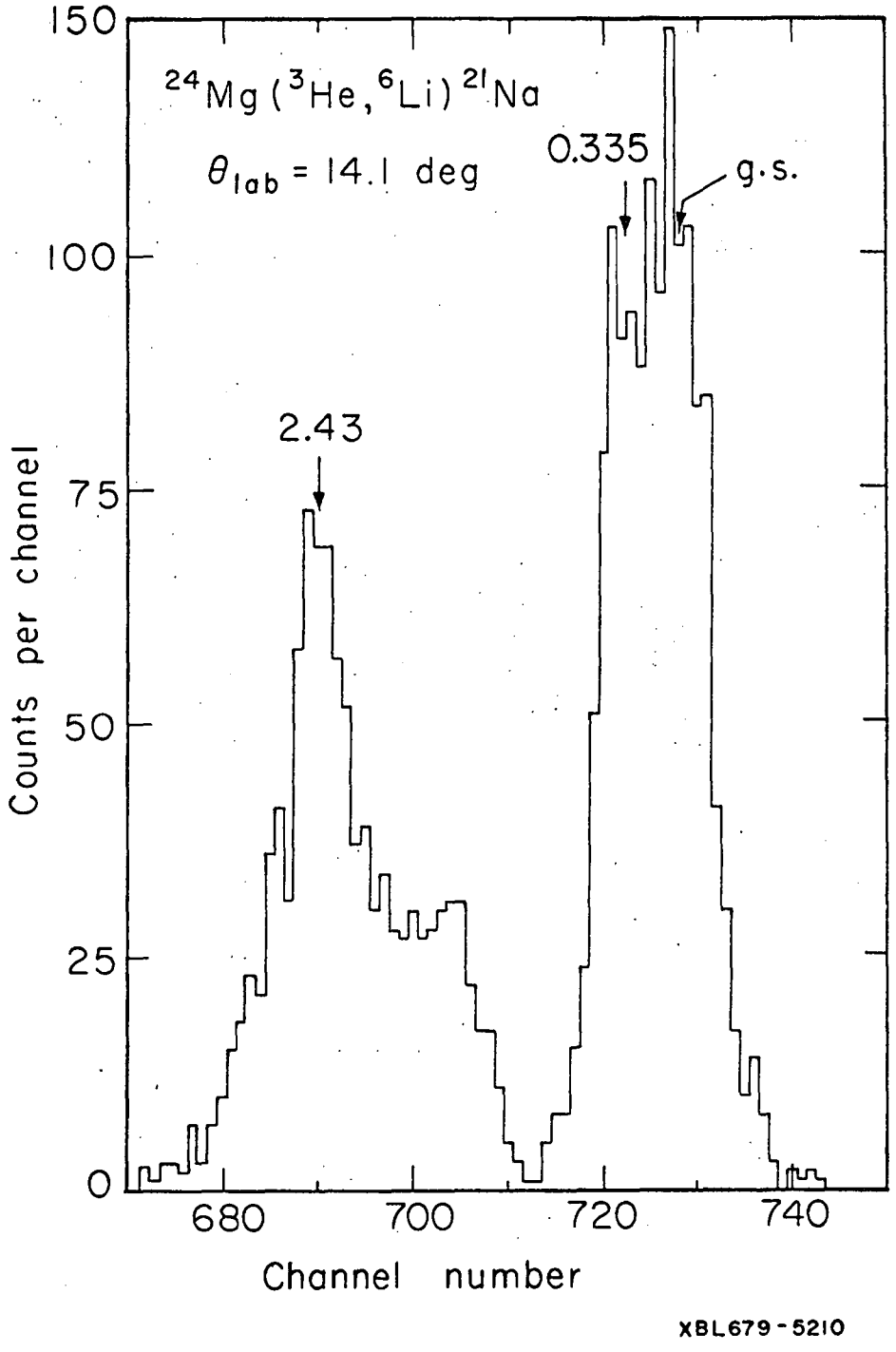

Fig. 19. Energy spectrum of the ^{24}Mg(^{3}He,^{6}Li)^{21}Na reaction at 55.9 MeV.

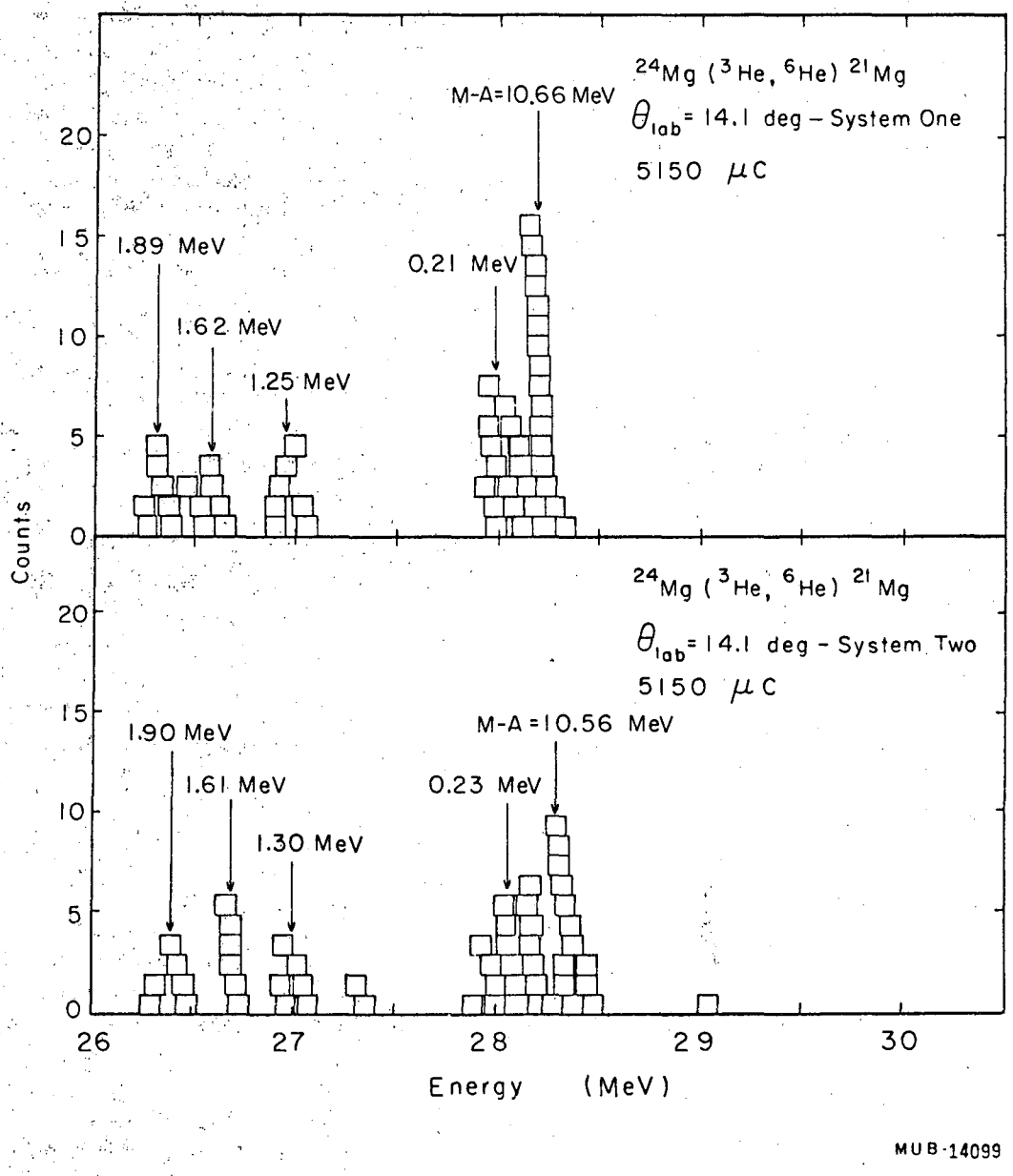

Fig. 20. Two independent ^{6}He energy spectra from the ^{24}Mg(^{3}He,^{6}He)^{21}Mg reaction at 55.9 MeV and a scattering angle of 14.1 deg. Each block represents one count and the block width is 100 keV.

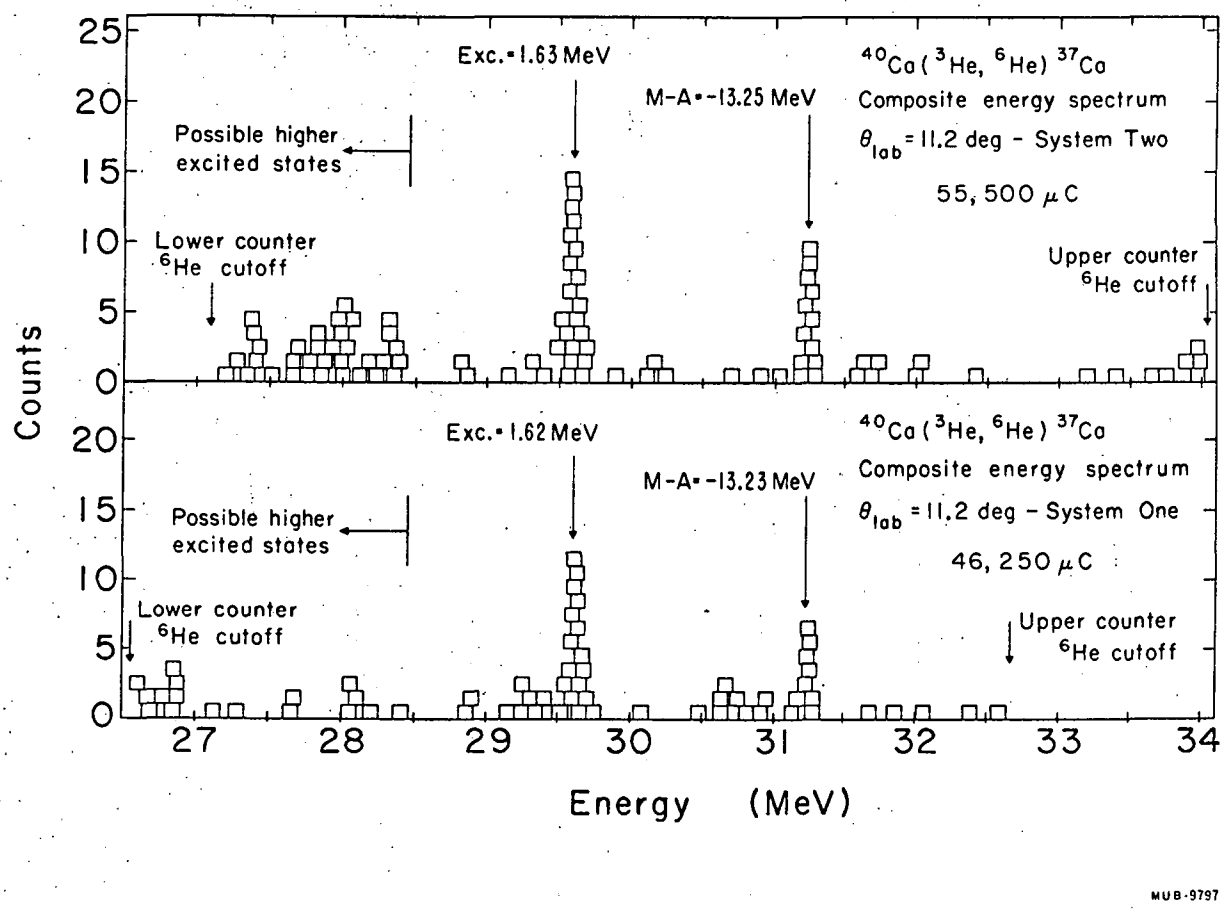

Fig. 21. Two independent ^{6}He energy spectra from the ^{40}Ca(^{3}He, ^{6}He)^{37}Ca reaction at 55.9 MeV; the data from both systems were kinematically corrected to 11.2 deg. Each block is one count and the block width is 100 keV.

in one system and three angles in the other system, all the data have been kinematically corrected to 11.2 deg. Each ^{6}He spectrum contains two sharp states which correspond to the ground and first excited states of ^{37}Ca. The average cross section for the ^{37}Ca ground-state transition at 11.2 deg (lab) was 0.175 μb/sr and the Q-value was determined to be -24.27±0.05 MeV, which corresponds to a ^{37}Ca mass excess of -13.24±0.05 MeV (^{12}C = 0). Hence ^{37}Ca is stable to proton emission by 3.2±0.2 MeV (the mass excess of ^{36}K is not known very well, but the value calculated in Ref. 30 is probably good to ±0.2 MeV). The first excited state of ^{37}Ca appears at an excitation energy of 1.62±0.03 MeV, which is consistent with the known first excited state of the T_z = +3/2 nucleus ^{37}Cl at 1.72 MeV.[31]

Table II presents the forward angle center-of-mass differential cross sections for the four (^{3}He,^{6}He) reactions that have been utilized at this laboratory[7,23] for mass determinations of T_z = -3/2 nuclides. As can be noted from this table, there appears to be a marked decrease in cross section with increasing mass number A. Unfortunately, the general behavior of these (^{3}He,^{6}He) cross sections with angle and with bombarding energy has not been determined, so that this apparent pattern could easily be a property of our experimental conditions. To further characterize the mechanism of the (^{3}He,^{6}He) reaction, an angular distribution of the ^{16}O(^{3}He,^{6}He)^{13}O reaction was obtained and the results are presented in Sec. IV C.

B. Location of Low-Lying T = 3/2 Levels In T_z = +1/2 And -1/2 Nuclei

In order to completely characterize the mass 21 and mass 37 isospin quartets, it was necessary to perform various one- and two-nucleon transfer reactions to locate low-lying T = 3/2 levels in the T_z = +1/2 (^{21}Ne and ^{37}Ar) and -1/2 (^{21}Na and ^{37}K) members of these two quartets—the results of these investigations are presented below.

1. T = 3/2 States in ^{21}Ne and ^{21}Na

The ^{22}Ne(d,t)^{21}Ne and ^{22}Ne(d,^{3}He)^{21}F reactions at 39.6 MeV were

Table II. Forward angle differential cross sections for (^{3}He, ^{6}He) reactions.

Reaction	Bombarding Energy (MeV)	c.m. (deg)	$d\sigma/d\Omega_{c.m.}$ (μb/sr)
^{12}C(^{3}He, ^{6}He)^{9}C g.s.	65.5	15.8	1.6 ± 0.4
^{16}O(^{3}He, ^{6}He)^{13}O g.s.	65.3	15.3	0.76 ± 0.12
^{24}Mg(^{3}He, ^{6}He)^{21}Mg g.s.	55.9	18.0	0.53 ± 0.12
^{40}Ca(^{3}He, ^{6}He)^{37}Ca g.s.	55.9	12.9	0.13 ± 0.03

studied simultaneously to characterize the T = 3/2 states in ^{21}Ne. Triton and ^{3}He energy spectra from these reactions are shown in Fig. 22; energy resolutions (FWHM) were 160 keV for tritons and 182 keV for ^{3}He. The lowest T = 3/2 level in ^{21}Ne was expected to lie near 8.9 MeV excitation since its analogue level in the mirror nucleus ^{21}Na was observed at 8.90±0.04 MeV excitation.[32] Three sharp states at 8.92±0.025, 9.21±0.04, and 10.04±0.03 MeV were observed in the ^{22}Ne(d,t)^{21}Ne spectra; they are indicated as T = 3/2 levels in Fig. 22 and are the presumed analogues of the ^{21}F ground, 0.28- and 1.10-MeV levels, respectively.

Angular distributions of the ^{22}Ne(d,t)^{21}Ne transitions to the ground state ($3/2^{+}$), 0.35-MeV ($5/2^{+}$), and 8.92-MeV levels, together with the distribution of the ^{22}Ne(d,^{3}He)^{21}F ground-state ($5/2^{+}$)[33] transition, are shown in Fig. 23. All these transitions are expected to involve L = 2 angular momentum transfers. The abscissa in Figs. 23-25 is the dimensionless quantity QR, where Q is the center-of-mass linear momentum transfer and R is the radius of interaction calculated from the formula $R(\text{fermis}) = 1.5(A_{\text{target}})^{1/3} + 1.2$ for incident deuterons. The error bars on the data are based on counting statistics only and the absolute cross sections are expected to be accurate to ±10%. It is of particular interest to compare the ^{22}Ne(d,^{3}He)^{21}F ground-state transition with the ^{22}Ne(d,t)^{21}Ne* 8.92-MeV transition since these two states are expected to be analogues. Assuming the charge independence of nuclear forces, transitions populating these analogue states proceed from identical initial to identical final states and hence should possess identical cross sections after phase space and isospin coupling corrections are made. These corrections involve (compare Bayman[34]);

$$\frac{\sigma(d,t)}{\sigma(d,{}^{3}\text{He})} = \frac{1}{2T_a + 1} \times \frac{k(t)}{k({}^{3}\text{He})} ;$$

where T_a is the isobaric spin of the target nucleus and k(t), k(^{3}He) are the center-of-mass momenta of the particles. Noting Fig. 23 one

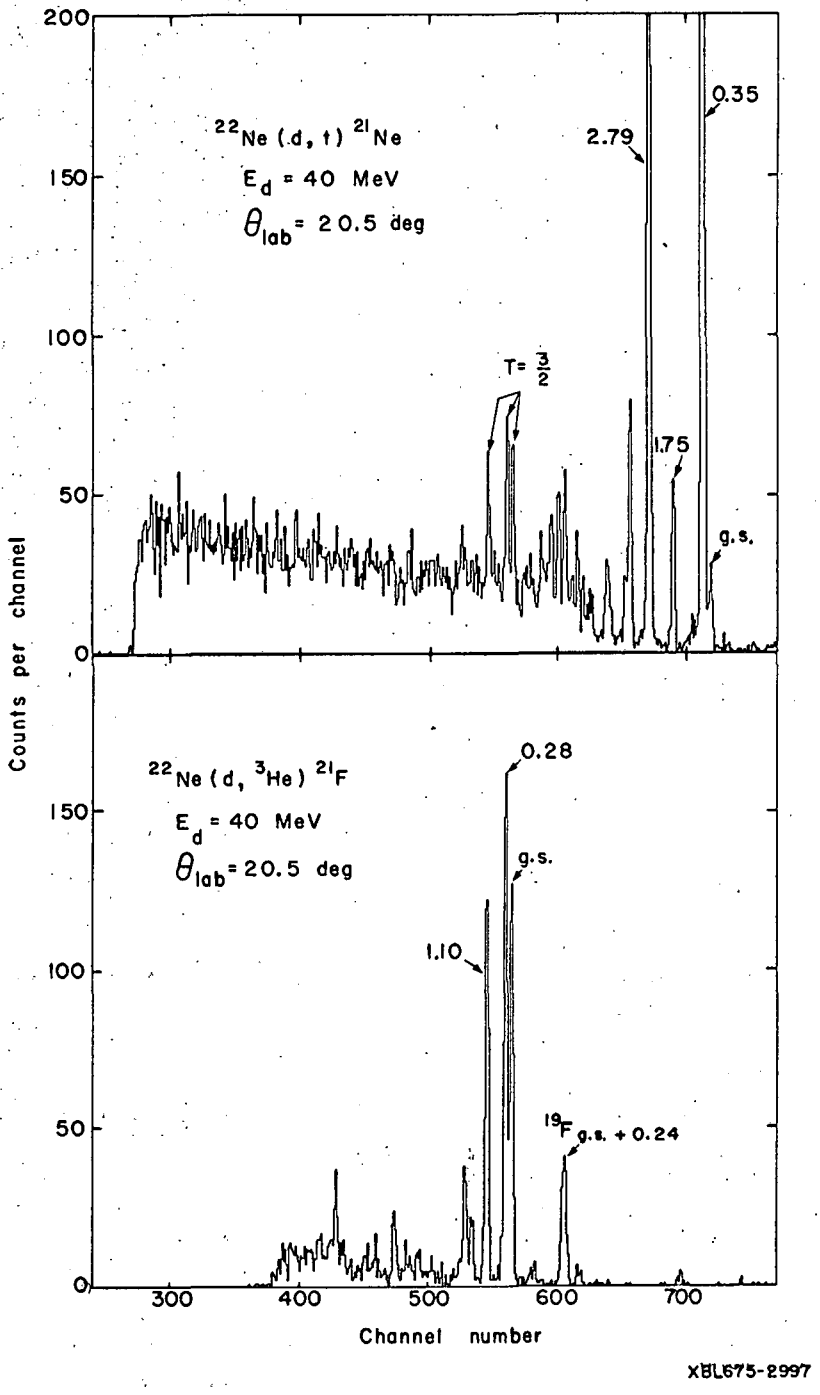

Fig. 22. Energy spectra from the ^{22}Ne(d,t)^{21}Ne and ^{22}Ne(d,^{3}He)^{21}F reactions at 20.5 deg. The ^{21}Ne spectrum has been adjusted to align the first three T = 3/2 levels in ^{21}Ne with their analogues in the ^{21}F spectrum.

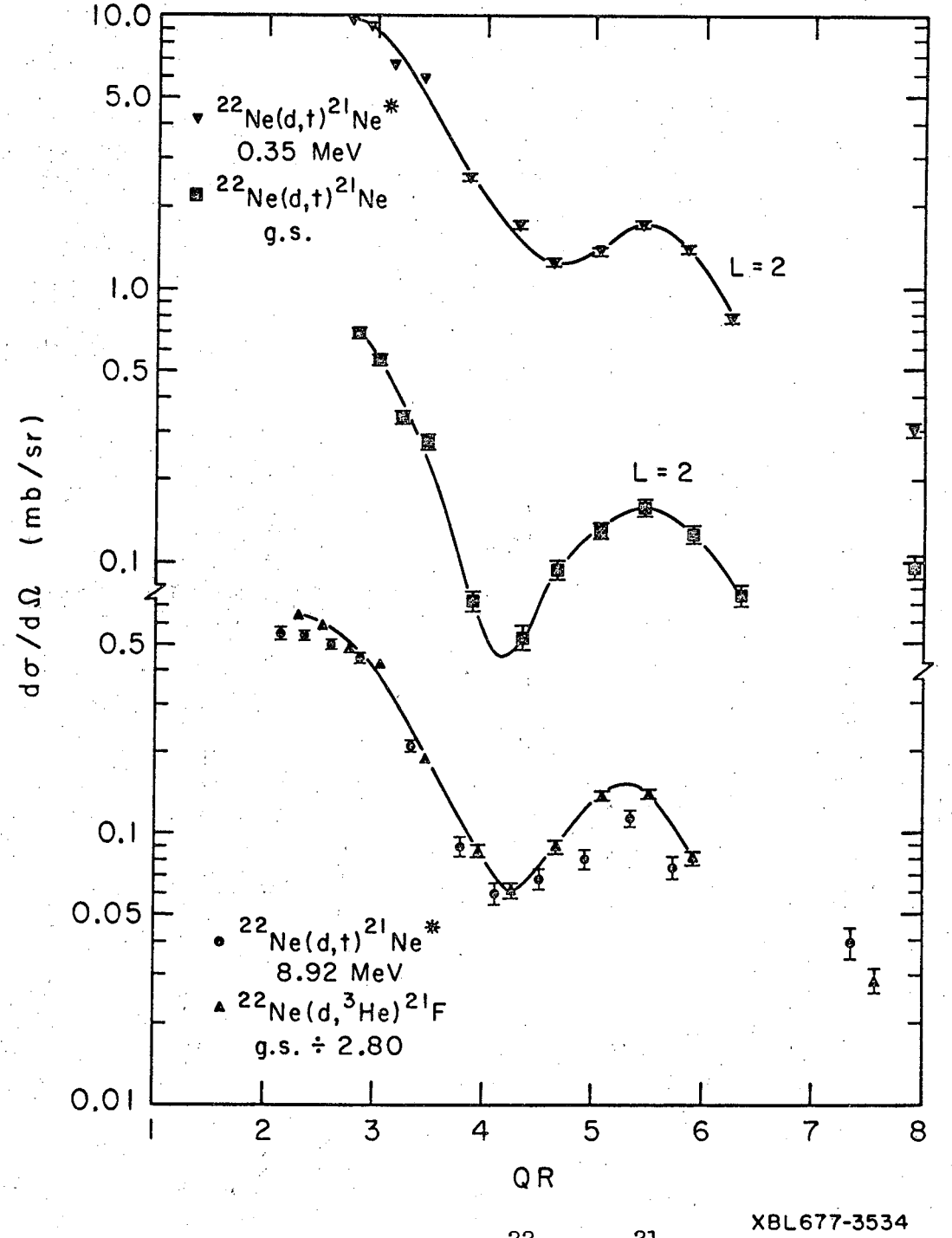

Fig. 23. Angular distributions of the ^{22}Ne(d,t)^{21}Ne transitions to the ground state ($3/2^+$), 0.35-MeV ($5/2^+$), and 8.92-MeV levels and of the ^{22}Ne(d,^{3}He)^{21}F ground-state ($5/2^+$) transition. In all cases smooth curves have been drawn through the experimental points to guide the eye; the abscissa is the dimensionless quantity QR, where Q is the momentum transfer and R is the interaction radius.

sees that the angular distributions of the $^{22}Ne(d,t)^{21}Ne^*$ 8.92-Mev state and the $^{22}Ne(d,^3He)^{21}F$ ground state have similar L = 2 shapes and that their adjusted cross sections agree quite well. Therefore the 8.92-MeV level of ^{21}Ne has been assigned T = 3/2 and $J^\pi = 5/2^+$ to agree with its analogue.

Angular distributions of the $^{22}Ne(d,^3He)^{21}F^*$ 0.28-MeV $(1/2^+)$[35] transition and the $^{22}Ne(d,t)^{21}Ne^*$ 9.21-MeV transition are presented in Fig. 24. The $(d,^3He)$ cross sections have again been divided by 2.80 to correct for isospin coupling and phase space factors. Upon comparison of the magnitudes (and L = 0 shapes) of these two angular distributions, the 9.21-MeV level of ^{21}Ne can be assigned as a $1/2^+$, T = 3/2 state. Angular distributions of the $^{16}O(d,^3He)^{15}N$ ground $(1/2^-)$ and 6.33-MeV $(3/2^-)$ states,[36] together with the distributions of the $^{22}Ne(d,^3He)^{21}F^*$ 1.10-MeV level and the $^{22}Ne(d,t)^{21}Ne^*$ 10.04-MeV level, are shown in Fig. 25. The spin and parity of the 1.10-MeV level of ^{21}F are not known, but when the angular distribution of this level is compared to the known L = 1 transitions to ^{15}N, it appears to possess an L = 1 shape so that it may be tentatively assigned as $J^\pi = (1/2, 3/2)^-$. The angular distributions of the $^{21}Ne^*$ 10.04-MeV and the $^{21}F^*$ 1.10-MeV levels (the latter cross section has been divided by the appropriate phase space and isospin coupling factor in Fig. 25) are similar in shape and have the proper relative magnitudes, so that the $^{21}Ne^*$ 10.04-MeV state is the third T = 3/2 level in ^{21}Ne and it is also tentatively assigned spin and parity $(1/2, 3/2)^-$.

The $^{23}Na(p,t)^{21}Na$ and the $^{23}Na(p,^3He)^{21}Ne$ reactions were studied at 42 MeV in order to locate T = 3/2 levels in ^{21}Na through comparison of (p,t) transitions with $(p,^3He)$ transitions to the now established T = 3/2 levels in ^{21}Ne. An energy spectrum from the $^{23}Na(p,t)^{21}Na$ reaction is shown in Fig. 26 with typical triton energy resolution (FWHM) of 150 keV. Peak 19 in the spectrum possessed an average excitation energy of 8.92±0.03 MeV and was presumed to be the lowest T = 3/2 level since this excitation agreed with the value of 8.90±0.04 MeV reported earlier.[32] Due to the large amount of oxygen in the target, the $(p,^3He)$ transitions to the ^{21}Ne analogues of the 8.92-MeV

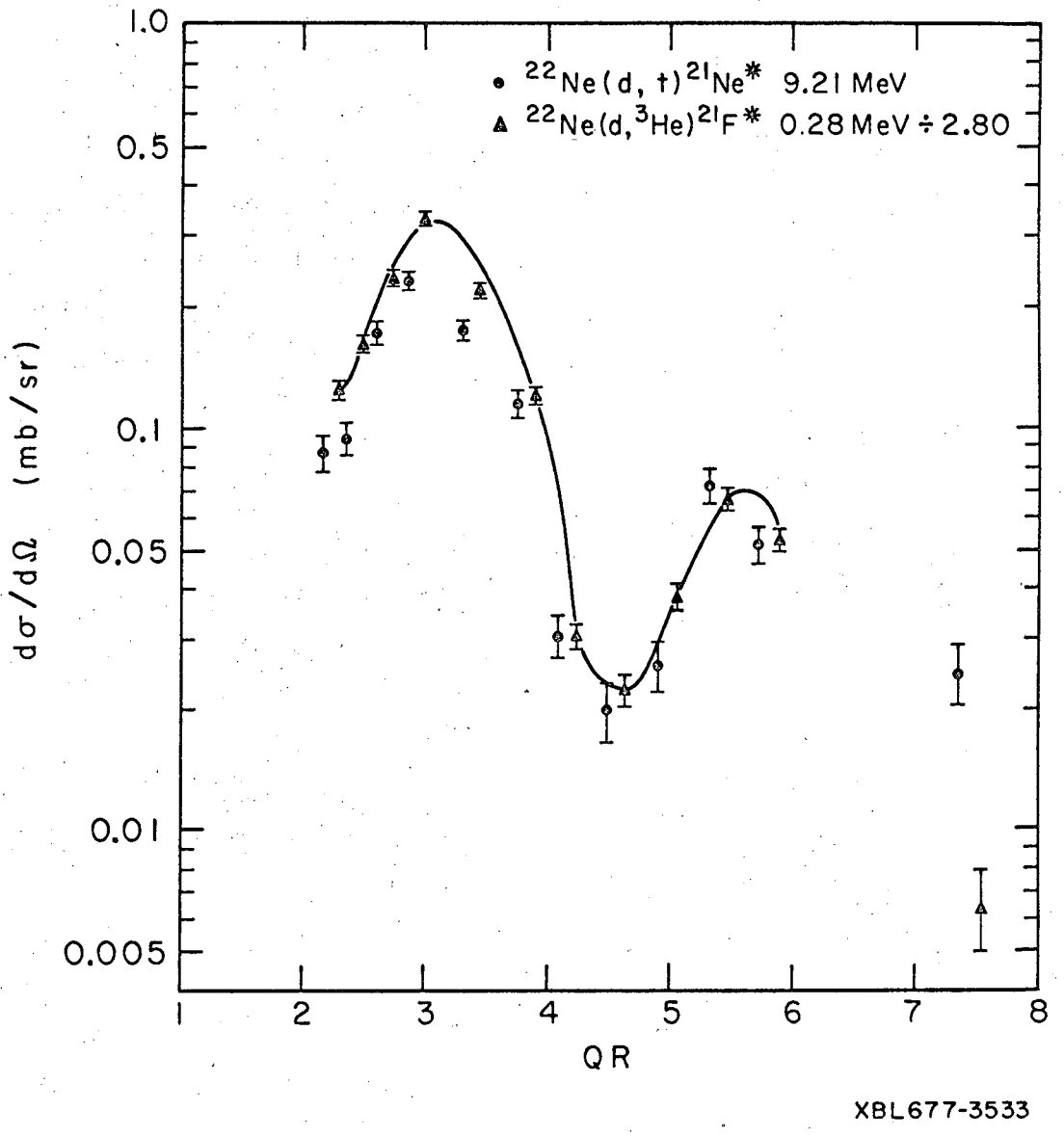

Fig. 24. Angular distributions for the ^{22}Ne(d,^{3}He)^{21}F* 0.28-MeV ($1/2^{+}$) and the ^{22}Ne(d,t)^{21}Ne* 9.21-MeV transitions.

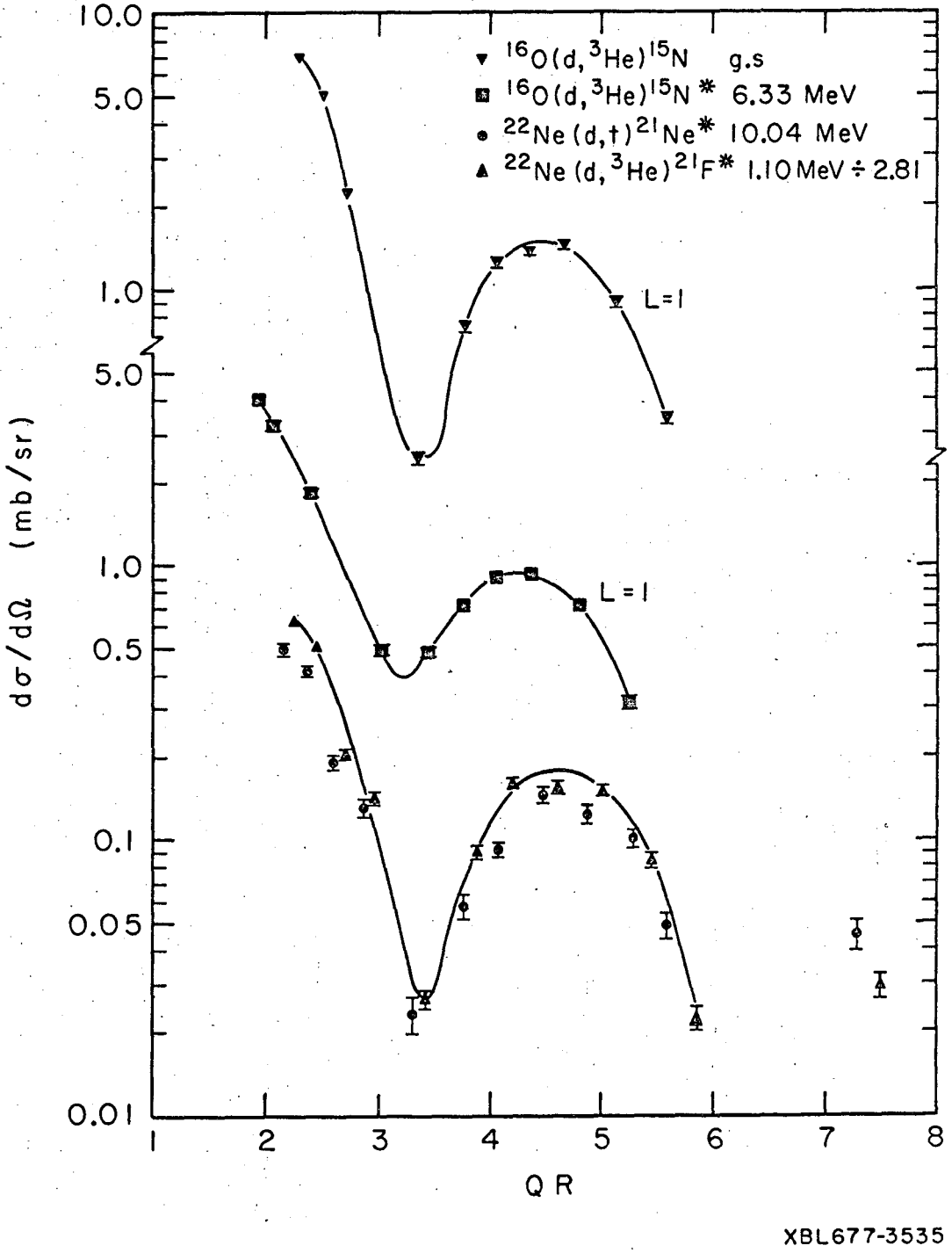

Fig. 25. Angular distributions of the $^{16}O(d,^3He)^{15}N$ ground-state ($1/2^-$) and 6.33-MeV ($3/2^-$) transitions, the $^{22}Ne(d,^3He)^{21}F^*$ 1.10-MeV transition and the $^{22}Ne(d,t)^{21}Ne^*$ 10.04-MeV transition.

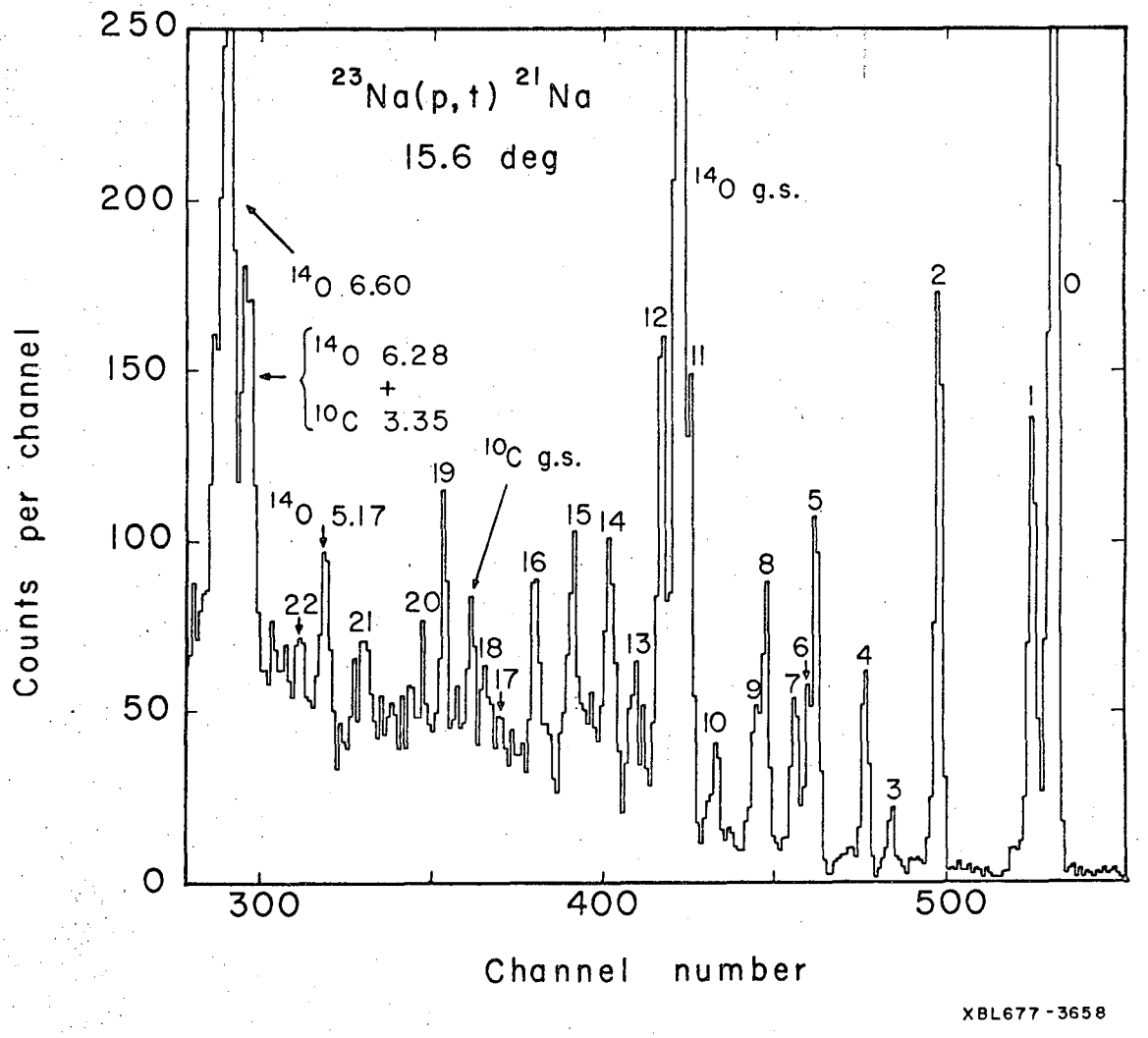

Fig. 26. Triton energy spectrum from the ^{23}Na(p,t)^{21}Na reaction at 42 MeV. The numbered levels are ^{21}Na levels whose average excitation energies are listed in Table III.

and higher levels of ^{21}Na were not observed. Several previously unreported energy levels of ^{21}Na were observed in this experiment and the results are presented in Table III along with a summary[37-39] of previously published data on states of this nucleus. No new spin and parity assignments have been made by us, and, in fact, some of the excited levels may be unresolved doublets. In general, the results of this experiment are in good agreement with the published data on the energy levels of ^{21}Na.

These new data on the mass 21 isospin quartet are summarized in Fig. 27, which shows energy level diagrams for the members of the quartet. For clarity, ground-state energies of mirror nuclei have been equated and many of the energy levels of ^{21}Ne and ^{21}Na below 10 MeV excitation have been deleted. The four members of the completed ground-state T = 3/2 quartet are shown and T = 3/2 analogue levels are connected by dashed lines.

2. T = 3/2 States in ^{37}K and ^{37}Ar

The ^{39}K(p,t)^{37}K and ^{39}K(p,^{3}He)^{37}Ar reactions at 45 MeV were used to locate the lowest T = 3/2 levels in ^{37}K (T_z = -1/2) and ^{37}Ar (T_z = +1/2). Triton and ^{3}He energy spectra from these reactions at a laboratory angle of 26 deg are shown in Fig. 28. Energy resolutions (FWHM) were about 180 keV for tritons and 280 keV for ^{3}He-particles. Sharp states were observed in these spectra in the expected regions for the T = 3/2 levels, as predicted from Coulomb calculations and the ^{37}Cl mass, at excitations of 5.010±0.030 and 5.035±0.025 MeV in ^{37}Ar and ^{37}K, respectively. This excitation for the lowest T = 3/2 level of ^{37}K agrees with that of 5.030±0.018 MeV obtained previously.[40] Angular distributions to these two states and to the ^{37}K ground ($3/2^+$) and 1.37-MeV ($1/2^+$) states are shown in Fig. 29. Since a spin transfer of S = 0 is required to first order for (p,t) reactions, the ^{37}K* 1.37-MeV transition is expected to be a pure L = 2 angular momentum transfer. Although the ^{37}K ground-state transition is allowed by angular momentum and parity selection rules to proceed via either L = 0 or L = 2 angular momentum transfers, previous (p,t) experiments[41] have shown that

Table III. Levels in ^{21}Na observed in the ^{23}Na(p,t)^{21}Na reaction at 42 MeV. The J^{π} assignments were all taken from the references cited.

Level Number	Excitation This Work (MeV ± keV)	Excitation Other Work (MeV ± keV)	J^{π}	References
0	0.0		$3/2^{+}$	31
1	0.335 ± 10	0.338 ± 3	$5/2^{+}$	37
2	1.71 ± 10	1.72	$(7/2^{+})$	31
3	2.42 ± 30	2.430 ± 3	$1/2^{+}$	38
4	2.81 ± 20	2.81 ± 40		31
5	3.54 ± 20	3.540 ± 2	$5/2^{+}$	37
6	3.64 ± 30			
7	3.83 ± 20	3.88, 3.82		31, 37
		4.15	$3/2^{-}$	31, 37
8	4.28 ± 30	4.29 ± 4	$5/2^{+}$	37
9	4.41 ± 30	4.41 ± 20		37
		4.46 ± 5	$3/2^{+}$	37
10	4.99 ± 30	5.00 ± 50		31
11	5.34 ± 30			
		5.47		31
		5.70		31
12	5.78 ± 30	5.83		31
13	6.16 ± 30			
		6.26		31
14	6.54 ± 30	6.52 ± 50	$3/2^{+}$	31, 39
15	7.06 ± 30			
		7.21 ± 50	$1/2^{+}$	39
		7.45 ± 50	$5/2^{+}$	31, 39
16	7.60 ± 60			
17	8.11 ± 30			
18	8.31 ± 30			

Table III. (continued)

Level Number	Excitation This Work (MeV ± keV)	Excitation Other Work (MeV ± keV)	J^{π}	References
19	8.92 ± 30	8.90 ± 40	$(5/2^{+})$, T=3/2	32
20	9.19 ± 30			
21	10.05 ± 40			
22	11.00 ± 30			

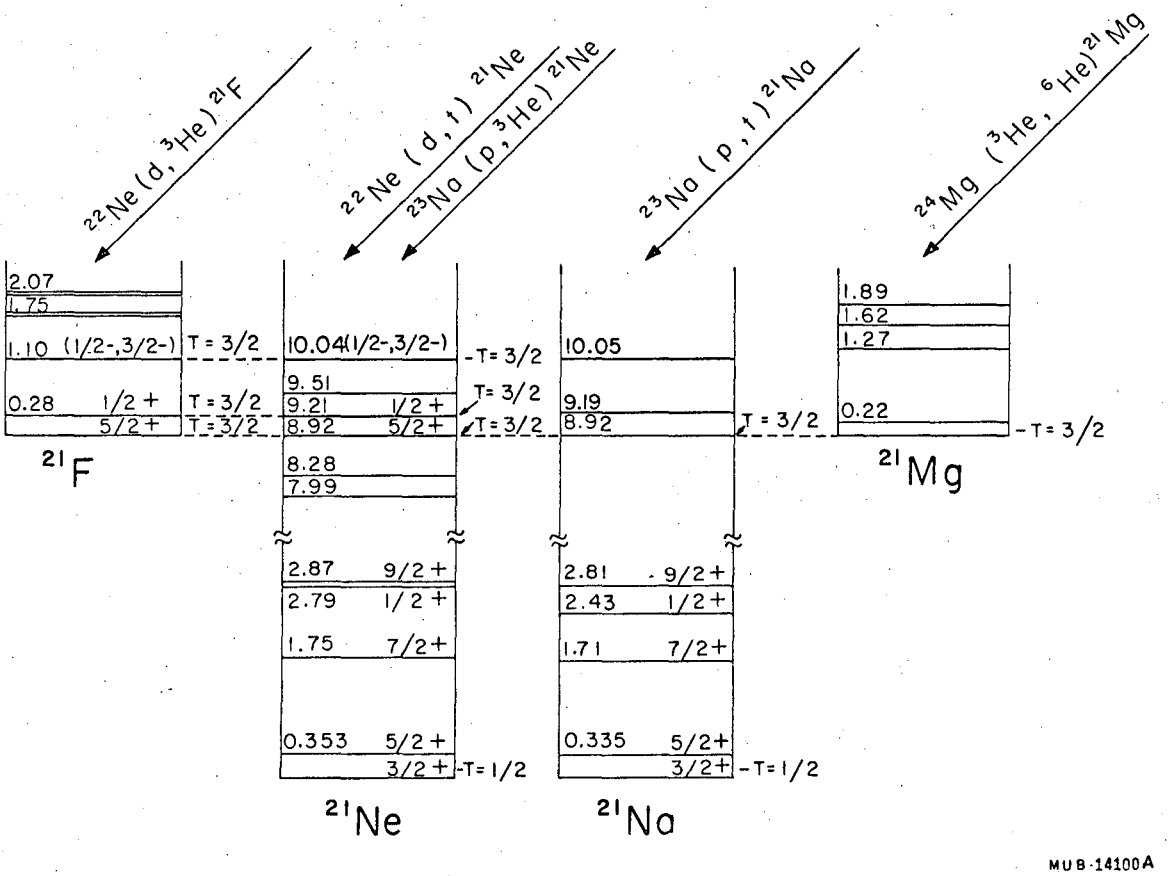

Fig. 27. Energy level diagrams for the members of the mass 21 isospin quartet showing the positions of the T = 3/2 levels in each nucleus. For the sake of clarity the ground-state energies of mirror nuclei have been equated and many of the excited levels of ^{21}Ne and ^{21}Na below 10 MeV excitation have been deleted.

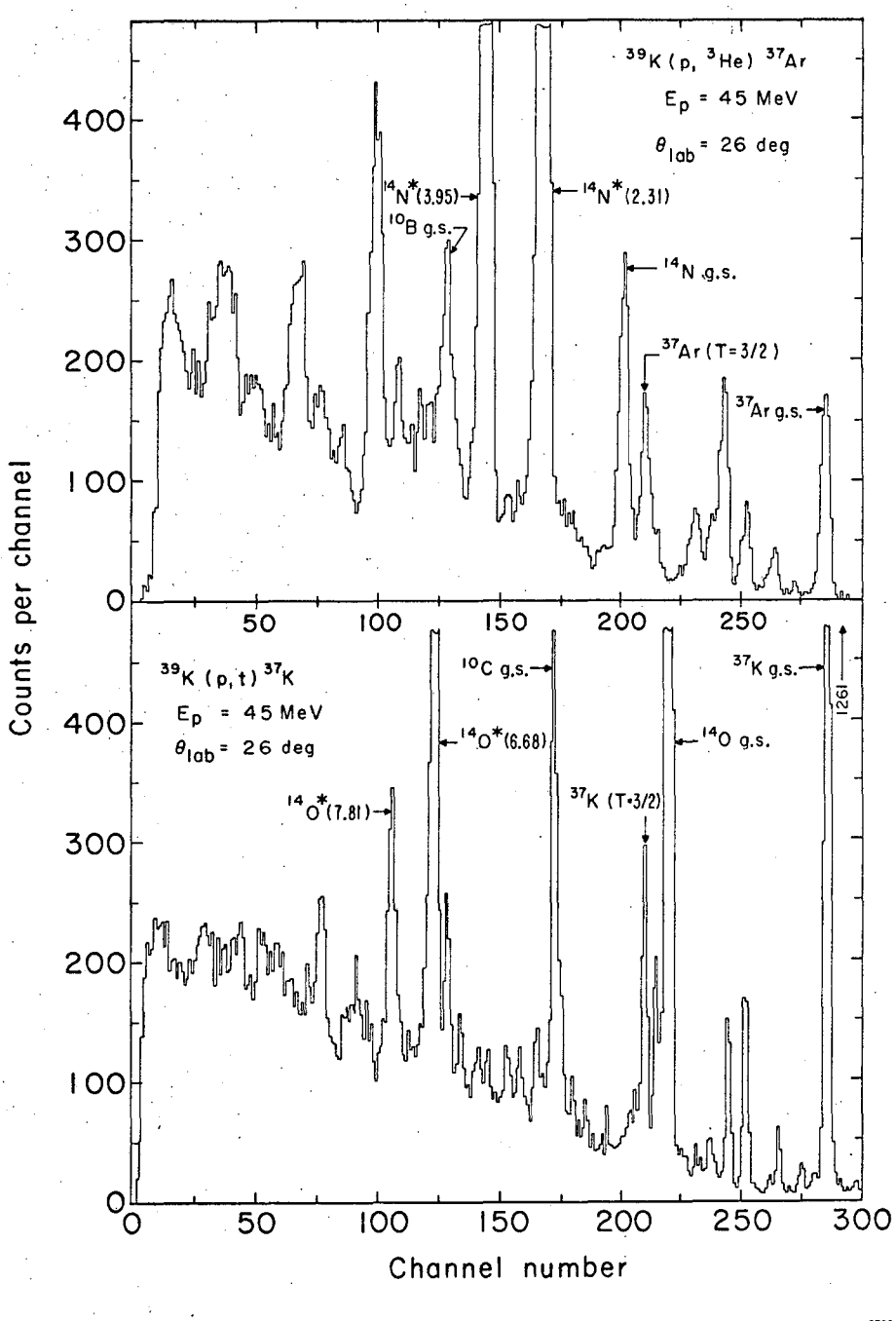

Fig. 28. Energy spectra from the $^{39}K(p,^{3}He)^{37}Ar$ and $^{39}K(p,t)^{37}K$ reactions at 45 MeV and a scattering angle of 26 deg. The spectra have been adjusted to align the positions of the ground state peaks.

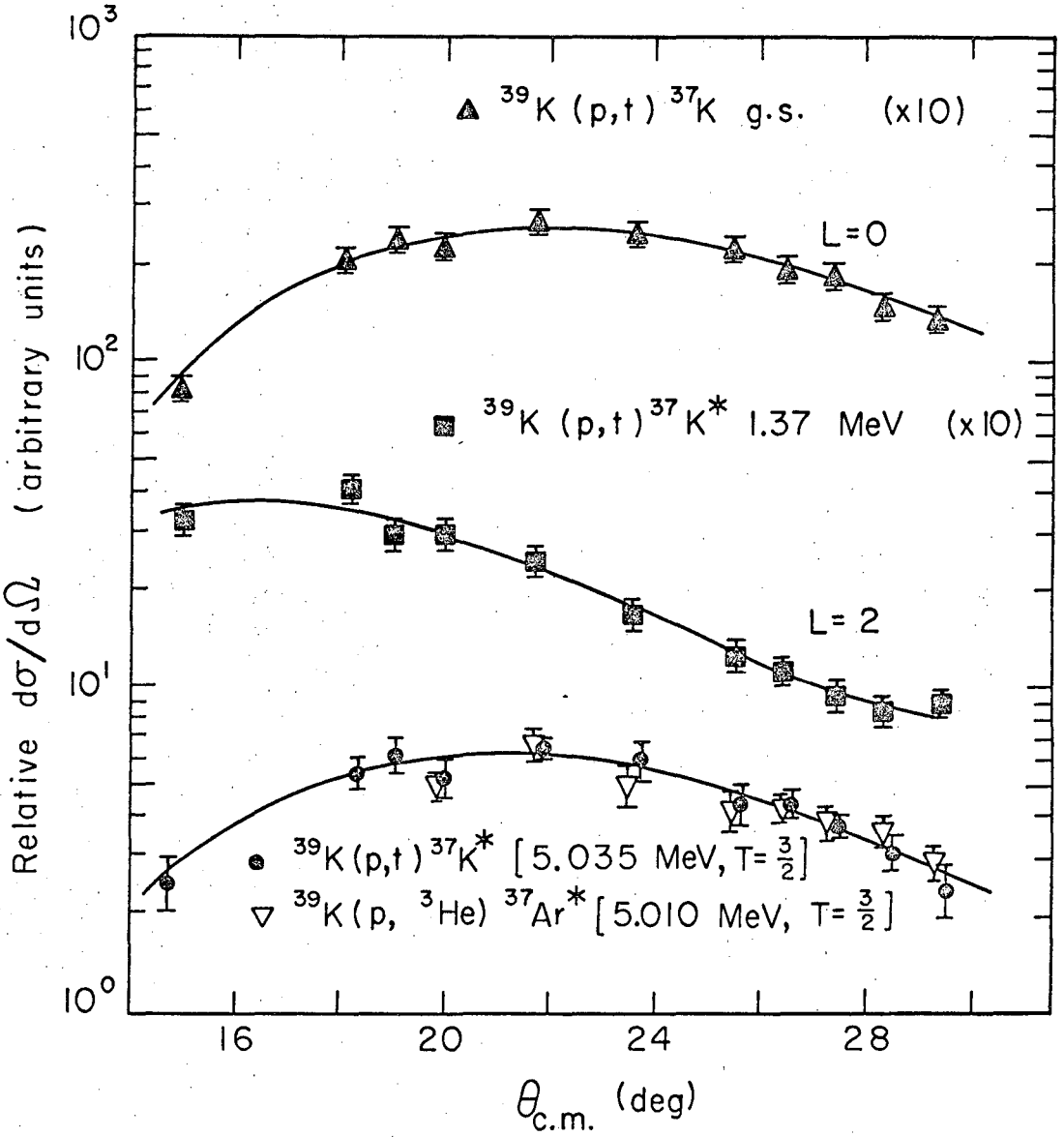

XBL675-2990

Fig. 29. Relative angular distributions for the $^{39}K(p,t)^{37}K$ ground ($3/2^+$), 1.37-MeV ($1/2^+$), and 5.035-MeV (T = 3/2) states and for the $^{39}K(p,^3He)^{37}Ar^*$ 5.010-MeV (T = 3/2) state. The cross section of the last transition has been corrected for phase space and isospin coupling factors.

such transitions appear to proceed by relatively pure L = 0 transfers. Assuming the charge independence of nuclear forces, (p,t) and (p,^{3}He) transitions to T = 3/2 analogue states proceed from identical initial to identical final states primarily through only S = 0, T = 1 pick-up of two nucleons. The lowest T = 3/2 states in ^{37}K and ^{37}Ar, which are the analogues of the known ^{37}Cl ground state ($3/2^+$), should therefore have identical cross sections after isospin coupling and phase space corrections have been made; L = 0 behavior is again expected. Indeed, Fig. 29 shows that the angular distributions to these supposed analogue states possess L = 0 and are essentially identical, thereby confirming that they are T = 3/2 analogue levels with expected spins and parities of $3/2^+$.

Figure 30 summarizes the mass 37 isospin quartet data. Ground-state energies of mirror nuclei have been equated for the sake of clarity and only a few of the levels of ^{37}Ar and ^{37}K below 5 MeV excitation are shown—the level structure of ^{37}K is from Goosman and Kavanagh.[42] The lowest T = 3/2 level in each nucleus is shown and they are connected by dashed lines.

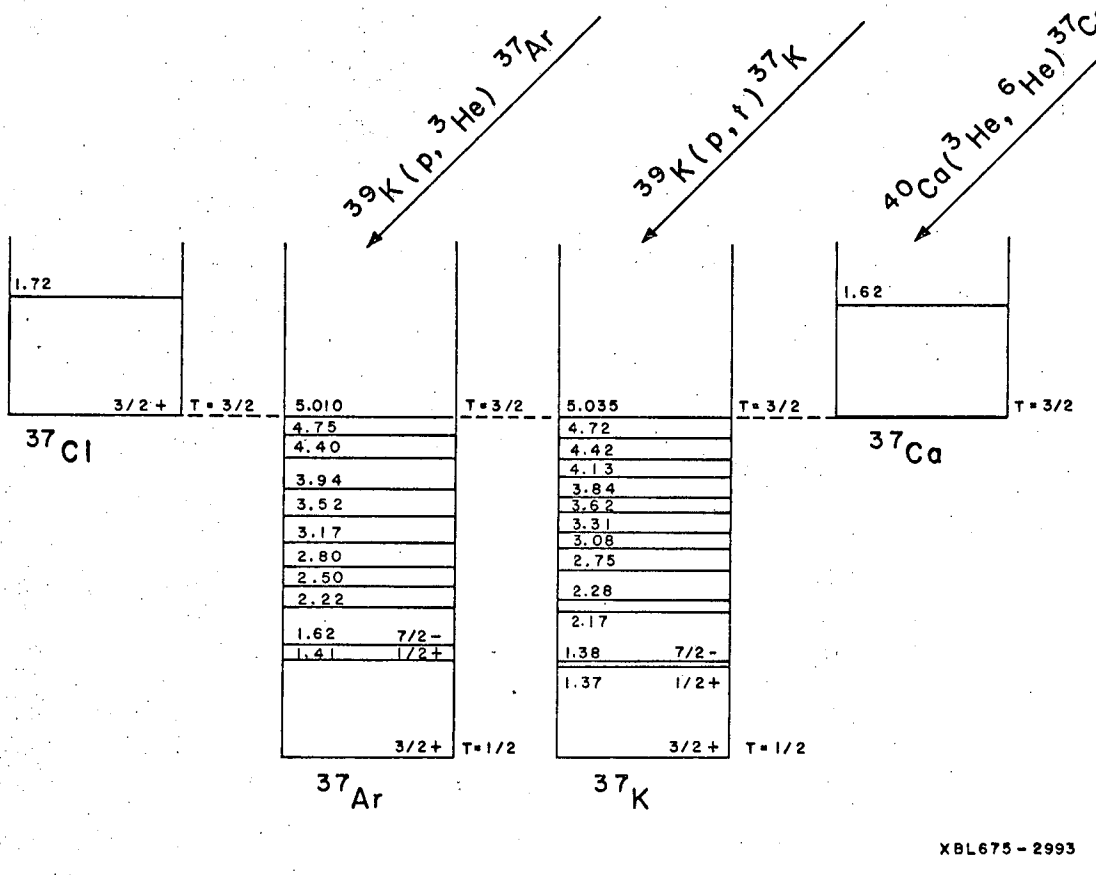

Fig. 30. Energy level diagrams of the members of the mass 37 isospin quartet showing the positions of the T = 3/2 levels in each nucleus. For clarity the ground-state masses of mirror nuclei have been equated and several of the ^{37}Ar and ^{37}K energy levels have been deleted.

C. Preliminary Studies of Three- and Four-Nucleon Transfer Reactions

Angular distributions of the reaction products from the $^{16}O(^{3}He,^{6}He)^{13}O$, $^{16}O(^{3}He,^{6}Li)^{13}N$, $^{16}O(^{3}He,^{7}Li)^{12}N$, and $^{16}O(^{3}He,^{7}Be)^{12}C$ reactions at 70 MeV were obtained and the results are presented in this section. Most of these studies were peripheral to the main concern of this thesis, but the results are presented to be available to others.

1. The $^{16}O(^{3}He,^{6}He)^{13}O$ Reaction

In an effort to determine the mechanism of the $(^{3}He,^{6}He)$ reaction, a further study of the $^{16}O(^{3}He,^{6}He)^{13}O$ reaction was made utilizing the triple-counter particle identifier. An identifier spectrum from the bombardment of an ^{16}O gas target with 70-MeV ^{3}He-particles is shown in Fig. 31. As described previously, all the events in the ^{6}He region of the identifier spectrum were sent to an on-line computer and were later individually analyzed in order to eliminate chance coincidence events. The small cross sections required 8-hour runs at beam intensities of 0.5 to 1.5 μA (depending on the scattering angle) in order to obtain the ^{13}O ground-state angular distribution which is presented in Fig. 32. No transitions to excited ^{13}O states were observed. The spin and parity of the ^{13}O ground state is expected to be $3/2^{-}$, since that is the spin and parity[29] of the ground state of the mirror nucleus ^{13}B. Therefore the ^{13}O ground-state transition is restricted to an L = 1 angular momentum transfer, assuming the reaction is a direct reaction. For comparison, this $(^{3}He,^{6}He)$ transition, the $^{16}O(^{3}He,^{6}Li)^{13}N^{*}$ 3.51-MeV $(3/2^{-})$ transition [the $(^{3}He,^{6}Li)$ data are presented in the next subsection], and the $^{16}O(p,^{4}He)^{13}N^{*}$ 3.51-MeV transition,[43] are shown in Fig. 33, where the abscissa is QR (angular momentum transfer times radius of interaction), which is perhaps a more meaningful representation of the data. Assuming that the $(^{3}He,^{6}Li)$ and $(p,^{4}He)$ reactions proceed by a direct triton pick-up mechanism, these two transitions in Fig. 33 would be expected to possess L = 1 angular momentum transfers. The $^{16}O(^{3}He,^{6}He)^{13}O$ angular distribution appears to have a maximum at the larger angles studied, but the shape does not

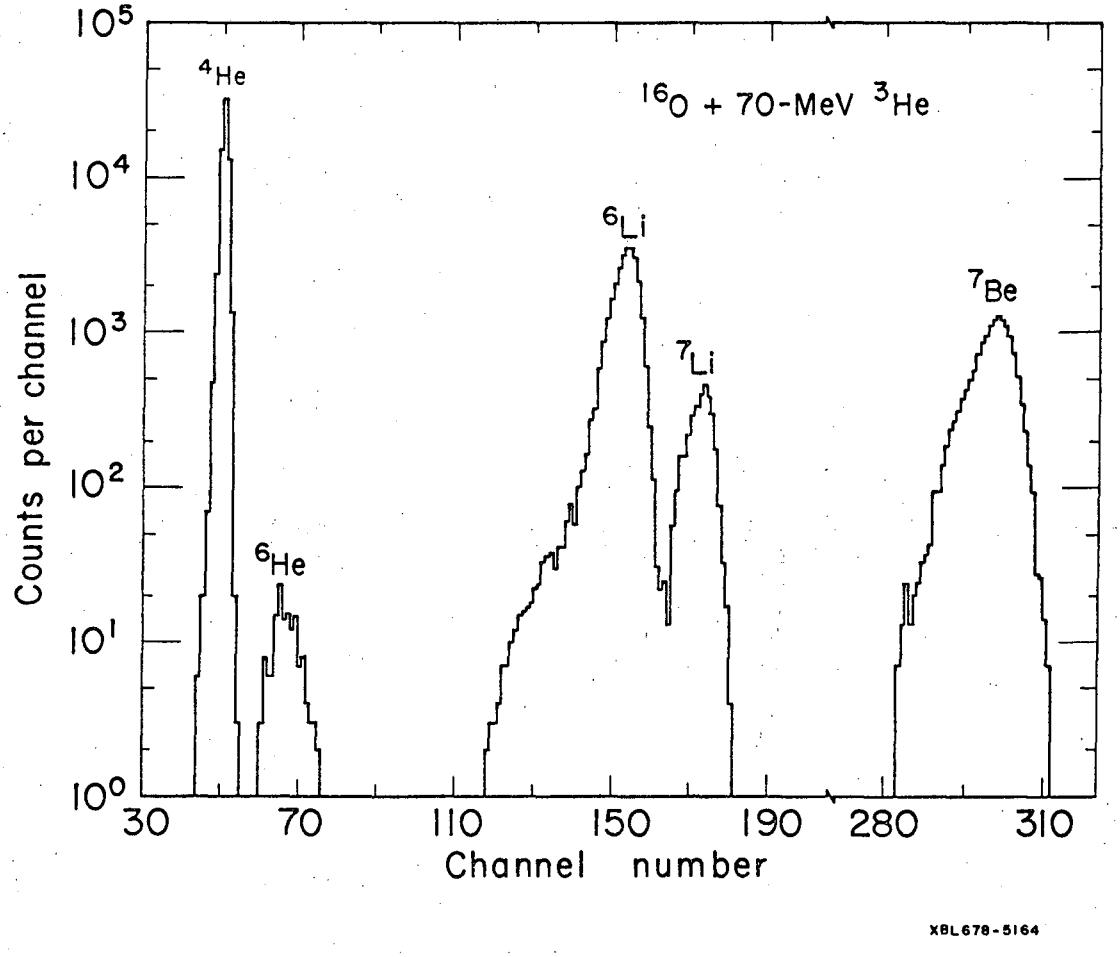

Fig. 31. Triple-counter particle-identifier spectrum from the bombardment of an oxygen gas target with 70-MeV ^{3}He-particles. The $\Delta E2$, $\Delta E1$, and E counter thicknesses were 3.2 mils, 2.4 mils, and 20 mils, respectively.

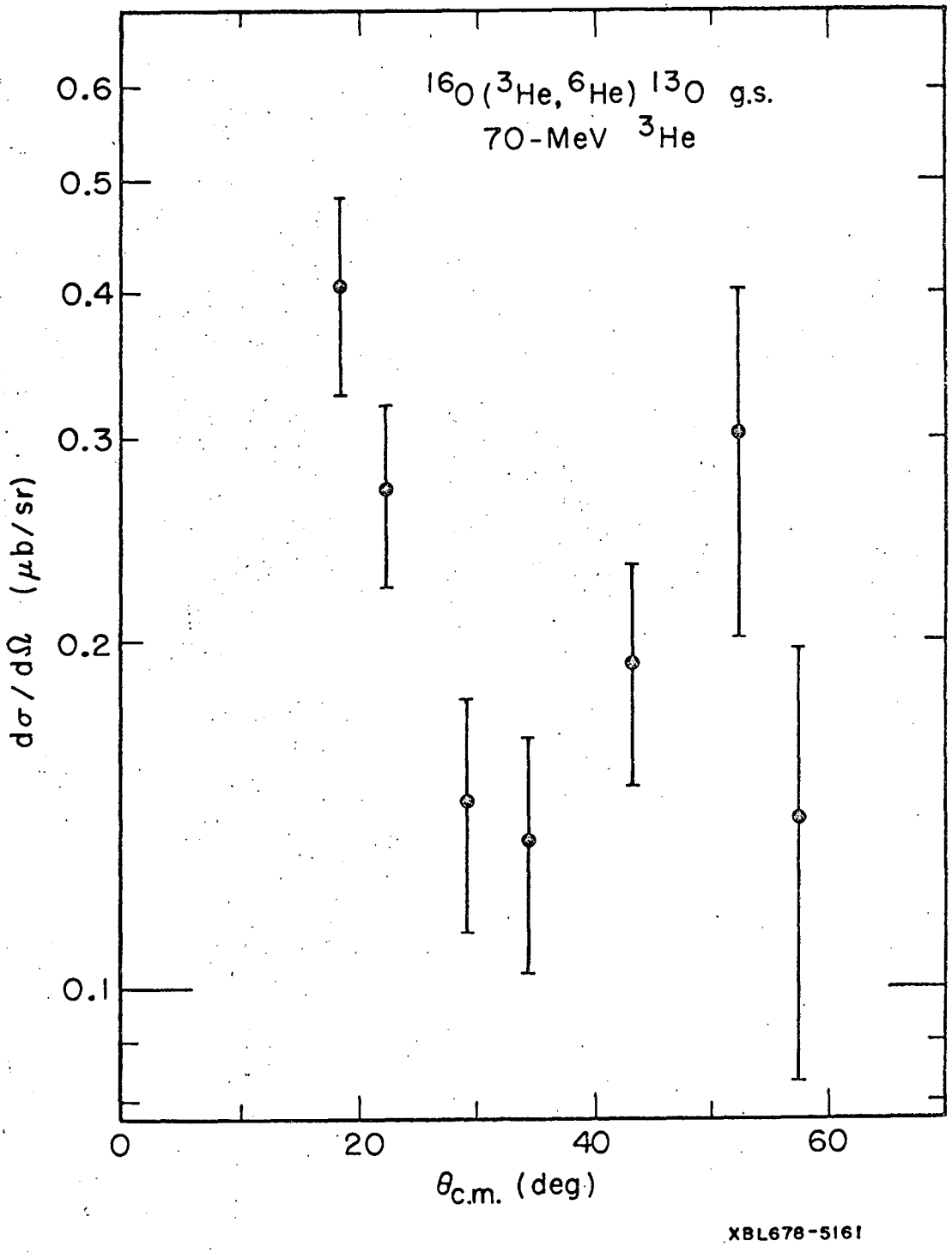

Fig. 32. Angular distribution of the $^{16}O(^{3}He,^{6}He)^{13}O$ ground-state transition.

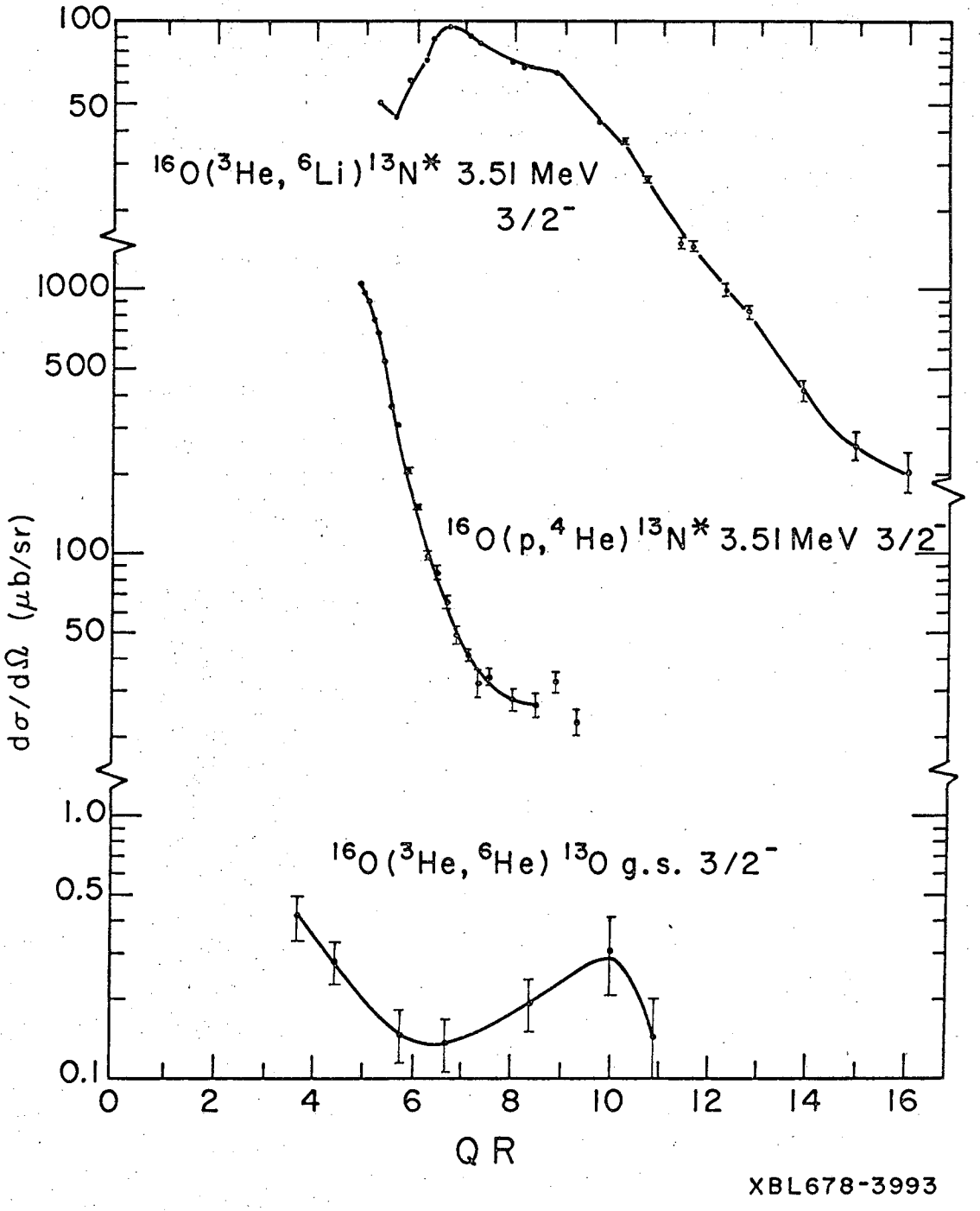

Fig. 33. Angular distribution comparison of $^{16}O(^{3}He,^{6}He)^{13}O$, $^{16}O(^{3}He,^{6}Li)^{13}N^{*}$, and $^{16}O(p,^{4}He)^{13}N^{*}$ reactions leading to $J^{\pi} = 3/2^{-}$ states.

correspond to the shape of either of the other two transitions in Fig. 33. The differential cross sections of the ($p,^4He$) and ($^3He,^6Li$) transitions to the ground state and 3.51-MeV state of ^{13}N, together with that of the ^{13}O ground-state transition, have been integrated over the same angular range and the results are given in Table IV. Clearly the transfer of three neutrons is much more difficult than the transfer of one proton and two neutrons. Since this was only a preliminary study, more data are needed in order to establish the characteristics and mechanism of the ($^3He,^6He$) reaction.

2. The $^{16}O(^3He,^6Li)^{13}N$ Reaction

A ^6Li energy spectrum from this reaction is shown in Fig. 34; the typical ^6Li energy resolution (FWHM) was about 300 keV. Angular distributions of the transitions to four levels of ^{13}N are presented in Fig. 35. Under the assumption that the ($^3He,^6Li$) reaction proceeds by the direct pick-up of a triton cluster from the target nucleus by the incident ^3He-particle, the $^{16}O(^3He,^6Li)^{13}N$ transitions to the ground and 3.51-MeV states of ^{13}N would possess L = 1 angular momentum transfers, whereas the 7.39-MeV ($5/2^-$) transition would proceed via an L = 3 transfer. The angular distributions of the ground and 3.51-MeV states show very little structure other than a peaking at the smaller angles, whereas the 7.39-MeV level has a more constant cross section and it becomes the strongest state in the spectrum at the larger angles. Angular distributions of the ($^3He,^6Li$), ($p,^4He$),[43] and ($^4He,^7Li$) reactions (we obtained the $^{16}O(^4He,^7Li)^{13}N$ data utilizing the standard particle identifier) proceeding to the ground state and 7.39-MeV state of ^{13}N are presented in Figs. 36 and 37 (refer back to Fig. 33 for a comparison of ($^3He,^6Li$) and ($p,^4He$) transitions to the 3.51-MeV state of ^{13}N). In all cases the various reactions have quite different shapes, possibly indicating different reaction mechanisms. The integrated cross sections for these three reactions leading to several states in ^{13}N are presented in Table V. In general, the ($p,^4He$) reaction has a larger cross section than the ($^3He,^6Li$) or ($^4He,^7Li$) reactions to the same strong final state. A systematic study of these reactions on several

Table IV. Integrated cross sections for several three-nucleon transfer reactions.

Reaction	Energy Level (MeV)	Bombarding Energy (MeV)	Angular Range (c.m. deg)	Integrated Cross Section (μb)
$^{16}O(^{3}He,^{6}He)^{13}O$	g.s.	70.1	18.2-57.4	0.54
$^{16}O(^{3}He,^{6}Li)^{13}N$	g.s.	70.1	18.2-57.4	40.8
	3.51		18.2-57.4	109.0
$^{16}O(p,^{4}He)^{13}N$[a]	g.s.	54.1	18.2-57.4	56.3
	3.51		18.2-57.4	375.5

[a] See Ref. 43

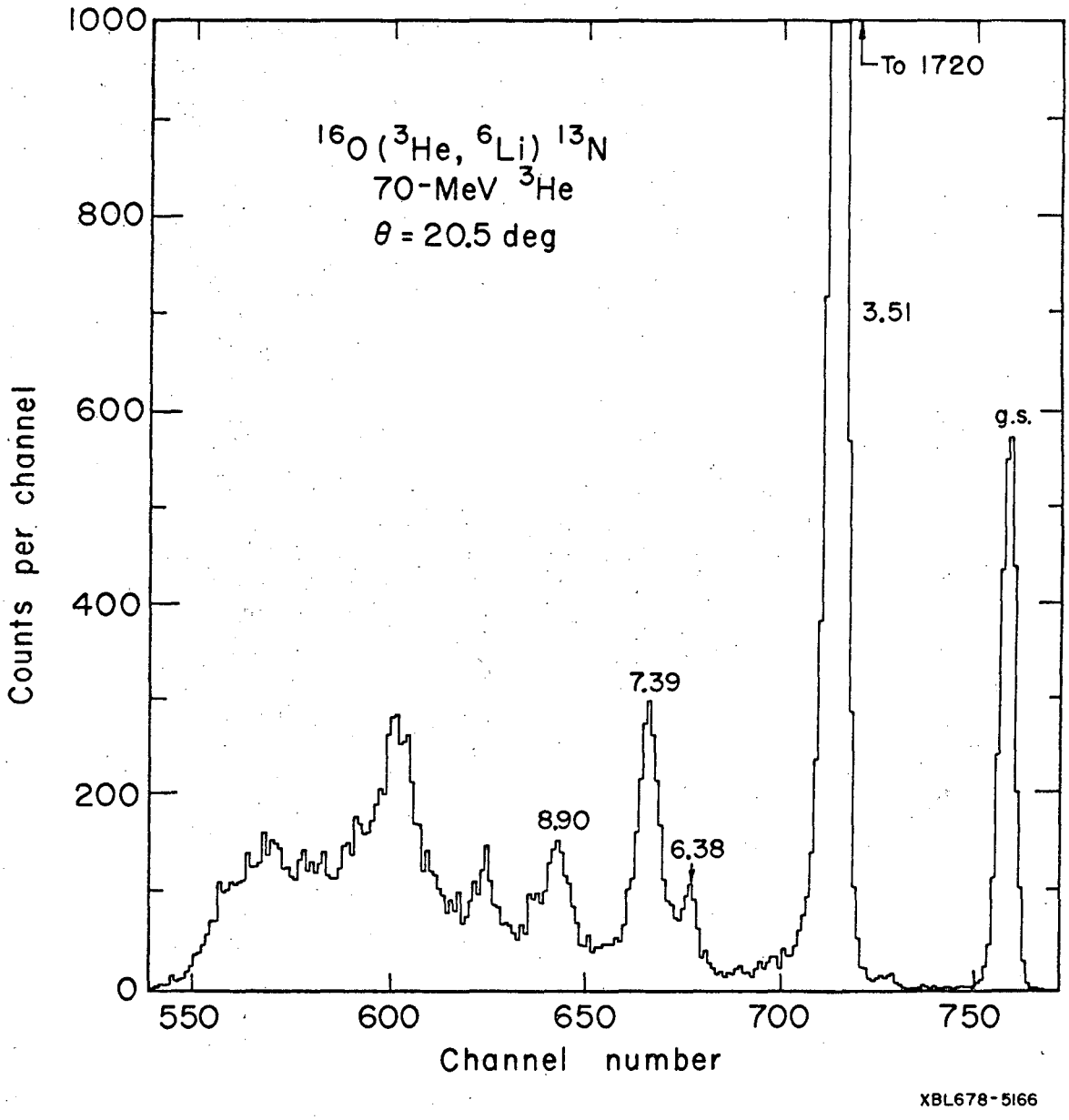

Fig. 34. Energy spectrum of the $^{16}O(^{3}He,^{6}Li)^{13}N$ reaction at 70 MeV and a scattering angle of 20.5 deg.

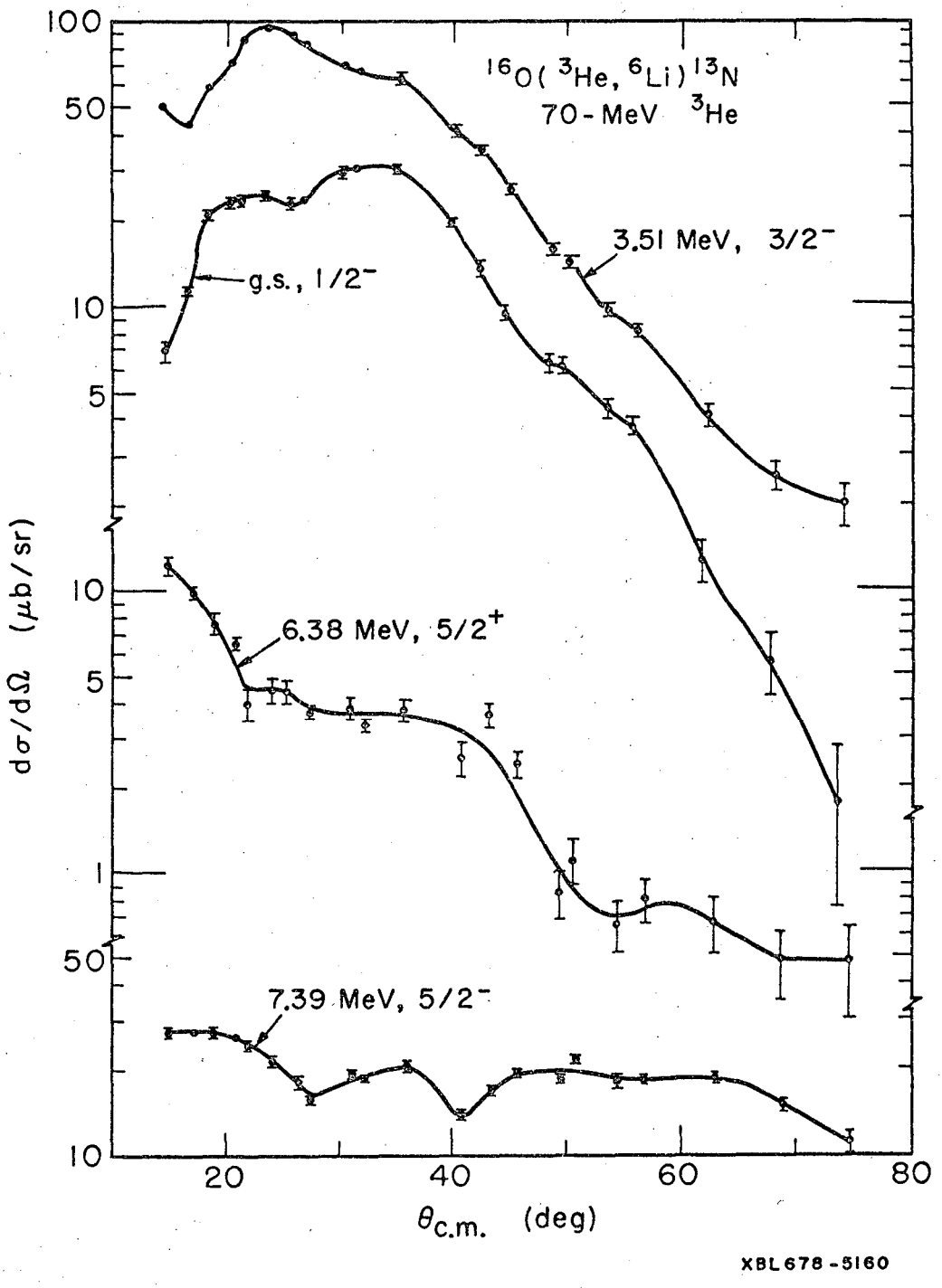

Fig. 35. Angular distributions of several $^{16}O(^{3}He,^{6}Li)^{13}N$ transitions.

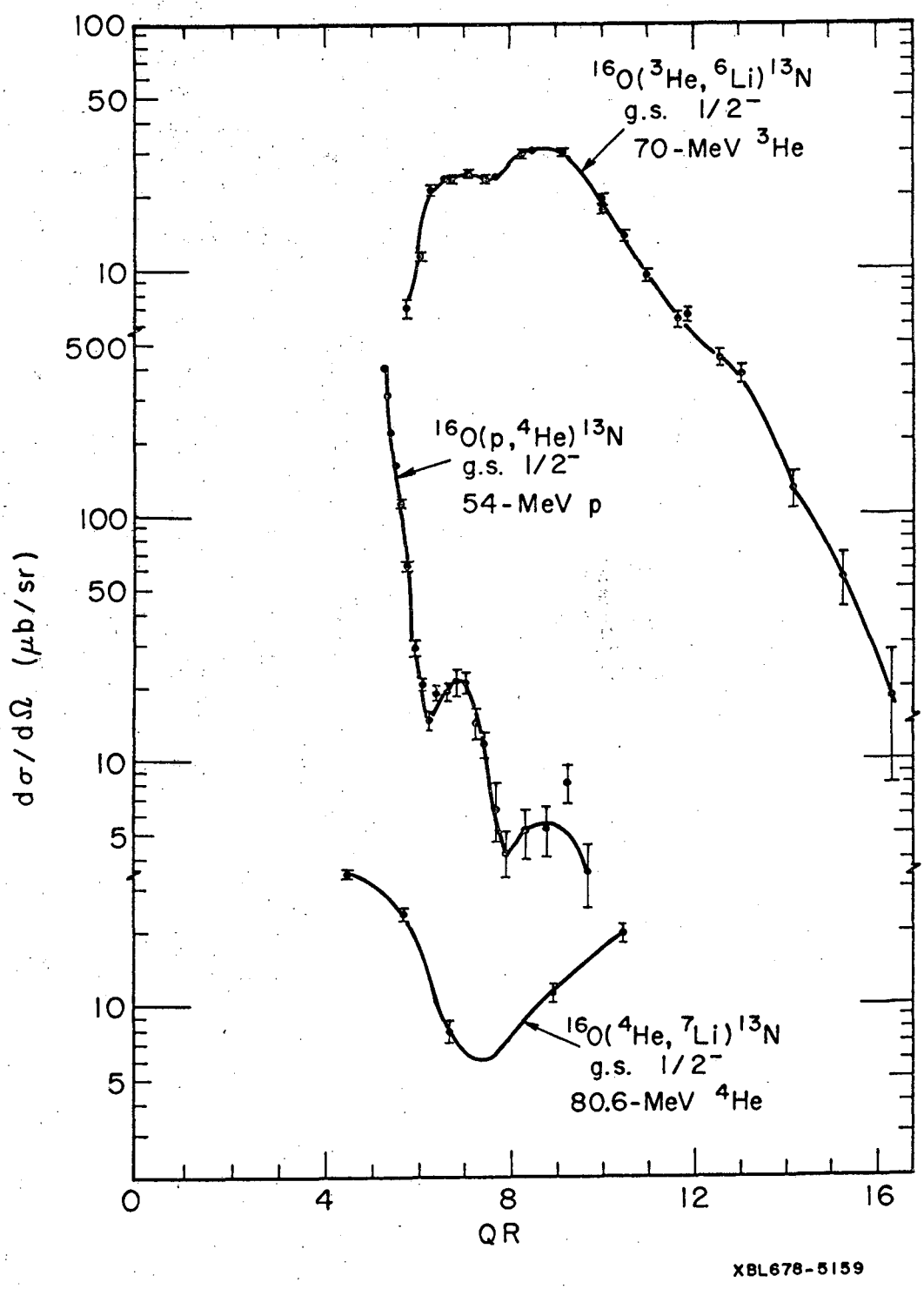

Fig. 36. Angular distributions of $^{16}O(^{3}He, ^{6}Li)^{13}N$, $^{16}O(^{4}He, ^{7}Li)^{13}N$, and $^{16}O(p, ^{4}He)^{13}N$ ground-state transitions.

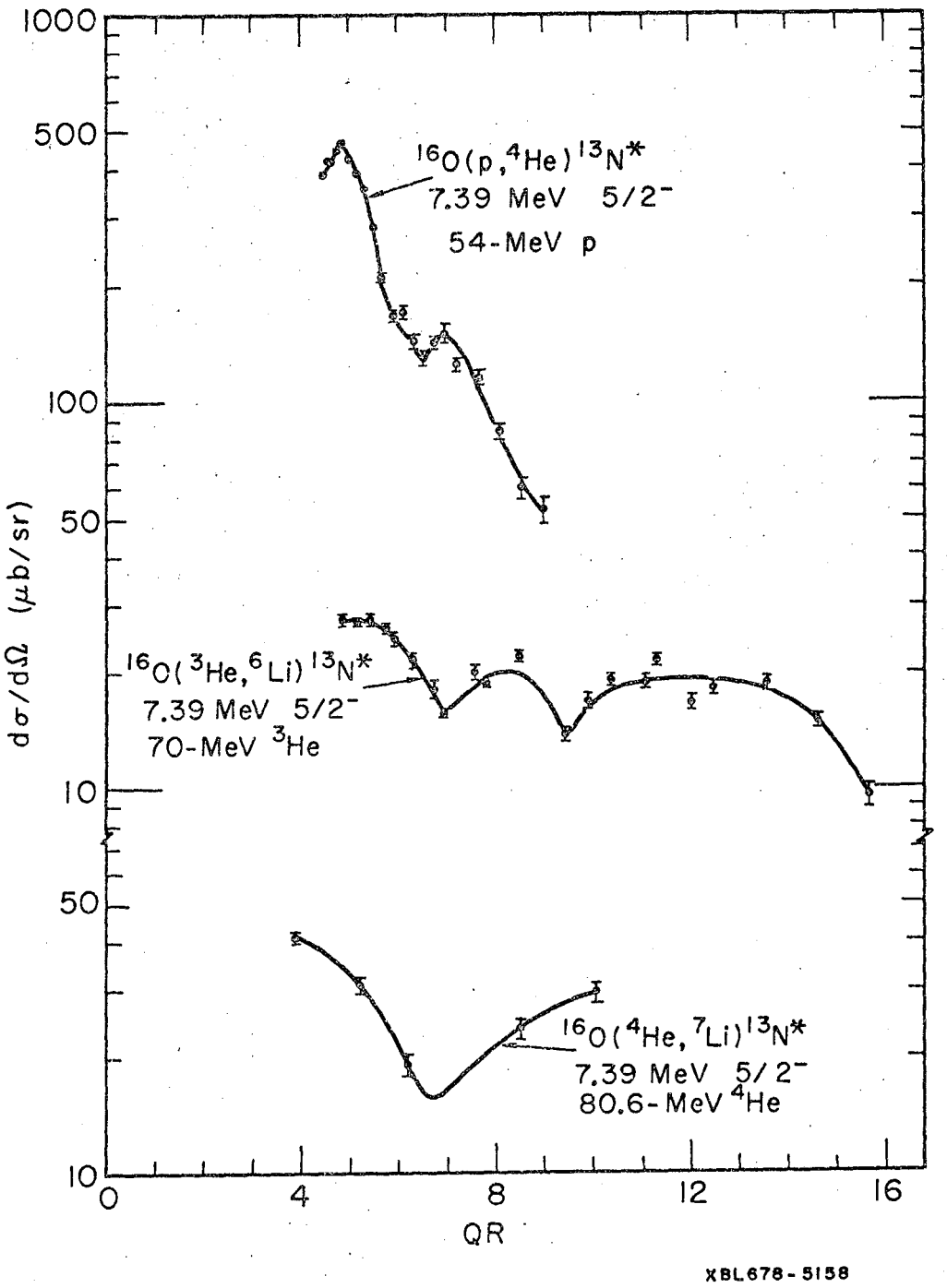

Fig. 37. Angular distributions of $^{16}O(^{3}He,^{6}Li)^{13}N^{*}$, $^{16}O(^{4}He,^{7}Li)^{13}N^{*}$, and $^{16}O(p,^{4}He)^{13}N^{*}$ transitions to the 7.39-MeV ($5/2^{-}$) level of ^{13}N.

Table V. Integrated cross sections for three different reactions proceeding from ^{16}O to the same final states in ^{13}N.

Energy Level (MeV)	Angular Range (c.m. deg)	Integrated Cross Sections (μb) $^{16}O(^{3}He,^{6}Li)^{13}N$ 70.1-MeV ^{3}He	$^{16}O(\alpha,^{7}Li)^{13}N$ 80.6-MeV α	$^{16}O(p,\alpha)^{13}N$[a] 54.1-MeV p
g.s.	16.0-43.3	34.4	28.9	62.3
2.37	16.2-43.7	1.28	5.52	1.69
3.51	16.3-43.9	94.8	115.4	386.7
6.38	16.5-44.5	6.34	11.1	34.8
7.39	16.5-44.7	29.6	40.0	411.2

[a] See Ref. 43.

targets should be made in order to obtain a better understanding of the possible reaction mechanisms.

3. The $^{16}O(^{3}He,^{7}Li)^{12}N$ and $^{16}O(^{3}He,^{7}Be)^{12}C$ Reactions

Energy spectra from these reactions are presented in Figs. 38 and 39—the ^{7}Be energy resolution (FWHM) was about 500 keV. The angular distributions of the $^{16}O(^{3}He,^{7}Li)^{12}N$ ground-state and 0.96-MeV transitions are shown in Fig. 40 and angular distributions of several $^{16}O(^{3}He,^{7}Be)^{12}C$ transitions are shown in Fig. 41. For both the $(^{3}He,^{7}Li)$ and $(^{3}He,^{7}Be)$ transitions, the first excited states (^{7}Li = 0.478 MeV, ^{7}Be = 0.431 MeV) of the exit particles were not resolved from the ground states, so the angular distributions in Figs. 40 and 41 are really sums of transitions to the ground states and first excited states of ^{7}Li or ^{7}Be. The $(^{3}He,^{7}Be)$ angular distributions show little structure and a rapid decrease in cross section with increasing angle. Angular distributions of the $(^{3}He,^{7}Be)$, $(^{4}He,^{8}Be)$,[44,45] and $(d,^{6}Li)$[46] reactions leading to the ground state and to the 4.43-MeV state of ^{12}C are presented in Figs. 42 and 43. Although the $(d,^{6}Li)$ and $(^{3}He,^{7}Be)$ angular distributions are qualitatively similar, the $(d,^{6}Li)$ data do not extend to high enough QR to permit a sufficient comparison to be made. However, the $(^{4}He,^{8}Be)$ and $(^{3}He,^{7}Be)$ angular distributions are quite different, thus making it impossible to reach any conclusions concerning the mechanism of the $(^{3}He,^{7}Be)$ reaction. Integrated cross sections for these three reactions leading to states in ^{12}C are given in Table VI. Obviously the $(^{3}He,^{7}Be)$ reaction has a lower cross section than the other two reactions. Future studies will have to be made to learn more about the nature of these α-particle transfer reactions.

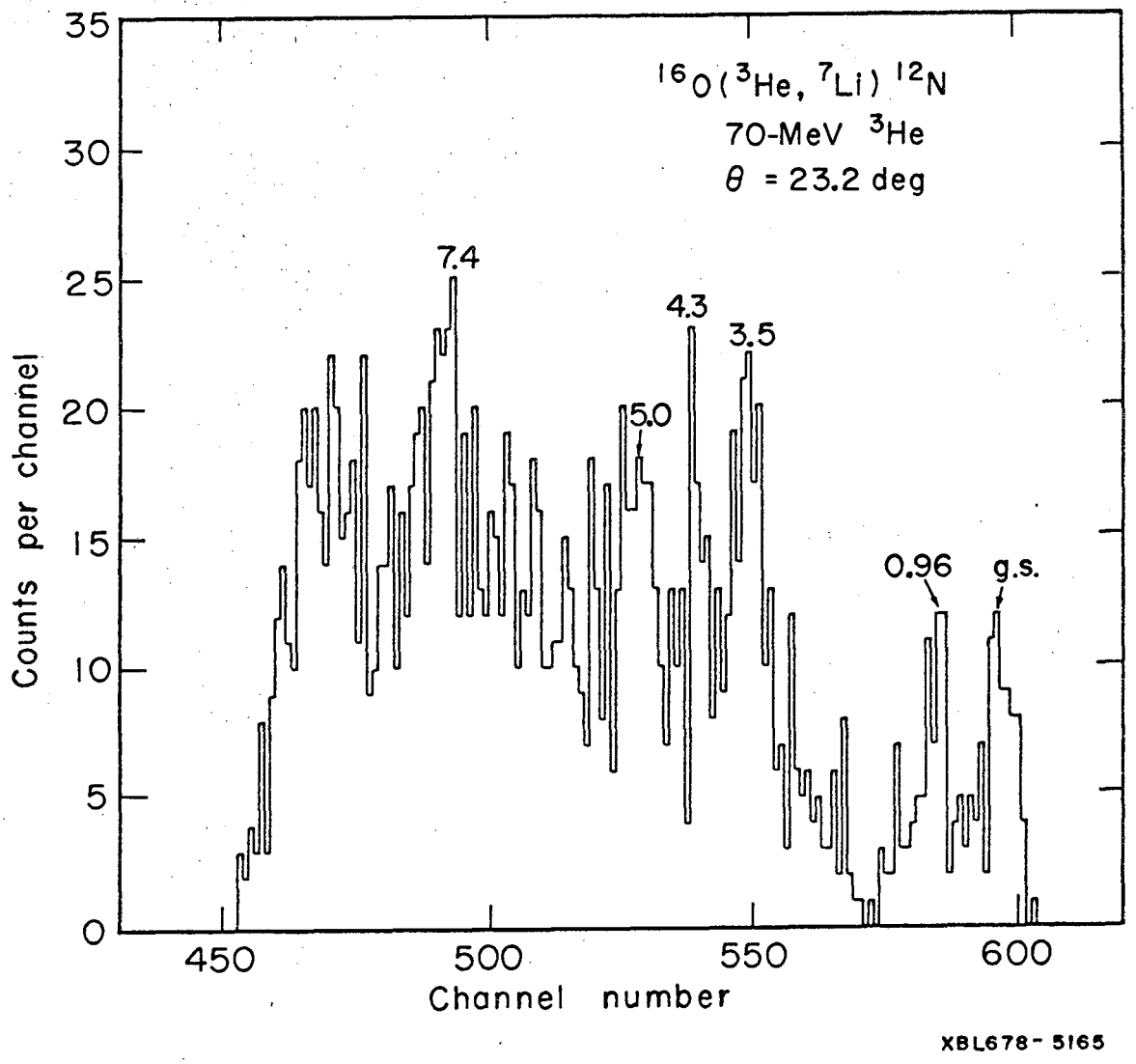

Fig. 38. Energy spectrum of the $^{16}O(^{3}He,^{7}Li)^{12}N$ reaction at 70 MeV and a scattering angle of 23.2 deg.

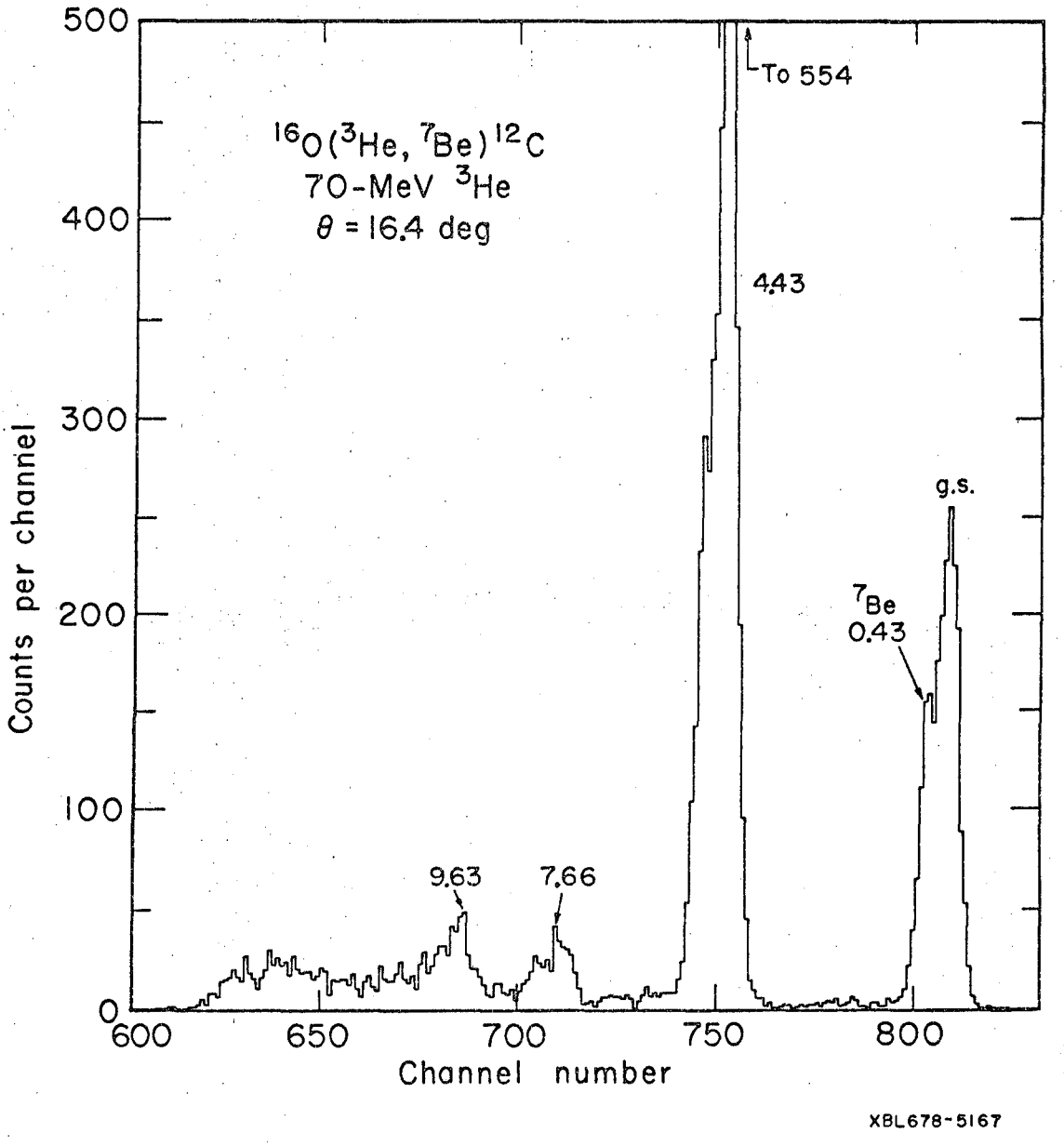

Fig. 39. Energy spectrum of the $^{16}O(^{3}He, ^{7}Be)^{12}C$ reaction at 70 MeV and a scattering angle of 16.4 deg.

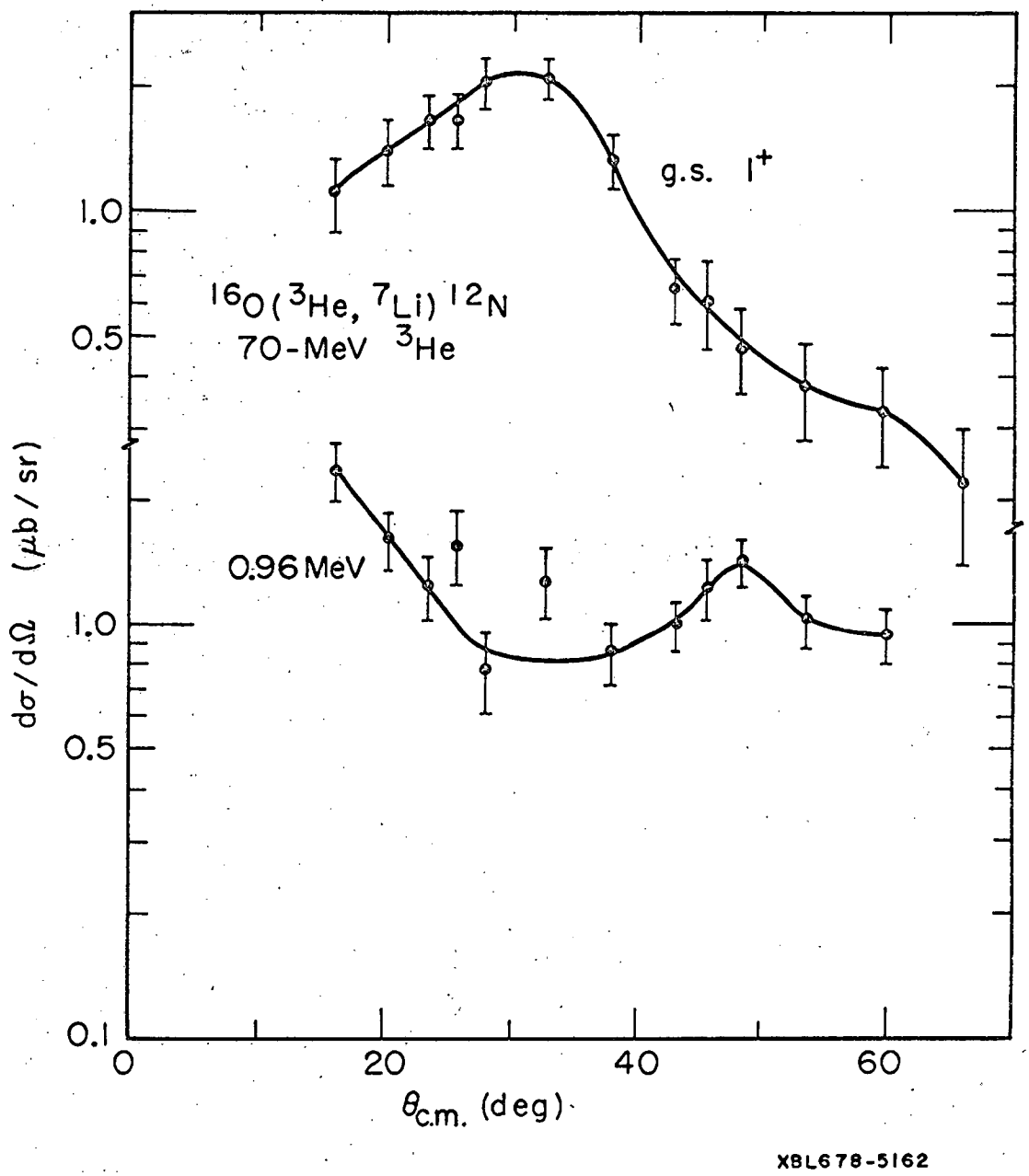

Fig. 40. Angular distributions of the $^{16}O(^{3}He,^{7}Li)^{12}N$ transitions to the ground and 0.96-MeV states of ^{12}N.

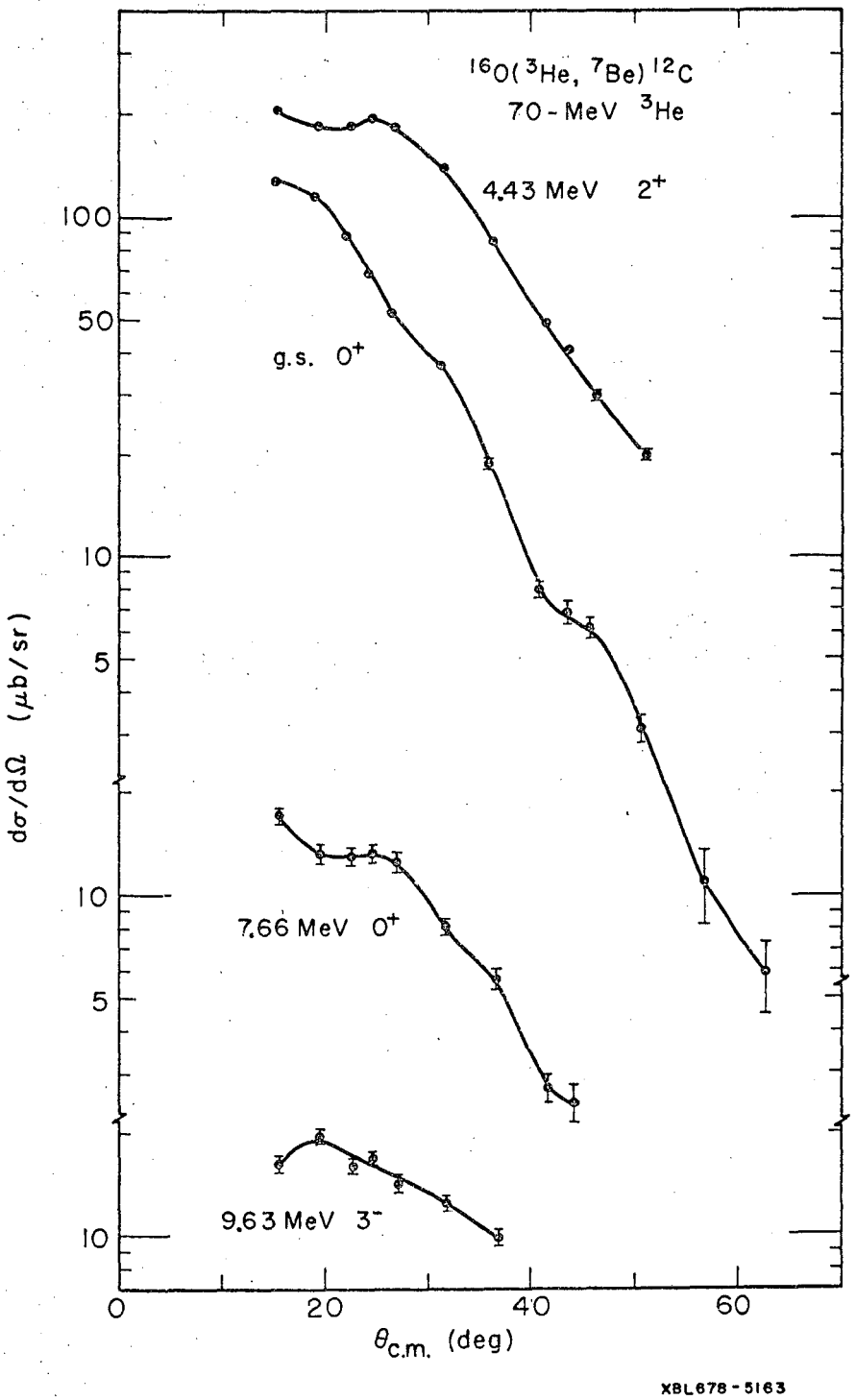

Fig. 41. Angular distributions of several $^{16}O(^{3}He,^{7}Be)^{12}C$ transitions at 70 MeV.

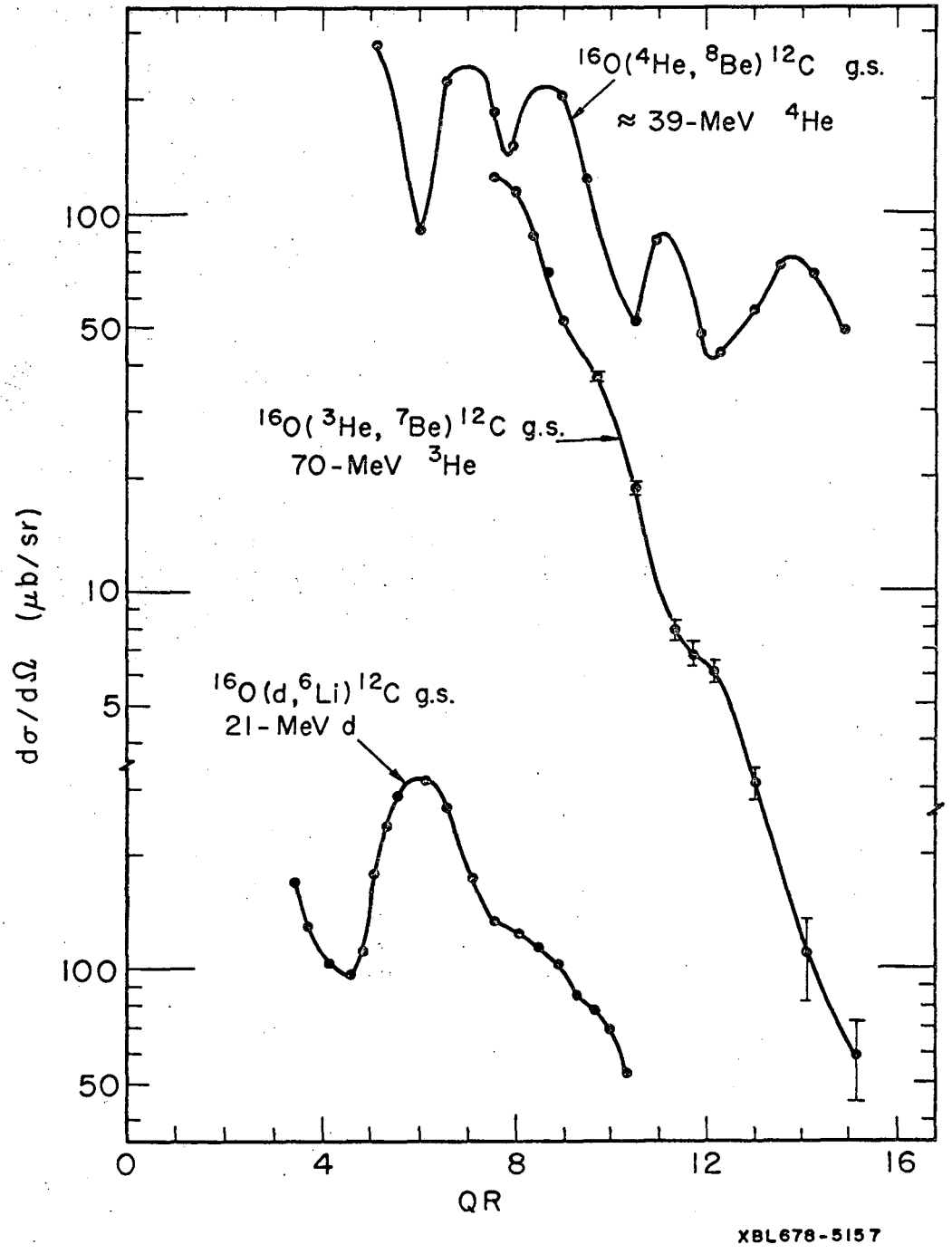

Fig. 42. Angular distributions of $^{16}O(^{3}He,^{7}Be)^{12}C$, $^{16}O(^{4}He,^{8}Be)^{12}C$, and $^{16}O(d,^{6}Li)^{12}C$ ground-state transitions.

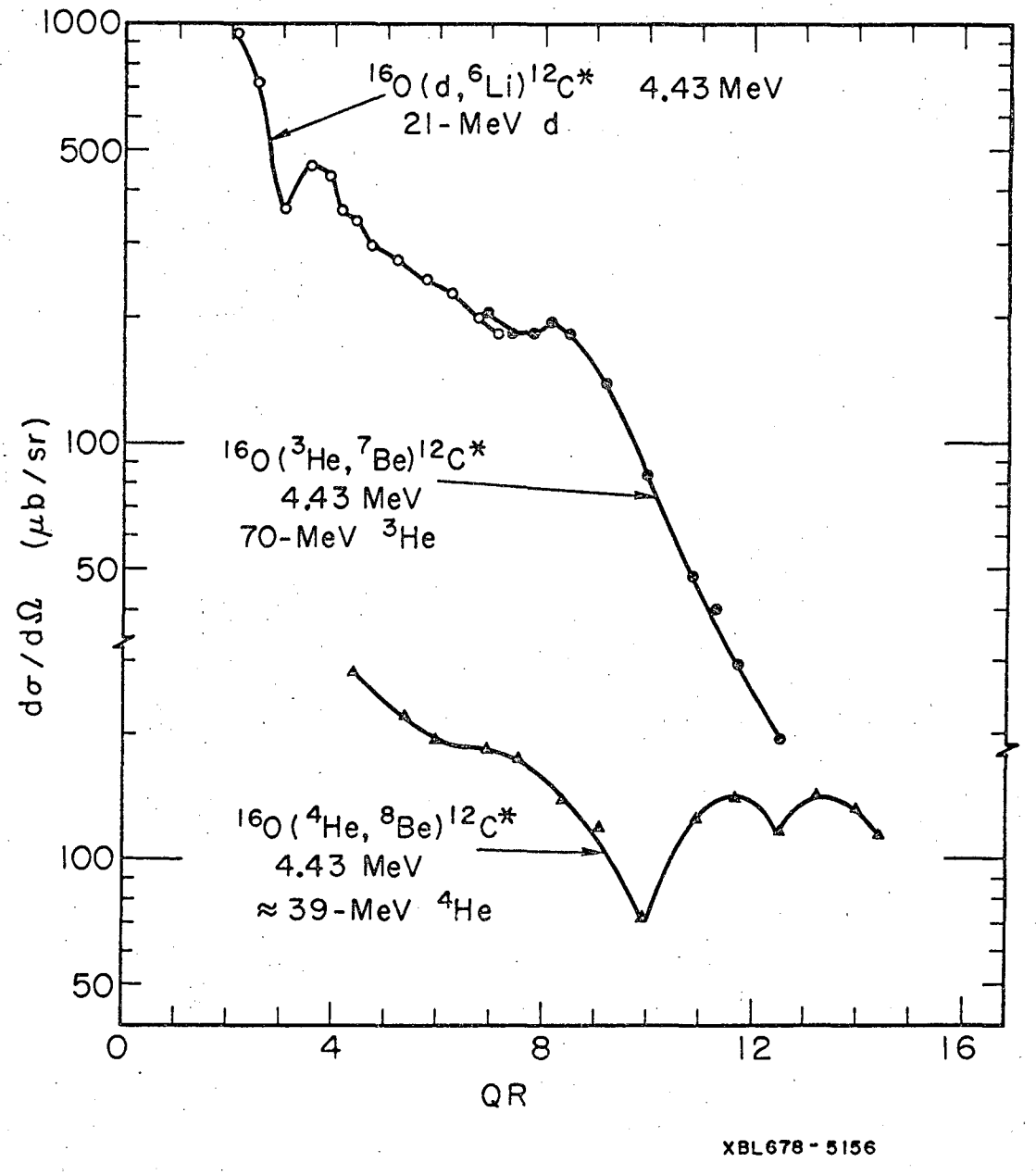

Fig. 43. Angular distributions of $^{16}O(^{3}He,^{7}Be)^{12}C^*$, $^{16}O(^{4}He,^{8}Be)^{12}C^*$, and $^{16}O(d,^{6}Li)^{12}C^*$ transitions to the 4.43-MeV state of ^{12}C.

Table VI. Integrated cross sections for three different reactions proceeding from ^{16}O to the same states in ^{12}C.

Energy Level (MeV)	Angular Range (c.m. deg)	Integrated Cross Sections (μb) $^{16}O(^{3}He,^{7}Be)^{12}C$ 70.1-MeV ^{3}He	$^{16}O(\alpha,^{8}Be)^{12}C$[a] 39-MeV α	$^{16}O(d,^{6}Li)^{12}C$[b] 21-MeV d
g.s.	22.0-62.9	43.4	449	649
4.43	23.9-51.3	153.8	358	699
7.66	15.4-44.2	13.0	-	-
9.63	15.5-36.9	14.9	-	-

[a] See Ref. 45.

[b] See Ref. 46.

V. DISCUSSION OF THE COMPLETED ISOSPIN QUARTETS

If the wave functions of the members of an isospin multiplet can be regarded as identical and if any charge-dependent forces are of a two-body character that can be treated as perturbations, then the masses of the members are given by the isobaric multiplet mass equation (IMME) ;

$$M(A,T,T_z) = \underline{a}(A,T) + \underline{b}(A,T)T_z + \underline{c}(A,T)T_z^2.$$

(See Sec. II for a discussion of this equation.) The completion of the mass 13, 21, and 37 isospin quartets permits three further independent tests of the parabolic character of the IMME since the coefficients can be determined from three of the members of a quartet and then used to predict a mass for the fourth member. We have chosen to use these data to predict the mass of the $T_z = -3/2$ nucleus in each quartet. A list of the $T_z = -3/2$ nuclei whose mass excesses have been measured, together with the coefficients and the predictions of the IMME for the four isospin quartets which have been completed to date, is presented in Table VII. In all four of the completed isospin quartets there is very good first order agreement between the predicted and experimental mass excesses within the relatively large experimental errors, which indicates that the IMME is accurate over a fairly large variation in atomic number Z. An apparent discrepancy in the much more accurate mass 9 quartet data[47] was interpreted as indicating a possible (and ultimately to be expected[23]) need for the inclusion of a higher order term $\underline{d}(A,T)T_z^3$ in the IMME, but unfortunately no explicit theoretical estimate of the magnitude of such a coefficient is available. These $\underline{d}(A,T)$ coefficients of an IMME containing a $\underline{d}(A,T)T_z^3$ term were calculated from the four experimental masses in each quartet and the results are listed in Table VII. Clearly such a coefficient is no greater than $\overline{Z}\alpha\underline{c}$, where $\overline{Z}$ is the average atomic number of the four members of an isospin quartet and α is the fine structure constant. Theoretical predictions of the magnitude of the expected second order corrections would be quite valuable.

Table VII. Isobaric multiplet mass equation predictions and calculated coefficients.

Isobaric Multiplet Mass Equation

$$M(A,T,T_z) = \underline{a}(A,T) + \underline{b}(A,T)T_z + \underline{c}(A,T)T_z^2 \quad [+ \underline{d}(A,T)T_z^3]$$

T_z=-3/2 Nucleus	Experimental Mass Excess (MeV)	Predicted Mass Excess (MeV)	b(A,T) (MeV)	c(A,T) (keV)	[d(A,T)] (keV)	$\overline{Z\alpha c}$ (keV)
^{9}C	28.99 (70)[a,b]					
^{9}C	28.916 (5)[c]	28.961 (29)	-1.332 (7)	278 (11)	7 (5)	9
^{13}O	23.11 (70)	23.10 (49)	-2.180 (16)	254 (11)	-1 (14)	12
^{21}Mg	10.62 (120)	10.59 (120)	-3.545 (40)	154 (24)	-5 (28)	12
^{37}Ca	-13.24 (50)	-13.24 (118)	-6.176 (39)	176 (25)	1 (21)	24

[a] All errors are in parentheses and are in keV.

[b] See Ref. 7.

[c] See Ref. 47.

Various systematic mass predictions for ^{9}C, ^{13}O, ^{17}Ne, ^{21}Mg, and ^{37}Ca, which are all the $T_z = -3/2$ nuclei whose masses are known, together with the experimentally measured masses, are shown in Table VIII. Only the Kelson-Garvey predictions (Ref. 4) cover all five nuclei and their predictions appear to be in excellent agreement with the experimental masses except for ^{13}O. In general, though, all three sets of predictions are in reasonable agreement with the data and a more stringent test of such predictions would appear to require investigations of nuclei nearer proton-instability, such as ^{12}O and ^{36}Ca, which could be reached through the $(\alpha, ^{8}He)$ reaction.

Table VIII. Comparison between various systematic mass predictions and the experimental masses.

Nucleus	Experimental[a] Mass Excess (MeV)	Goldanskii[b] Mass Excess (MeV)	Jänecke[c] Mass Excess (MeV)	Kelson-Garvey[d] Mass Excess (MeV)
^{9}C	28.916 (5)[e]	-	29.3	28.88
^{13}O	23.11 (70)[f]	23.2	23.4	23.52
^{17}Ne	16.47 (190)[g]	16.2	16.3	16.63
^{21}Mg	10.62 (120)	10.9	10.8	10.79
^{37}Ca	-13.24 (50)	-12.9	-	-13.17

[a] Values in parentheses are the mass excess errors in keV.

[b] See Ref. 1.

[c] See Ref. 3.

[d] See Ref. 4.

[e] See Ref. 47.

[f] See Ref. 23.

[g] See Ref. 48.

ACKNOWLEDGMENTS

I am indebted to all those associated with the 88-inch cyclotron and I take particular pleasure in thanking:

Professor Joseph Cerny III, my research adviser, for suggesting this experiment and for his assistance, advice, and encouragement during the course of this work;

Dr. Richard H. Pehl for many enlightening discussions and for significant contributions to this research;

Dr. Sam W. Cosper and Dr. Robert L. McGrath for a great deal of assistance with the experimental work and for several helpful discussions;

Dr. Bernard G. Harvey and Dr. David L. Hendrie for helpful discussions;

Mr. Frederick S. Goulding and Mr. Donald A. Landis for their invaluable assistance with the electronic equipment and counters;

Mr. Robert Lothrop, Mr. Morris Roach, and Mr. Harry Smith for providing the silicon detectors used in these experiments;

Dr. Claude Détraz, Mr. Donald G. Fleming, Mr. Gordon C. Ball, Mr. Heinz Brunnader, and Mr. George W. Goth for their aid in the actual experiments and for several discussions, many of which were relevant and helpful;

Mr. Creve C. Maples, Jr. for writing several data analysis programs and for his assistance in these experiments;

Mr. Nolan F. Mangelson, Mr. Chi Chang Lu, Miss Mary F. Reed, Mr. John Esterl, and Mr. Gordon Wozniak for many conversations, some of which were helpful;

Mr. Claude Ellsworth for preparing several targets;

Mr. John Meneghetti and all the accelerator technicians for the construction of several pieces of experimental equipment;

Mr. John Bowen and the operating crew of the 88-inch cyclotron for their cooperation.

This work was performed under the auspices of the U. S. Atomic Energy Commission.

REFERENCES

1. V. I. Goldanskii, Nucl. Phys. 19, 482 (1960).
2. A. I. Baz, V. I. Goldanskii, and Ya. B. Zeldovich, Usp. Fiz. Nauk 3, 211 (1961); [Trans.: Soviet Physics USPEKHI 3, 729 (1961)]; A. I. Baz, V. I. Goldanskii, and Ya. B. Zeldovich, Usp. Fiz. Nauk 85, 445 (1965); [Trans.: Soviet Physics USPEKHI 8, 177 (1965)].
3. J. Jänecke, Nucl. Phys. 61, 326 (1965).
4. I. Kelson and G. T. Garvey, Phys. Letters 23, 689 (1966); G. T. Garvey and I. Kelson, Phys. Rev. Letters 16, 197 (1966).
5. E. P. Wigner and E. Feenberg, Rept. Progr. Phys. 8, 274 (1941).
6. E. P. Wigner, Proc. Robert A. Welch Foundation Conf. on Chemical Research, 1957, Vol. I, ed. by W. O. Milligan (The Robert A. Welch Foundation, Houston, 1958), p. 67; S. Weinberg and S. B. Treiman, Phys. Rev. 116, 465 (1959); D. H. Wilkinson, Phys. Letters 12, 348 (1964).
7. J. Cerny, R. H. Pehl, F. S. Goulding, and D. A. Landis, Phys. Rev. Letters 13, 726 (1964).
8. M. A. Tuve, N. P. Heydenburg, and L. R. Hafstad, Phys. Rev. 50, 806 (1936).
9. D. H. Wilkinson, Proc. Conf. on Isobaric Spin in Nuclear Physics, 1966, ed. by J. D. Fox and D. Robson (Academic Press, Inc., New York, 1966), p. 30.
10. D. H. Wilkinson, Phys. Letters 11, 243 (1964).
11. D. H. Wilkinson, Phys. Rev. Letters 13, 571 (1964).
12. C. C. Maples, Jr. and J. Cerny, Lawrence Radiation Laboratory Report UCRL-17214, 1967 (unpublished).
13. C. Williamson and J. P. Boujot, Tables of Range and Rate of Energy Loss of Charged Particles of Energy 0.5 to 150 MeV, Centre D'Etudes Nucleaires de Saclay (1962); and L. C. Northcliffe, Studies in Penetration of Charged Particles in Matter, National Academy of Sciences - National Research Council, Washington, D. C. (1964), pp. 173-186.
14. P. Darriulat, G. Igo, H. G. Pugh, J. M. Meriwether, and S. Yamabe, Phys. Rev. 134, B42 (1964).

15. Hamilton Watch Company, Metals Division, Lancaster, Pennsylvania.
16. Monsanto Research Corporation, Mound Laboratory, Miamisburg, Ohio.
17. Isomet Corporation, Palisades Park, New Jersey.
18. Union Carbide Nuclear Company, Oak Ridge National Laboratory, Oak Ridge, Tennessee.
19. W. L. Briscoe, Rev. Sci. Instr. 29, 401 (1958); R. H. Stokes, J. A. Northrup, and K. Boyer, Rev. Sci. Instr. 29, 61 (1958).
20. F. S. Goulding, D. A. Landis, J. Cerny, and R. H. Pehl, Nucl. Instr. and Methods 31, 1 (1964).
21. J. H. Elliot and R. H. Pehl, Rev. Sci. Instr. 33, 713 (1962).
22. F. S. Goulding, Nucl. Instr. and Methods 43, 1 (1966).
23. J. Cerny, R. H. Pehl, G. Butler, D. G. Fleming, C. Maples, and C. Détraz, Phys. Letters 20, 35 (1966) and references therein.
24. F. S. Goulding, D. A. Landis, J. Cerny, and R. H. Pehl, IEEE Trans. Nucl. Sci. NS-13, No. 3, 514 (1966).
25. J. Cerny, S. W. Cosper, G. W. Butler, R. H. Pehl, F. S. Goulding, D. A. Landis, and C. Détraz, Phys. Rev. Letters 16, 469 (1966).
26. S. W. Cosper, J. Cerny, and R. C. Gatti, Phys. Rev. 154, 1193 (1967).
27. All atomic masses and reaction Q-values were taken from the following reference: C. Maples, G. W. Goth and J. Cerny, Nuclear Reaction Q-values, UCRL-16964, 1966 (unpublished).
28. C. M. Lederer, J. M. Hollander, and I. Perlman, Table of Isotopes, Sixth Edition, (John Wiley and Sons, Inc., New York, 1967), p. 405.
29. Nuclear Data Sheets, Energy Levels of Light Nuclei, National Academy of Sciences - National Research Council, Washington, D. C. (1962).
30. R. E. Berg, J. L. Snelgrove, and E. Kashy, Phys. Rev. 153, 1165 (1967).
31. P. M. Endt and C. Van der Leun, Nucl. Phys. 34, 1 (1962).
32. J. C. Hardy and R. E. Bell, Can. J. Phys. 43, 1671 (1965) and references therein.
33. M. E. Bunker, M. G. Silbert, J. W. Starner, R. K. Sheline, and N. Jarmie, Bull. Am. Phys. Soc. II, 8, 317 (1963); P. Kienle

and K. Wien, Nucl. Phys. 41, 608 (1963).

34. B. F. Bayman, Proc. Conf. on Isobaric Spin in Nuclear Physics, 1966, ed. by J. D. Fox and D. Robson (Academic Press Inc., New York, 1966), p. 503.

35. P. Horvat, Nucl. Phys. 52, 410 (1964); R. A. Mendelson, Jr. and R. T. Carpenter, Phys. Rev. 152, 1002 (1966); R. E. McDonald and J. A. Becker, Phys. Rev. 154, 1101 (1967).

36. The $^{16}O(d,^{3}He)^{15}N$ angular distributions at 39.6 MeV are from unpublished data of J. Cerny, et al.

37. C. Van der Leun and W. L. Mouton, Physica 30, 333 (1964).

38. J. G. Pronko, C. Rolfs, and H. J. Maier, Nucl. Phys. A94, 561 (1967) and references therein.

39. P. Bém, J. Habanec, O. Karban, and J. Nemec, Nucl. Phys. A96, 529 (1967).

40. A. M. Poskanzer, R. McPherson, R. A. Esterlund, and P. L. Reeder, Phys. Rev. 152, 995 (1966) and references therein.

41. G. Bassani, N. M. Hintz, and C. D. Kavaloski, Phys. Rev. 136, B1006 (1964); G. M. Reynolds, J. R. Maxwell, and N. M. Hintz, University of Minnesota Linear Accelerator Laboratory Annual Progress Report, p. 98, 1965 (unpublished); J. R. Maxwell, G. M. Reynolds, and N. M. Hintz, University of Minnesota John H. Williams Laboratory of Nuclear Physics, Annual Progress Report, p. 77, 1966 (unpublished); C. Détraz, J. Cerny, and R. H. Pehl, Phys. Rev. Letters 14, 708 (1965); J. Cerny, C. Détraz, and R. H. Pehl, Phys. Rev. 152, 950 (1966).

42. D. R. Goosman and R. W. Kavanagh, Nuclear Energy Levels of ^{37}K, April 1967 (preprint).

43. The $^{16}O(p,^{4}He)^{13}N$ data at 54 MeV are from unpublished data of C. C. Maples, Jr. and J. Cerny.

44. Since the ^{8}Be nucleus in its ground state is unstable with respect to breakup into two α-particles with a half life of about 10^{-16} sec, its detection requires the coincident detection of the two breakup α-particles; this was the technique used in Ref. 45 for studying the $^{16}O(^{4}He,^{8}Be)^{12}C$ reaction.

45. R. E. Brown, J. S. Blair, D. Bodansky, N. Cue, and C. D. Kavaloski, Phys. Rev. 138, B1394 (1965).

46. J. B. Gerhart, P. Mizera, and F. W. Slee, University of Washington, Nuclear Physics Laboratory Annual Report, p. 21, 1964 (unpublished).

47. C. A. Barnes, E. G. Adelberger, D. C. Hensley, and A. B. McDonald, Proc. Int. Conf. on Nuclear Physics, Gatlinburg, Tennessee, September 1966 (to be published).

48. R. A. Esterlund, R. McPherson, A. M. Poskanzer, and P. L. Reeder, Phys. Rev. 156, 1094 (1967).